UNIVERSITY of ROME

"TOR VERGATA"

Department of Chemical Science and Technology

XVII Ph.D. Course on "Materials for Environment and the Energy"

Thesis of Doctorate

POROUS SILICON MATERIALS DEVELOPMENT FOR APPLICATIONS IN ENVIRONMENTAL SENSORS

Dr. Veronica Valentini

Internal tutor

Prof. Riccardo POLINI

External tutor (CNR)

Dr. Giorgio MATTEI

Academic Years 2001-2004

CONTENTS

INTRODUCTION

In these last years we have seen the consolidation of a diffused interest in the environmental monitoring problems in its amplest meanings. The smog pollution problem, and in general, of the environmental impact consequential from all the activities developed in the urban centers, has been faced in a systematic way since the first '70s, using special tools both legislative and technological. According to the most recent indications of the EU the attention is concentrated on thematic of remarkable social-economic interest, and particularly on the following action areas: environment, health, innovation in product and process, microsystems and nanotechnologies.

Among the materials used in the environmental sensors porous silicon, PS, can also be enumerated. PS is the product of the partial anodic dissolution of a substrate of crystalline silicon in an electrolytic solution of hydrofluoric acid, HF. PS is a material of wide importance not only for fundamental studies, for example for quantum confinement studies and for the chemistry of the surfaces, but also in application for its properties of photoluminescence and electroluminescence in the visible, its large superficial area and its optical properties [1]. All these characteristics have greatly increased researchers' interest in PS, opening a very active research area in constant expansion, especially for applications in the fields of the opt-electronics, optics and sensors. With the use of PS, among of the applications, light emitters, solar cells, interferential filters and sensors devices have been made; other applicative purposes of PS production and industrial use of PS as a sacrificial insulating layer in electronic devices and as electrode in fuel cell are well known.

PS is a material of wide interest in the sensors field because of its large surface area, surface reactivity and natural integrability in the electronic circuits. Therefore, the study of the interaction between the environment, namely liquid phase and/or gas phase, and the PS surface is of great importance in applications. PS, can be used as transducer material in sensing application, and in particular in the detection of vapors, liquids and biochemical molecules. In fact, when exposed at chemical substances, several physical quantities, such as refractive index, photoluminescence, and electrical conductivity, can change drastically. Moreover, PS is an available, low cost material, with a large surface area that can assure a very effective interaction with several adsorbates, so that it could usefully be employed in the realization of sensors and microsystems.

For all these reasons we have prepared single layers and specially devised PS superstructures and studied in details some aspects of the interaction between the PS materials with the environment that is a crucial point for application in the sensor field. The first subject of our research has been the oxidation process of PS in air and its control. In fact, we know that in presence of air, or water and/or oxygen, PS inevitably gets oxidized so modifying its properties and the performances of its devices. But a controlled oxidation of PS materials can be also used as method to stabilize the properties of this material. Indeed oxidized PS can be used for different application, for example a laser light stimulated emission from nano-structured silicon in a silicon oxide matrix has been recently demonstrated [2]. Besides, applications of oxidized PS in the environmental sensor field have been reported [3 ÷ 7].

On the basis of these interests, a thorough study of PS oxidizing phenomena in different environments, namely air alone or saturated with vapors of some organic substances (in recent work the Pyridine has been suggested as a catalyst for PS oxidation in air [8]), has been performed.

During this research doctorate course we have verified that the use of PS multilayer optical systems, e. g. Fabry-Perot, FP, increases the response sensibility of the system (due to the optical signal amplification that occurs inside the structure) and thus of the sensibility of the possible optical sensors. Therefore we have applied one of our FP structure to realize a dosimeter for the urotropin, toxic organic substance commonly used in several application areas, e.g. rubber, explosives, fuel, pharmaceutical industries, etc.. Following the tendency of recent literature we start to work on the functionalization of PS with the aim of use organic molecules having peculiar properties “ad hoc” for sensor applications. Functionalize a PS sample means to substitute the Si-H bonds normally presents on the whole surface of fresh PS with Si-C covalent bonds that therefore bond in a stable manner a certain organic molecule to the PS surface (e. g. chemisorptions by hydrosilylation reaction). The coverage of the PS surface with suitable organic molecule can attribute new properties to the PS, those owning to the organic molecule and others deriving from the organic-PS match, but it can also stabilize the sample and reducing the effect of the oxidation due to the aging of the PS. In the PS functionalization activity we have, finally, invented a new PS functionalization method simple, fast and effective and that present the unique ability to allow the confined functionalization of a selected layer in a PS stack. We have developed this study with the aim to exploit at the best its potentialities, also as first step to realize sensors of novel design.

PS produced samples have been characterized by SEM and optical spectroscopies, FTIR, UV-Vis, Raman and sum frequency generation (SFG), which are particularly suitable for thin layers

and surfaces studies. After the post-treatments, the species present on the PS surface, resulting from the functionalization, have been determined using the FTIR reflection spectroscopy and, in the case of the study of oxidation, the evolution of the various species on time has been followed.

Finally, the presentation of the subjects of this thesis is the following:

- In chapter 1 after a short historical introduction general information regarding the PS main properties and the possible applications are presented;
- In chapter 2 is presented the experimental part that include information on the sample preparation and characterization;
- In chapter 3 are presented in detail and discussed the results of the research activity: the study of the PS induced oxidation in humid air saturated by H_2O, Pyridine and other organic base vapors; the study of the interaction between PS and saturated vapors of Urotropin (with the demonstration that our samples can be used as a dosimeter for this toxic substance used in several application areas, e.g. rubber, explosives, fuel, pharmaceutical industries, etc.); the first measurements of PS surface species using a non linear spectroscopy highly sensitive to the surface i.e. SFG spectroscopy; the results obtained on the functionalization of PS layers that include the description of a new original method of in-situ formation-functionalization PS;
- finally there is the summary.

At the end there are several annexes: some general information and properties about the crystalline Si (annex A); some indication about the theory of Raman (annex B) and Infrared (annex C) spectroscopies; an illustration of the SCOUT elaboration and of the used Bruggeman model (annex D); short notes describing general information about the SFG spectroscopy (annex E).

Finally a list of all the publications regarding the scientific research activity carried out during the last three years.

CHAPTER 1

Porous Silicon properties

PS which forms on the surface of crystalline Si substrate in hydrofluoric acid (HF), under an appropriate anodic polarization, was first observed by Uhlir in 1956 [9]. He investigated electropolishing of crystalline Si and found that below a certain current density a brownish layer develops, which is now known as PS. Later on, PS was investigated in detail by Turner (1958) [10]. As the name PS indicates, the bulk crystalline Si changes by the etching process into a kind of sponge-like structure with interconnected and hydrogen covered silicon columns and pores, as shown in Fig. 1.1.

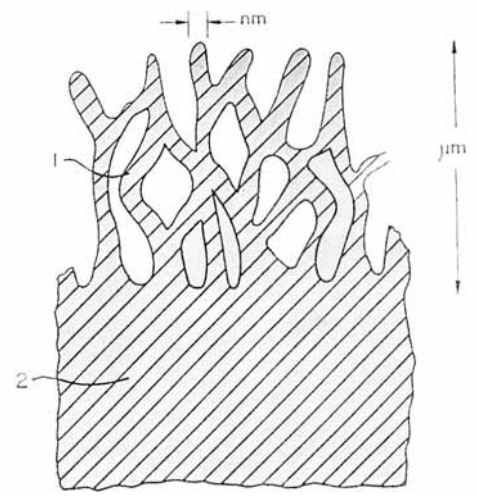

Fig.1.1. Scheme of PS layer structure (1) overhanging the crystalline Si substrate (2).

Uhlir had already noticed that flakes of PS appeared sometimes of red color (indicative of an increase of the "band gap" in comparison to the Si crystalline of the "bulk"), in 1984, Pickering et all. [11] had reported for PS the measure of photoluminescence (PL) in the visible at 4 K.
In 1990 Canham [12] found strong visible room temperature (RT) photoluminescence in a PS layer which had been etched chemically in HF after the anodic etching in order to widen the pores and therefore decrease the size of the remaining Si skeleton.
The observed luminescence was much more efficient, than the usual band gap related IR luminescence of crystalline bulk Si (which has an indirect gap of 1.1 eV) as showed in Fig. 1.2.

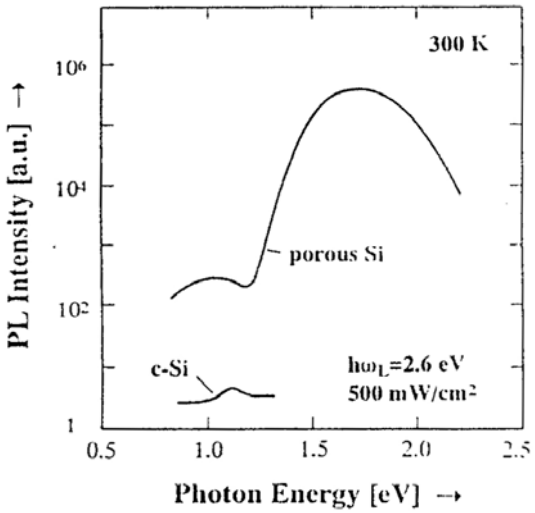

Fig. 1.2. Comparison between photoluminescence spectra at room temperature of the crystalline Si substrate and the PS. The photoluminescence intensity expressed in a logarithmic scale.

The observation of efficient room temperature (RT) photoluminescence in the visible range combined with the quantum confinement explanation attracted a large interest, both fundamental and applicative, on PS.

The main PS properties are:

1. Strong PL (and EL) in the visible: interesting for optoelectronic applications;
2. Large surface area (up to 900 m^2/g): interesting in chemical and biochemical sensing;
3. Dielectric function (ε) that can be easily modulated. Indeed by varying the porosity, defined as the vacuum volume fraction, it is possible to obtain several values of the dielectric function, which is basically the sum of contributions from the skeletal crystalline Si and the air on the pores.
4. It is also possible to produce multilayer systems with various porosity changing the applied current density during the anodization because the porosity depends on the current density and the thickness on the anodization time. One of these multilayer systems is the Fabry-Perot (FP) that is a structure of PS at high reflectivity (100%), with a cavity, a reflectivity minimum, in the center of this high reflectivity region. This property makes the PS interesting for optical, spectroscopic and sensing applications.
5. PS is also a biodegradable and biocompatible material, property interesting for medical and biological application.
6. Easy integrability in the Si microelectronics.

General information, also about possible applications, are reported in numerous reviews and articles devoted to the PS [1, 13 ÷ 17].

1.1 PREPARATION: Electrochemical Reactions and Formation Processes

The partial anodic dissolution of crystalline Si samples occurs under suitable conditions in electrochemical teflon cells containing an HF electrolytic solution.

In Fig. 1.3 are shown some typical electrochemical cells in use. In this work the typology of cell used was the (c) one that is simple and allows to realize homogeneous samples presenting a good control of the porosity and thickness.

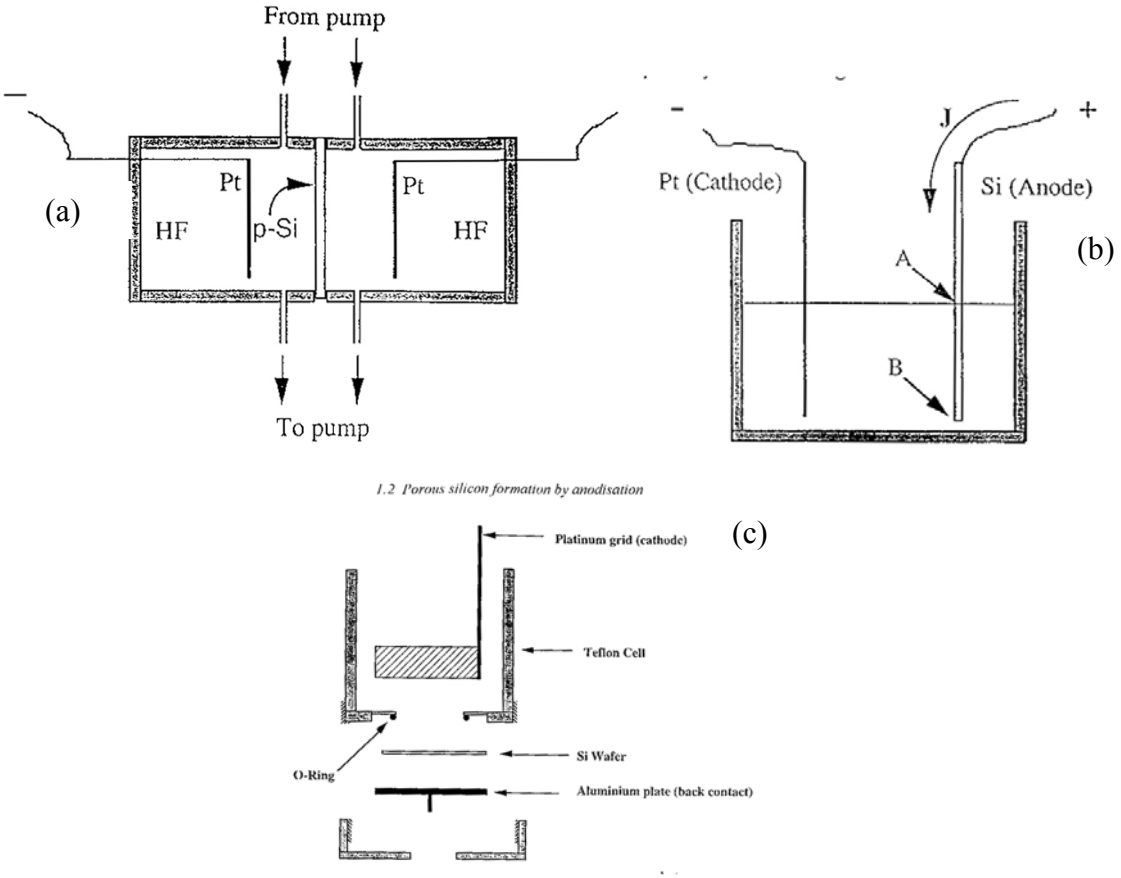

Fig. 1.3. Schemes of anodization cells used for the electrochemical PS formation reaction: (a) cross section of a double tank cell; (b) cross section of a lateral anodization cell; (c) cross section of a conventional single tank cell.

Observing a typical current density (J)/electrodic potential (V) curve, Fig. 1.4, for $J > J_{ep}$ the electropolishing occurs and for $J \leq J_{ep}$ the PS formation occurs.

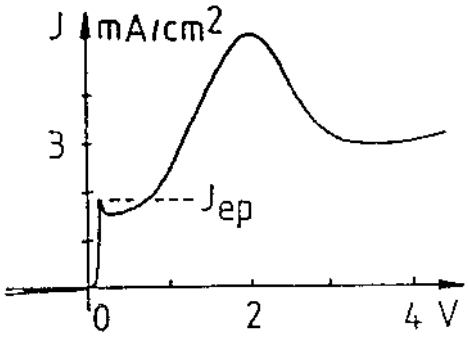

Fig. 1.4. Dependence of the current density on the potential in a Si sample submitted to the anodization.

The J_{ep} depends mostly on the composition of the HF solution in EtOH and little on the substrate. A large variety of layers morphologies (pore diameter, pore spacing, direction of propagation, etc.) may be obtained with single crystalline Si, according to the substrate (surface orientation, doping level and type) as well as the composition of the aqueous solutions (pH, HF concentration, etc.) and to the anodization conditions (J and t).

The skeleton remaining among the channels preserves its original crystallinity, showing that pore formation occurs through a direct dissolution of the bulk of the material and not by some redeposition or recrystallization process.

The exact Si dissolution chemistry is still matter of discussions, although it is generally accepted that the holes are necessary in the initial oxidation stage both for the electropolishing and for the pore formation. *In-situ* and *ex-situ* spectroscopy has confirmed the presence of Si-H bonds in the surface during the PS formation. The hydrogen exists on the Si surface in at least two different forms, Si-H and $Si-H_2$, with a third possible form $Si-H_3$ (the superficial concentration of the dihydride, $Si-H_2$, increases with the increase of the anodic potential).

The (100) plane has the more sterically favorite geometry for the Si divalent superficial state, that is two bonds symmetrically direct inside the solution, important preferential site of the anodic etching.

The presentation and discussion of the various proposed models, in literature, for the PS electrochemical formation processes in the HF various solutions, go beyond the purposes of the present treatment. Therefore, the interested reader can consult the specific articles quoted in the bibliography and associated to the various models indicated in the following list:

1. The “Beale” model [18, 19];
2. The “diffusion-limited” model [18, 20];
3. The “quantum-based” model [18, 21];
4. The “Zhang” model [19];
5. The “Lehmann” model [19];

6. Mathematical models with growing simulations [22 ÷ 24].

We present here a general scheme of p-type Si dissolution process, in HF ethanoic solution, the aim is to emphasize the two fundamental steps of the process (universally accepted): (i) The Si dissolution that involves hole (h^+) participation, at the interface Si/electrolyte and (ii) the passivation, namely the end of this process, when the hole supply is interrupted, and that causes the stability of the produced PS structure.

Before to start the anodic dissolution the Si thin plate is kept in contact for few minutes with the HF solution to eliminate the native oxide (SiO_2) always and inevitably present on the crystalline Si surface leaving it H-terminated [10]. Indeed, although the bond energy for the Si—F bonds is the highest of all superficial species (see table 1.1), such bonds, thermodynamically more stables, are not observable on the Si surface, because they hydrolyze easily to Si —OH and Si —H in presence of water. The SiH species present on the Si surface depends on the Si substrate orientation; PS layers produced from a (100) Si plate, as in our case, present their surface mostly SiH_2-terminated.

Table 1.1. *Bond energies for various bond type presents on the crystalline Si surface.*

Bond type	Bond energy (Kcal/mol)
Si—F	129.3
Si—O	88.2
Si—H	70.4
Si—Si	42.2

In some detail the formation process of PS during the anodization procedure can be summarized as it follows:

- When a hole (h^+) reaches the Si hydrogenated surface fluoride ions nucleophilic attack can occurs on Si—H bonds and a Si—F bond is established (step 1 Fig. 1.5).

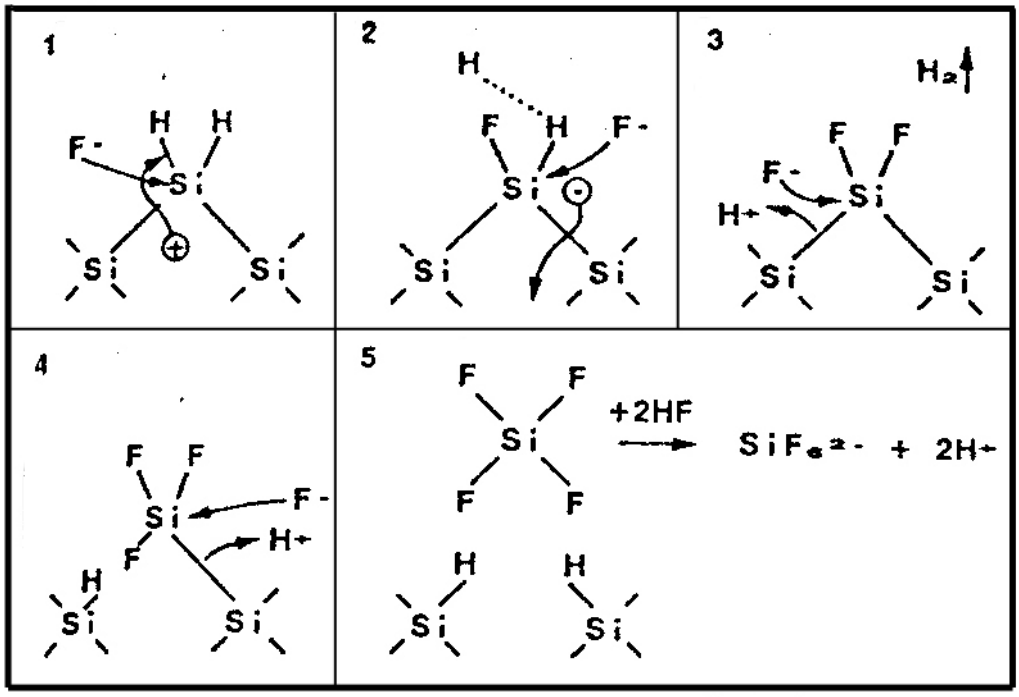

Fig. 1.5. Porous Si formation reaction scheme starting from a crystalline Si substrate in an HF ethanoic solution by anodic dissolution reaction.

- Due to the polarizing influence of the first fluorine Si-bonded atom, another F^- ion can attack the other Si-H bond of the same Si atom under generation of an H_2 molecule and injection of one electron into the electrode (step 2). Due to the polarization induced by the Si—F groups, the electron density of the Si—Si back bonds is lowered and these weakened bonds will now be attacked by HF or H_2O (step 4 and 5) in such a way that the Si surface atoms remain bonded to hydrogen (step 5). The dissolved Si will remain in solution as species H_2SiF_6 that appear in some ionized forms according to the concentration and pH of the HF solution.
- If a Si atom is removed from an atomically flat surface by this reaction, an atomic size dip remains. This modification in surface geometry will change the electric field distribution in such a way that hole (h^+) transfer occurs at this location preferentially. The defect points on the Si surface generates a local concentration of the electric field that increases the hole concentration in these regions that becomes larger than in the other Si surface regions passivated by Si-H bonds.
- At a certain point the dissolution reaction breaks off. This self-limiting process, that gives rise to the Si surface passivation and to the stabilization of the produced PS structure, can be attributed to different mechanisms: (i) if the pore walls are lacking in holes they will be protected against further dissolution. While the Si skeleton size decreases the supply of free carriers diminishes (hole depletion) and its resistivity increases until reach the intrinsic Si

value [1 (g), 25]. (ii) The thinning of the Si skeleton can reduce and stop the dissolution reaction, because of the quantum confinement of the charge carriers due to the small pore wall dimensions. This quantum confinement provokes a gap widening and an energy barrier $\mathbf{D}E_V$ for holes and $\mathbf{D}E_C$ for electrons formation to come into the Si region between the etched pores [21].

Similar processes occur for the n-type Si samples, in this case, because they have an excess of electrons, the necessary holes for the anodic dissolution process are produced exposing the samples to a controlled lighting. In the dark n-type Si samples anodization occurs only at high potential and the resulting structure is different from that obtained at same operative conditions but under illumination.

1.2 DISSOLUTION CHEMISTRIES

When Si samples remain in contact with the HF solution for long times, a dissolution of purely chemical nature is added to the phenomenon of the electrochemical dissolution. The contribution of the chemical dissolution has therefore a larger impact in the layers formation of thicker PS, in fact, for p-type Si samples, increasing the layer thickness of a factor 5 the average porosity increases of 10% and the peak of the pore size distribution increases of 3 nm [1 (a)].

For the substrates heavily doped (e. g. $\rho = 0.01\ \Omega$cm) the effect of the chemical dissolution on the porosity is negligible and not measurable due to the low specific surface area (200 $m^2 \cdot cm^{-3}$) of the material, compared to that of the layers obtained from low resistivity Si (~600 $m^2 \cdot cm^{-3}$).

In the case of n-type porous layers, the pore radii increase and the distribution broadens when the sample thickness is increased, because the contribution of the chemical dissolution is added to the electrochemical one.

1.3 RELATIONS BETWEEN PREPARATION AND PROPERTIES OF THE PS LAYERS

In this paragraph the relations are described between the parameters preparations (for example the type of substrate, the composition of the electrolytic solution, etc.) and the characteristics of the PS produced layers (porosity, morphology, pore dimensions, etc.).

All the properties of the PS layer, such as porosity, thickness, pore diameter, microstructure, are strongly dependent on the anodization conditions. These conditions include the HF concentration, the pH of the solution and its chemical composition, current density, wafer type

and resistivity, crystallographic orientation, temperature, anodization duration, stirring conditions and illumination conditions during anodization. Optimum control of the porous layers fabrication and the reproducibility are possible only if all the parameters listed above are taken into account.

In the most general sense a "pore" is an etch pit whose depth, d, exceeds its width, w. Generally single pores are generally closed at one end and partially interconnected to some degree. The most common shape by far is that of cylindrical pores with varying degrees of "branching" and "necking". The use of chemically aggressive electrolytes, excessively long anodization times or light-assisted etching all act to generate a funnel-type shape. The anodization of (100) oriented wafers can generate pores of square cross-section whilst (111) oriented wafers can exhibit triangular shaped pores [1 (b)].

The IUPAC defines pore size ranges, reported in the table 1.2, where are associated different PS typologies:

Table 1.2. *Definition of the pore typology as a function of the width range.*

Pore width (nm)	**Pore type**
§ 2	Micro
2**π**50	Meso
> 50	Macro

Clearly, pore size only has a precise meaning when the geometrical shape of the pores is well defined and known. For low porosity macroporous Si, and sometimes of mesoporous Si, this is the case, but micro pore shape is currently ill-defined. Extreme caution, however, is needed to distinguishing rough surface from incipient pore formation via surface topography measurements relying on "Atomic Force Microscopy" (AFM) or "Scanning Tunneling Microscopy" (STM) alone. Such images can be significantly distorted in the vertical direction and completely miss or underestimate the depth of very narrow features. Individual pore examination is most frequently made by high resolution transmission electron microscopy (HRTEM) or high resolution scanning electron microscopy (HRSEM).

Pore size determines much of the absorptive properties of a material, and that are important in application area such as sensing or biofiltration.

1.3.1 Properties dependence from the used Si type

The pore nucleation starts from the defect sites on the crystal surface, therefore the doping atoms are selectively removed during the anodization process leaving an intrinsically porous structure. This allows to explain the dependence of the pore density on the doping level. A gradual increase of the pore number and the decrement of their radius to the increasing of the semiconductor doping level occur. The pore size increases with the decrease of the resistivity for the p-types and vice versa for the n-types (that is the size increases with the increasing of the resistivity) [19].

Increasing the doping concentration also the pore diameter and the average skeleton dimensions slightly increase (the p^+-type produce formation of channels) [18].

The characteristic curves J/V for p-type Si wafers of different dopant concentrations in an HF solution are independent of the thickness of the PS layer and successive potential sweeps on the same Si electrode lead to the same dependence [1 (c)]. When the doping concentration increases the curves shift towards cathodic potential, as we can observe in Fig. 1.6 [1 (c)]. As a consequence, of this if a Si wafer with an average dopant concentration is anodized the PS formation takes place previously in the heavily doped regions producing a spatial selectivity.

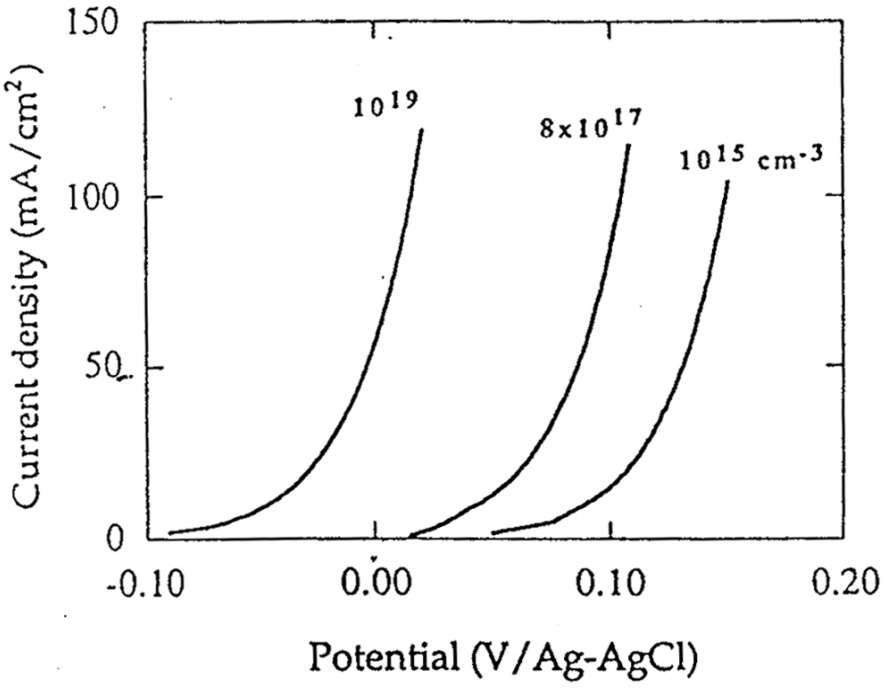

Fig. 1.6. Anodic current density-voltage characteristics of p-type Si in a 35% HF solution and with e of different substrate doping concentrations.

The relation J/V depends also on the relative doping of the material: the curves J-V for every type of samples are moved to the right in the general order $n^+ < p^+ < p < n$, see Fig. 1.7 [1 (c)].
If the potential is controlled with care to the appropriate value, the pore formation occurs in preferential way for the different types of dopants: n^+ can be preferentially anodized over p^+, p or n; p^+ can be preferentially anodized over p or n; etc…

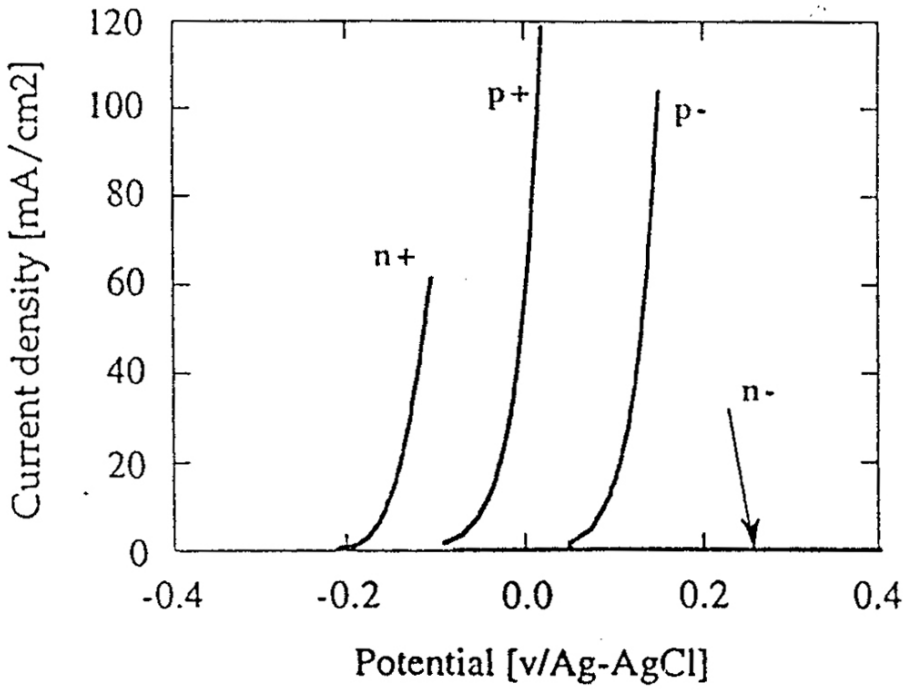

Fig. 1.7. Comparison of the anodic current density-voltage characteristics obtained from p- and n-type Si in a 35% HF solution using substrates of different doping levels (n^+ and p^+: 10^{19} cm^{-3}, n^- and p^-: 10^{15} cm^{-3}).

1.3.2 Effect of Illumination

Si dissolution requires holes (h^+). When lightly doped n-type Si (~10^{18} cm^{-3}) is anodized in the dark, PS formation is observed only at high voltages (>5V) and macroporous layers are obtained (pore diameter ~0.2 μm). If the anodization is performed under illumination, PS is formed at lower potentials (< 1V) and the resulting material consists of two parts: the top surface layer is nanoporous (d ~3 nm) and its thickness lies in the 0.2 ÷ 1 μm range, depending on the doping of the substrate. The underlying part is macroporous. For a heavily doped substrates (~10^{19} cm^{-3}) PS formation is observed even in the dark [1 (c)].
The anodic dissolution of p-type Si generally is performed to the dark because the p-type generally is not very sensitive to the presence to the lighting.

1.3.3 Effect of the solution composition

When for the PS formation a purely aqueous HF solution is used, the hydrogen bubbles stick to the surface inducing lateral and in-depth inhomogeneity. To improve the uniformity of the PS layer these bubbles must be quickly eliminated and one of the most appropriate means to overcome this problem is to add surfactant agents to the HF solution.

The more used surfactant in the case of the PS formation is absolute ethanol and it is known that for an efficient elimination of the bubbles the ethanol concentration should not be less than 15% [1 (c)]. It has been shown [26, 27] that the ethanoic HF solution completely infiltrates the pores, while a purely aqueous solution does not, due to wettability and capillary phenomena (the Si surface hydrogen terminated is hydrophobic [26, 27]).

These phenomena play an important role in the smoothness of the interface between Si and PS and thus in the uniformity of the PS thickness. In fact, the role of the ethanol is to improve the uniformity of the PS layer by elimination of the hydrogen bubbles and to improve the penetration of the electrolyte in the pores.

When the electrolytic HF concentration is decreased: the radii corresponding to the maximum distribution shift to higher values, and the distributions broaden [1 (a)]. Increasing the HF concentration in the electrolyte solution decreases the PS layer porosity [1 (c)]. Lower porosity can be obtained using a higher HF concentration, at the most a solution of pure HF (50%). Nevertheless the PS layers obtained in such a solutions, without ethanol, exhibit poor homogeneity and the best way to obtain lower porosity with good homogeneity is to use acetic acid as surfactant [1 (c)].

Although commonly the most used method for the PS formation is the anodization at constant current density, in some cases (thick layers, > 50 μm, obtained at high current density, > 100 mA cm^{-2}) to reduce the effects of the local concentration inhomogeneity of the electrolytic solution in the PS, a pulsed current is used. Indeed during the pauses of the anodic current there is regeneration of the active species (HF) and the out-diffusion of the inactive species through the pore network. Such current regime contributes to maintain an almost constant HF concentration in the pore tips and leads to a more in-depth homogeneous layer [1 (c)].

1.3.4 Current density effects

In general at low current density the pore are randomly direct and filamentous. At current density close to the electropolishing regime, the pores assume a pipe shape [18]. Porosity increases with the increase of the current density.

For given anodization conditions (current density and HF concentration) the porosity is much higher for the thicker layer (we remember that the thickest layer is more porous due to the extra chemical dissolution of the PS layer in HF).

For p-type substrates, when the forming current density is increased, the porosity increases, and the radii of the maximum of the distribution widen, while the distribution also broaden.

1.3.5 Anodization time effects

The layer thickness linearly increases with the increase of the anodization time, therefore it is useful to know the anodic etching rate for the specific Si substrate. Thönissen et al [1, 28] have planed a model from which they have obtained an expression for the anodic etching rate as a function of the formation parameters, that is in good agreement with the experimentally results.

The anodic etching rate r, defined as the PS volume obtained in the unity of time, is correlated to the porosity P (j), which is function of the current density, j, through the equation:

$$r = [j/ (P (j) n (j))][A_r / [e N_A \mathbf{r}]$$

where n (j) it is the number of exchanged charge carriers per dissolved silicon atom (valence that for PS = 2) also it function of the current density, ρ the Si density (2.33 g/cm^3), A_r the Si relative atomic mass (28.08 g/mol), e is the charge of the electron, N_A the moles number [1, 28].

1.4 POST TREATMENT AND OXIDATION, FUNCTIONALIZATION

Some post-treatments of PS samples are shortly described, that are important for the stabilization and for successive modifications (also in sight of possible applications) of the properties of the materials, i.e.: drying, storage, controlled oxidation, capping and functionalizations.

1.4.1 Drying

After the formation of a PS samples and rinsing in some liquids (water, ethanol, pentane, etc.), during the drying the cracking of the layer can occurs, the drying, in fact, is particularly critic, especially for microporous samples.

The origin of the cracking is due to the large capillary stresses associated with the nanometric size of the pores. Based on the PS mechanical properties and on the X rays diffraction data can be seen that the cracking occurs for PS layers thicker than a critical thickness h_c which mainly depends both on the porosity of the layer and on the surface tension of the drying liquid. The use of highly porous Si films has been limited from the mechanical fragility provoked during the drying. So among the techniques of drying, that have recently been set, trying to decrease or suppress the capillary stresses we can list the supercritical drying [1 (d), 29 ÷ 31], the freeze drying [1 (d), 32, 33], the drying with pentane [1 (d), 34] and the drying by slow evaporation rate [1 (d), 35].

1.4.2 Storage of PS

The morphology of PS is such that as-prepared layers can have extremely large internal surface areas (up to 900 m^2/g) and are largely passivated through relatively weak Si—H bonds. A consequence of this is that as-anodized material is unstable and chemically very reactive to the surrounding ambient. Indeed such layers readily oxidize if stored in air. The extension of the oxidation depends on the ambient humidity, temperature and storing time. The concentration of F and H atoms decrease, and impurity elements (such as C, B, S and N) gradually accumulate inside the resulting native oxide. The oxidation extent and the atmospheric contamination depends on both storage time and temperature, and is influenced by other factors such a spore morphology (macro-, micro-, or meso-porous) and storage conditions (light or dark ambient, type of container). Changes in material properties, such as electrical resistivity, strain, and optical properties, such as refractive index and photoluminescence, can accompany the ageing process.

The ageing of the PS results from the reaction of the material with the surrounding including its container.

In the most of the cases the PS is stored in air at RT. The exposure in air, however, changes gradually the structural and physical properties of the material, due to the oxidation of its inner surface. To minimize the variability and the extension of such storage effects various treatments have been suggested and applied:

- Intentionally oxidize the material in a controlled fashion [1 (e), (h)];
- isolate the inner surface by capping film or by storage in inert gases such as nitrogen or helium, or, finally by storage in UHV (<10^{-9} torr) [1 (e), (f)];
- modify its surface [1 (e), (f)];
- Impregnate the pores by suitable non-aqueous liquids such as ether or alcohols [1 (e), (f), (i)];
- Try to optimize storage time and conditions for the given application requirements [1 (e), (f)].

The storage and characterization in inert gas as N_2 or He clearly show a lower growth of native oxide, but a complete suppression is unlikely for periods of storage of weeks, unless the humidity levels and O_2 are lowered below the level of the ppm. Similar considerations are valid for storages in not aqueous liquid like ether or alcohols. Even with the drying of the electrolyte by distillation under vacuum and the degassing, the residual water to levels of ppm can produce islands of oxide that after a week cover the 60% of the surface [1 (e), 36].

For short-term uses (times or few days) the storage in ultra-pure alcohol or HF gives relatively cleaned returns of free-oxide material [1 (e), 37 ÷ 39]. Nevertheless the used concentration (HF aqueous solution 1 ÷ 10%) can increase the layer porosity of a significant amount (variation of the porosity a day < 2%) [1 (e), 40]. The PS has shown a rapid adsorption of carbon and oxygen also under vacuum of ~10^{-6} Torr. This contamination is minimized in UHV (< 10^{-9} Torr). The storage under vacuum does appreciably slow the ageing process down but it does not eliminate it, the material still pick up C and O, mainly through the variety of residual species (hydrocarbons, water vapor) that can be present within a vacuum system.

The storage into the dark is generally recommended to minimize photochemical effects. These can occur not only at the air but also during the storage in liquids as alcohol and HF. Ultra-dry inert gases or UHV storage are necessary to minimize the oxidation at RT of fresh etched material.

Both not anodized Si wafers and the anodized ones commonly are stored in plastic containers, which, while they offer protection from the contaminants of the air, such containers are able to spread some contaminants for degassing of the same container material. Due to such pollution highly porous materials can become doped with the volatile constituents of the container in which it is stored. A non luminescent material could gradually become impregnated of chromophores for example (this has been verified by accelerated ageing studies [41]) [1 (e)].

1.4.3 Controlled Oxidation

PS controlled oxidation would seem to be a simple process to realize and to control by thermal way. Due to the porosity of the material and the easy penetration of the gaseous O_2 in the pore we would expect a fast oxidation with the formation of a superficial oxide layer. Nevertheless due to the mechanical fragility solicited during the thermal treatments of the material its oxidation requests for some precaution. In fact, when a PS layer is annealed, under vacuum or in a non oxidizing gas, the partial collapse occurs ("coarsening") of the pore structure at $T \geq 400°C$ that increases with the increase of the temperature. After heating at ~900°C inside the material wide voids are formed, surrounded of thick Si walls [42]. A quantitative measure of the "coarsening" can be obtained by the change determination of the specific superficial area induced by the thermal annealing under vacuum. The "coarsening" of the PS structure is attributed to the superficial diffusion of the Si atoms along the pore walls, which has the tendency to minimize the high surface energy. During the annealing there is desorbing of H_2 from the PS surface. The coverage of H seems to be stable up to ~300°C; for higher temperatures the H partial pressure increases reaching a maximum around 400°C and the total H desorbing is complete at ~600°C. The bonds Si—H are nevertheless a stabilizing factor that prevents the diffusion on surface of the Si atoms below the 300°C. For higher temperatures the microstructure can be stabilized against every "coarsening", by total coverage of the inside surface with a thin layer of SiO_2 that is thermally stable. Such layer of stabilizing oxide is obtained by thermal oxidation in two steps, first the formation of the spongy thin layer of SiO_2 at low temperature (~300°C) for ~2 hours and then a densification of such layer at higher temperatures than 1000°C [42].

Besides the thermal oxidation other oxidizing methods have been proposed, e. g. immersion in liquid water with or without surfactants, in organic bases saturated atmospheres. As anticipated in the introduction, a new method based on the exposure of humid air saturated with some organic bases will be presented and discussed in the chapter 3.

1.4.4 Capping

To minimize, or to take under control, the associated effects to the ageing the capping, namely the coverage of the PS surface by a protective film, has been proposed. The total effectiveness of all the means of coverage depends on many interconnected factors: morphology, topology and porosity of the underlying PS, thickness and type of covering layer. It also needs to consider the effect of the same capping process on the PS properties and the compatibility of the coverage

process with the other stages of the processes that can be involved in the PS devices fabrication. Also the applicability is an important factor to be considered when the type of coverage layer is chosen. For example, metallic layers or of opaque semiconductors (of enough thickness to stabilize the PS) could be useless for the transmission of the visible light from the photoluminescents or electroluminescents processes.

The photoluminescence degradation caused by the modification of the passivation layer on the inner pore walls can be, temporarily avoided by covering the PS surface with a thin paraffin film. PS can be covered with conductive polymers e. g. polyaniline and polypyrrole. This capping methodology is slightly different, since the polymers can be deposited in the PS, rather than simply on the surface; polymerization occurring from the pore bottom, upwards. Such a methodology prevents degradation by ambient oxidation. Another type of organic film deposited onto PS is based on carboxylic acid derivatives of the calixarenes, a molecular group consisting of methylene-linked phenolic macrocycles [1 (f)].

1.4.5 Functionalizations

An organic molecule can be immobilized by covalent bond (hydrosilylation) on the Si surface, replacing the Si-H superficial bonds with Si-C bonds and thus stabilizing or providing new properties to the PS materials. Indeed, the organic molecules eventually anchored on the PS surface would protect it from the oxidizing phenomena, being the Si-C bond energetically stronger and more stable (see table 1.1) of that Si-H. The PS functionalization can be also useful in sensors applications. In fact, if the anchored molecule has properties that respond to determined stimuli it can easily be integrated in some electronic device using PS as a support. Moreover, the elevated surface area of the PS allows to increase the response of the sensor device.

Functionalization reactions can be catalyzed from Lewis acids, from organometallic compounds and also from the UV radiations. PS surface has been functionalized with a vast range of molecules, both aromatic and aliphatic, with linear chain or branched, having double or triple bonds as centers of attack, using one of the three procedures up mentioned [3 ÷ 6].

The functionalization of PS surfaces by contact with species in liquid phase and aimed to the realization of a material suitable for sensors applications is the second important subject of this thesis and it will be treated in the following chapters.

1.5 APPLICATIONS

Finally, at the end of this chapter, we mention some applications in various fields in which PS materials are used or can be applied with promising results.

1.5.1 Applications in optoelectronics (PL and EL)

The integrated electronic circuits are based on crystalline Si, which is not able to emit light efficiently (see Fig. 1.2); Si, therefore, cannot be used as light emitter (LED or Laser). The lasers that read CDs and send light impulses in optical fiber are made of different semiconductors as gallium arsenide, which does not epitaxially grow on Si so that the semiconductors laser cannot easily be fabricated on Si chips. This makes the actual cumbersome optoelectronic technology and relatively expensive. If Si is shaped in wires, foils, pieces that measure in section some nanometers, characteristics typical of PS, its optical properties vary respect to crystalline Si. For nanostructured Si with crystallite size below 2 nm the band gap widens and the energy gap follows in the visible (see Fig. 1.8).

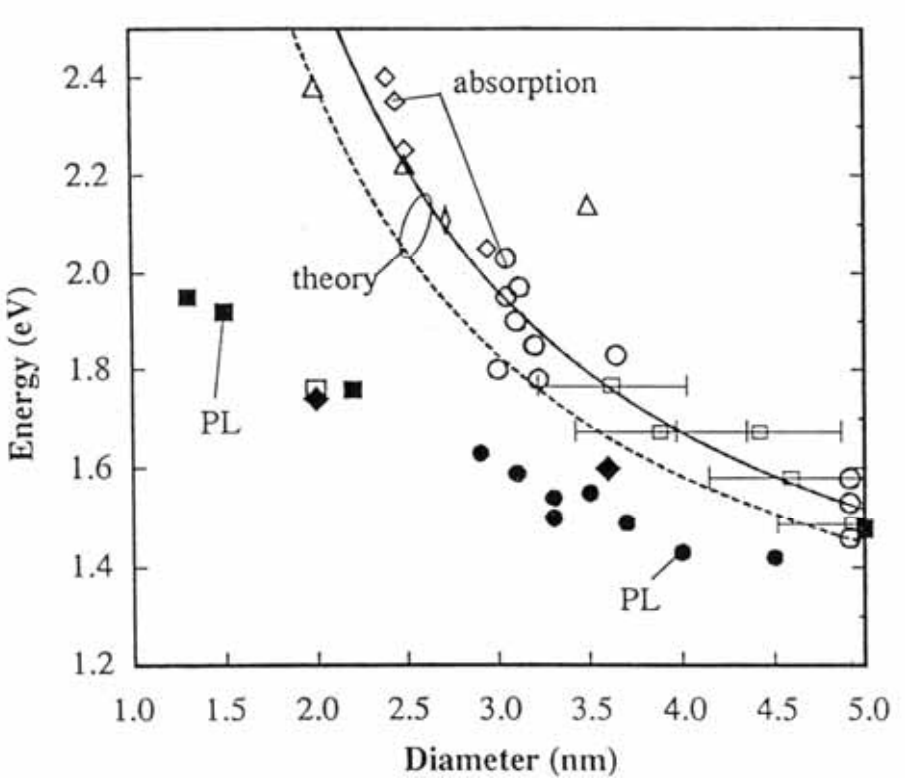

Fig, 1.8. Compilation of optical band gaps of silicon crystallites and porous silicon samples obtained from optical absorption (unfilled symbols) and luminescence (filled symbols). The dashed and continuous lines represent the calculated values with and without the excitonic correction.

For these reasons macroporous PS can emit visible radiation when excited by UV light (PL) or when electrically stimulated (EL).

In PS highly luminescent samples we know that the intensity of the luminescence and the position of the peak are strongly influenced by the presence of organic substances, which modify significantly also the electric conductivity of the samples. From all of this it derives the possibility to get a multi-parametric optical/electronic PS sensor. In fact, the position of the peak depends on the refraction index of the organic compound while the intensity of the luminescence from its dielectric constant at low frequency and the electric properties depend on the moment of dipole of the molecules. All these dependences associated to the variations of the PS samples optoelectronic characteristics allow to discriminate among different organic substances, so the specificity of the PS based optoelectronic sensor [7].

Also photoluminescent PS structures like Fabry-Perot, see also following paragraph, can be used as optoelectronic sensors, in fact the microcavity structure is highly sensitive to the environment and every small modification of the real optical thickness changes the reflectivity spectrum causing a shift of the interference peak in the spectrum. On the base of these considerations a biosensor has been built for DNA on a PS structure with multiple peak microcavity [43] in which luminescence peak shift are observed (selected by Fabry-Perot) for different concentrations of DNA.

Recently, Pavesi et al. [2], have shown that a crucial stage is possible for the creation of a Si based laser and that is the stimulated amplification of light in a system of Si nanoparticles in a SiO_2 matrix. This result is very important, because it can open the way to the construction of optoelectronic devices based entirely on nanostructured or porous crystalline Si opportunely oxidized.

For a review related to the PS optoelectronic properties (PL and EL) we suggest to interested reader to see references [1 (chap. 8 and 9), 44, 45].

1.5.2 Optic and Spectroscopic Applications of PS multilayer systems

The ability to control the porosity (and the morphology) as the PS layers thickness through the value of the current density J and the etching time, it allows to realize also PS multilayer systems through opportune modulations in the time of the values of J. In fact, since the Si dissolution proceeds at the interface between the electrolyte and the Si of the bulk, leaving nearly unchanged the PS layers already products and passivated above the same interface, varying the current

density for opportune times is possible to get further layers of different porosity and thickness, and predefined.

Structures of multilayer PS can be obtained also at constant anodization current but on a substrate consistent of alternate layers with different doping concentration.

The principal interest is the possibility to realize in controlled way PS systems constituted by layers with different microstructures and therefore with different optical properties useful for the construction and the functioning of optical devices.

As it is well known, the complex refraction index determines as the electromagnetic (e.m.) waves are propagated inside a material; being the square of the refraction index $\tilde{n}(\lambda)$ equal to the complex dielectric function $[\varepsilon(\lambda) = \tilde{n}^2(\lambda)]$. The e.m. radiation inside the material has a wavelength that differs of a 1/n factor from the corresponding wavelength in the vacuum. Since the wave frequency does not vary when the e.m. wave crosses an interface between two media the phase velocity differs by the same factor. Additionally, the wave amplitude exponentially decays propagating inside the material if the imaginary part of the refraction index is not null, namely there is an optical absorption.

It is clear that for every application of a material in optics or in optoelectronics it is essential to know its refraction index. For the PS n will depend on the morphology and porosity and it will be determined by the two principal components of the material: the air contained in the pore (increasing the porosity the refraction index decreases) and the Si of the skeleton. This approximation is more valid the smaller the dimensions of the pores, d, in comparison to those of the wavelength, λ, of the radiations (it is surely true for $d < 50$ nm, micro and mesoporous PS, in the IR and in the visible range). The morphology and the porosity are however both related to the anodization current, that implies a relation between the intensity of the current and the dielectric function, as illustrated in the Fig. 1.9, where is introduced the case of a p^+ Si sample (0.01 Ωcm) anodized in ethanoic solution 1:2 = HF:EtOH.

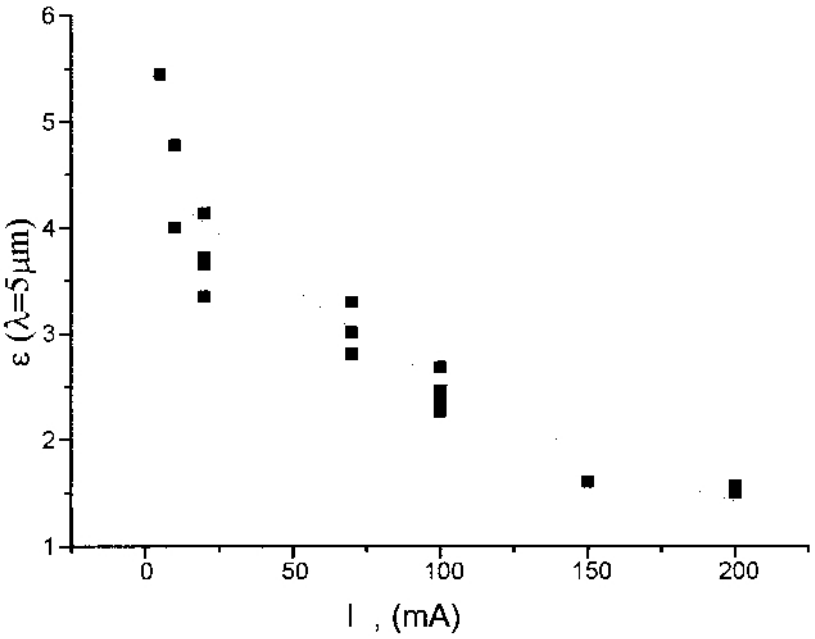

Fig. 1.9. The real part of the dielectric function, ε', to the wavelength of 5 μm, as a function of the current intensity applied during the anodization of a p+ type Si sample, of resistivity 0.01 Ωcm.

It is possible to obtain the refraction index of a material knowing the thickness of a layer that produces interference fringes in transmission or reflection spectra from the spectral distance between two adjacent minima or two maxima of the fringes. It is possible, besides, to obtain such quantity through theoretical models that simulate the spectra obtained in reflectance or in transmittance. The most used in the case of the PS is the Bruggeman model.

It is also possible to produce multilayers systems with various porosity by changing the applied current density during the anodization, because the porosity depends on the current density and the thickness on the anodization time.

It is clear that a PS layers stack of different porosities (and therefore refraction index) and thickness can be used to realize interferential devices and optical filters.

A PS antireflective optical filter, constituted by one or more PS layers, of opportune optical thickness, can show a reflectivity less than 2%, against 30% of the crystalline Si. High reflectivity (near 100%) PS structures, called Bragg mirrors, can be obtained alternating layers with low and high refraction index of appropriate thickness and such that the product of the refraction indexes of the single layers for their thickness, namely the optical thickness, is equal to $\lambda_0/4$, where λ_0 is the wavelength to which the 100% reflectivity zone is centered. We can also obtain complex structures as Fabry-Perot inserting a cavity layer of optical thickness $\lambda_0/2$ between two Bragg mirrors. In this case λ_0 correspond to the reflectivity minimum in the reflectance spectra, Fig. 1.10.

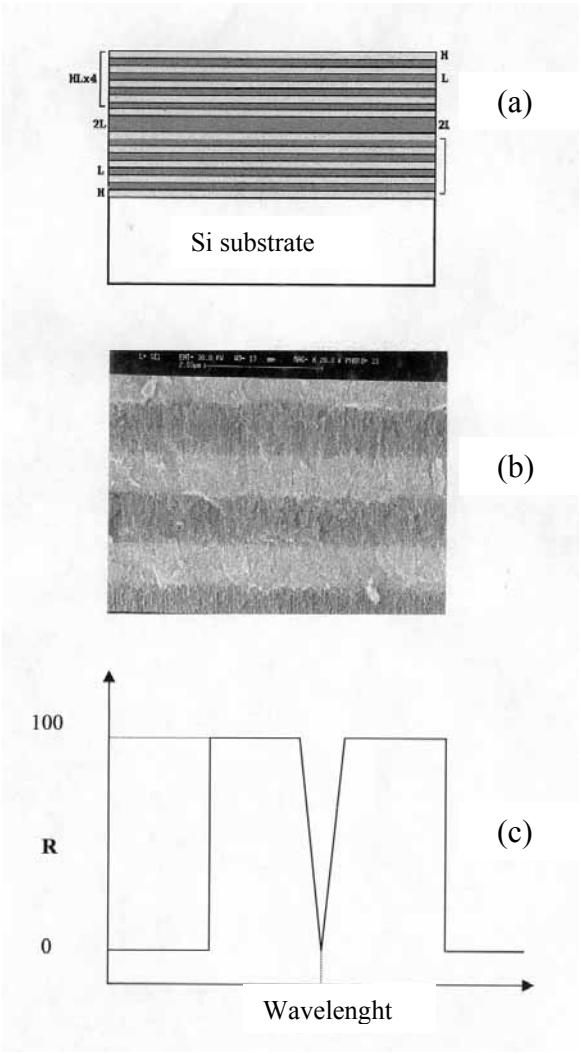

Fig. 1.10. Scheme of a PS Fabry-Perot (a), we alternate layer with high (H) and low (L) porosity; Photo SEM of a PS Fabry-Perot (b); PS Fabry-Perot characteristic Trend of the reflectivity as a function of the wavelength (c).

An example of a Fabry-Perot (FP) reflectance spectrum in the visible region is presented in Fig. 1.11. In this case we have a high reflectivity region and a cavity mode centered at 638 nm.

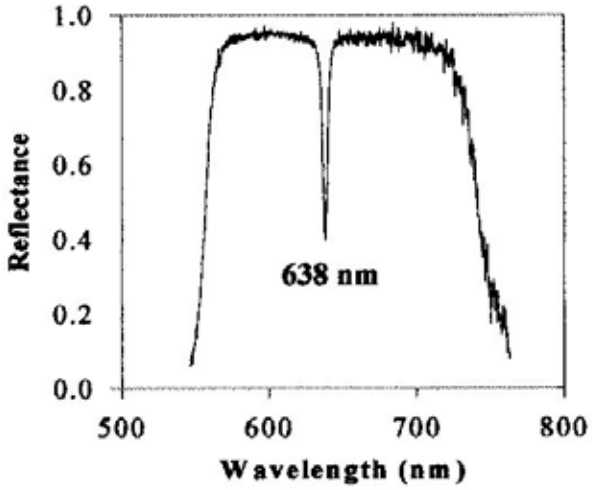

Fig. 1.11. Example of a Fabry-Perot (FP) reflectance spectrum in the visible region.

The presence of the cavity mode makes the PS interesting for optical, spectroscopic and sensing applications.

For example a Fabry-Perot microcavity has been realized in a PS multilayer sample in the region of the IR around the 2000 ÷ 2200 cm^{-1} and it has been observed that its interaction with the vibration modes of the Si-H_x species, which are in this spectral region, determines an enhancement of the IR absorption signal of these species [46]. The same type of amplification of the signal has been observed in the Raman spectra of the PS FP [47]. Obviously, a highly sensitive sensor that amplifying the signals will also give us a best signal/noise ratio and a lower detection limit.

1.5.3 Sensors and functionalization

PS could play an important role in the future of the chemical sensor since it is easy to be synthesized and to modify and it is easily integrable with the Si microelectronic. A PS sensor can be obtained exploiting the variations of its conductivity [48], capacity or photoluminescence. The fundamental limitations to the development in the sector of the PS chemical sensor derive from the chemical instability of the material in air or in aqueous means and from its lack of specificity. Nevertheless it has been shown possible the use of PS as sensor for NO_2 gas [49] with sensibility equal to 1 ppm at RT. More recently, beginning from the well known "quenching" of the PS photoluminescence due to the oxygen, a stable and reversible PS sensor for O_2 gaseous has been obtained [50], particularly important above all for applications in the food industry field.

The possible PS use in the medical sensor field has been considered for more than 10 years. The first of such studies used a membrane of PS as inside electrode reference that could easily be integrated with an ion-sensitive field effect transistor complementary with a metal oxide semiconductor [1 (k)]. Recently a PS device has been used to monitor in situ the proteins adsorbing in the man [51] and thoroughly studies have been made about the reactions of the animal tissues with PS [52] in sight of the numerous possibilities of application of this "new" biocompatible material [53].

1.5.4 Solar cells

PS is also a promising material for the applications in solar cells. In fact, PS thin layers (thick less than 100 nm), with a porosity in the 60 ÷ 70% range, prepared by either chemical or electrochemical etching, are effective as anti-reflective coatings (as previously shown), particularly for poly-crystalline Si solar cells [1 (j)]. It is possible to get reflected intensities lower than 2% in the spectral region from 400 to 1000 nm using PS coverage of the crystalline Si substrate constituents the solar cells [54].

It has been shown, besides, that PS active layers show a photovoltaic effect in the solar cells with structures of new conception, and the possibility to prepare substrates for purer solar cells using thin film of crystalline Si, deposited for epitaxial growth, and transform subsequently, by anodic etching, to PS has been also shown [55 ÷ 62]. The optimization of the PS use in the solar cells at industrial levels requires, to the moment, further studies necessary to improve the efficiency of the cells that use the PS and to exploit at the most its potentialities.

CHAPTER 2

Experimental part

2.1 SAMPLES PREPARATION

Preparation has been developed according to the following scheme:

- Anodization cell assemblage; in the anodization cell, realized in teflon (Fig. 2.1), we used as a cathode a gold wire and a gold coated brass plate as back contact of the Si plate (the anode). Hence with this geometry only the front side of the sample (a circle of 1.4 cm in diameter) is exposed to the anodizing solution.

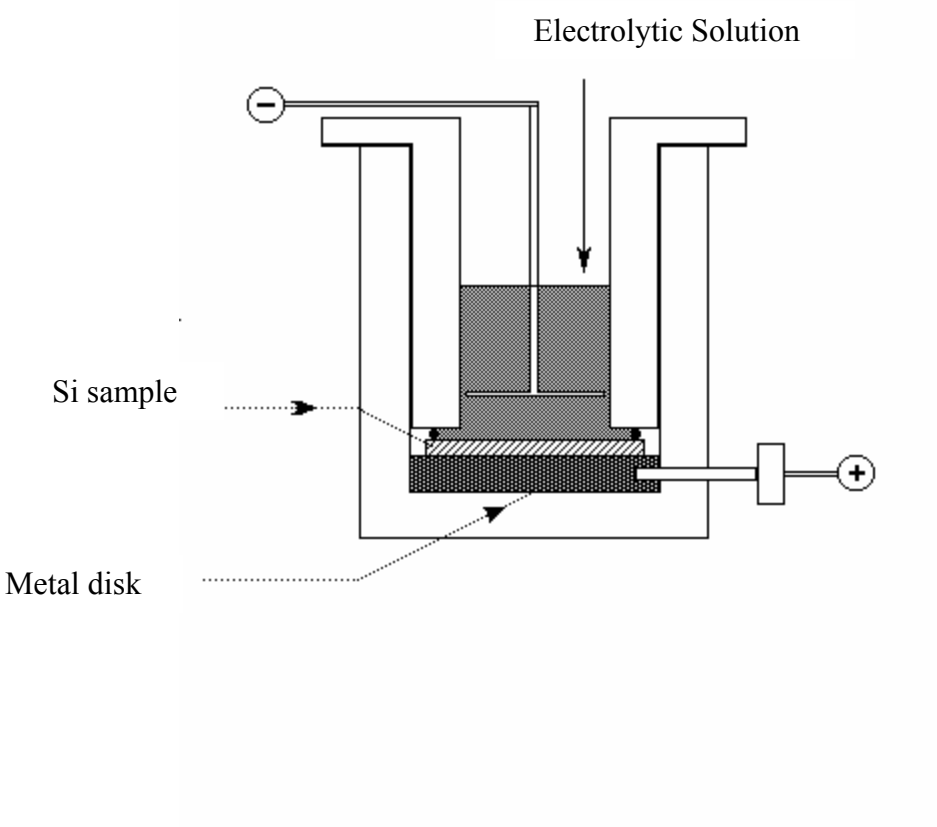

Fig. 2.1. Scheme of our electrochemical cell for the anodic etching PS generation starting by crystalline silicon.

- Cell filling with pure EtOH to verify the absence of any solution leakage, emptying and refilling with the electrolytic solution;

- Electric connection of the cell to the galvanostat (AMEL 594) linked to a PC (through an opportune software) that controls the current and the anodization time to realize the designed PS systems;
- We start the electrolysis after having kept the sample in the cell in contact with the electrolytic solution for 2 min and we wait for the planned time elapsing;
- Finally, once completed the PS formation reaction the samples were washed for 5 min with EtOH and/or H_2O, dried with flowing N_2 and stored in plastic boxes.

Some preparation tests have been performed following the procedures described above, with various solutions and types of Si substrates. At the end of these tests the choice of a p^+-type (0.01 Ωcm) Si substrate and of an electrolytic solution in the proportions 1: 2 = HF (50%): EtOH has been selected as optimal, for the preparation of mesoporous PS (pore of diameter 3 ÷ 50 nm) with low-level of luminescence.

After the preparations of several PS single layers at various current densities and times, some calibration curves i.e. porosity (q), (Fig. 2.2) and formation rate of the PS layer (μm/s)[1], (Fig. 2.3) as a function of the current intensity (I) were obtained.

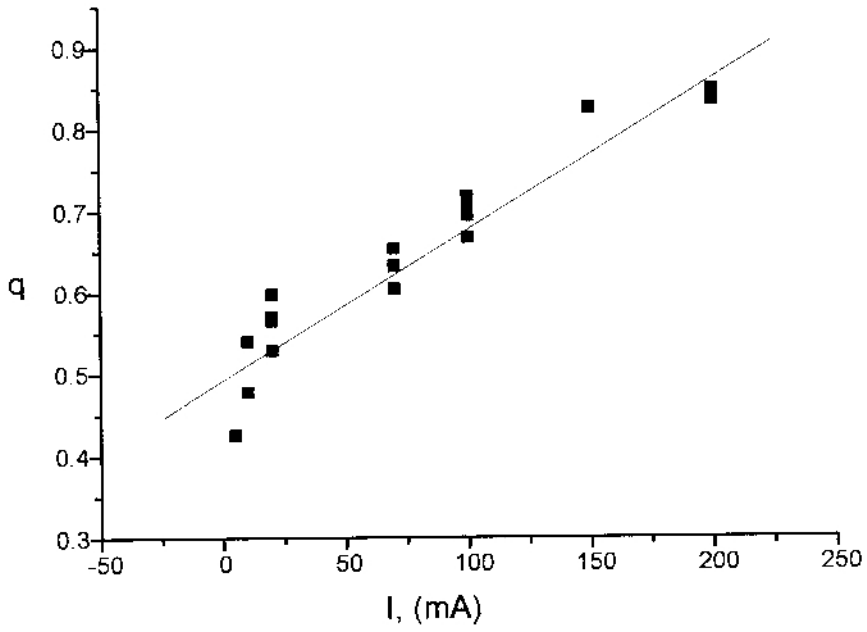

Fig. 2.2. Dependence of the porosity q (varying from 0 to 1) as a function of the current intensity for our PS samples.

We recall that the average current density, J (mA/cm^2), is obtained dividing the current intensity, I (mA), by the surface area (in our case 6.16 cm^2) of the Si samples.

[1] Defined as the thickness of PS product in the unit of time by the partial erosion of crystalline Si.

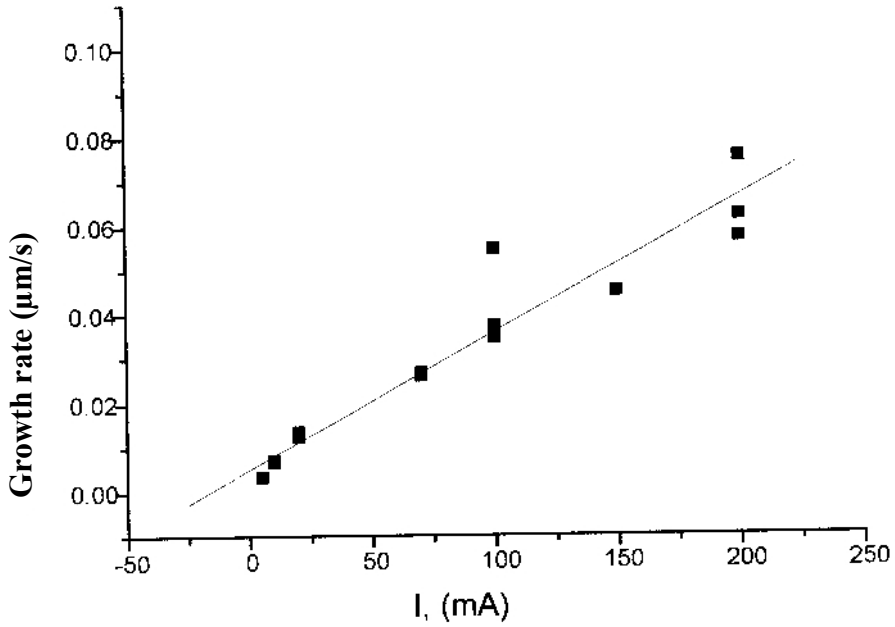

Fig. 2.3. Dependence of the porous layer growth rate from the current intensity applied during the electrochemical reaction of PS formation beginning from p^+-type crystalline Si, doped B, of 0.01 Ωcm resistivity.

The thickness was determined by: cross section SEM, weight loss measurements and IR or visible reflection spectra (see successive chapter).

Once defined the relation among the process parameters (J and t) and the characteristics of the produced PS layer, they have been used for preparing PS samples with well-established properties (both single layers and multilayer systems).

2.2 SAMPLES POST-TREATMENTS

2.2.1 Oxidation

For better comparing the results of the oxidizing processes, every sample has been cut in four parts, each of them was then separately treated with air saturated with vapors of H_2O of different liquid organic substances at RT. The liquids were poured in a glass and that was inserted inside a glass bell, acting as a sort of reaction chamber (Fig. 2.4). After two hours, when the environment was considered saturated, the PS sample was introduced (movement showed by the arrow in the left side of Fig. 2.4), having care to perturb as little as possible the equilibrium formed inside the chamber. The samples have been kept in contact with the saturated vapors, for predefined times. The induced oxidation was then studied by FTIR spectroscopy.

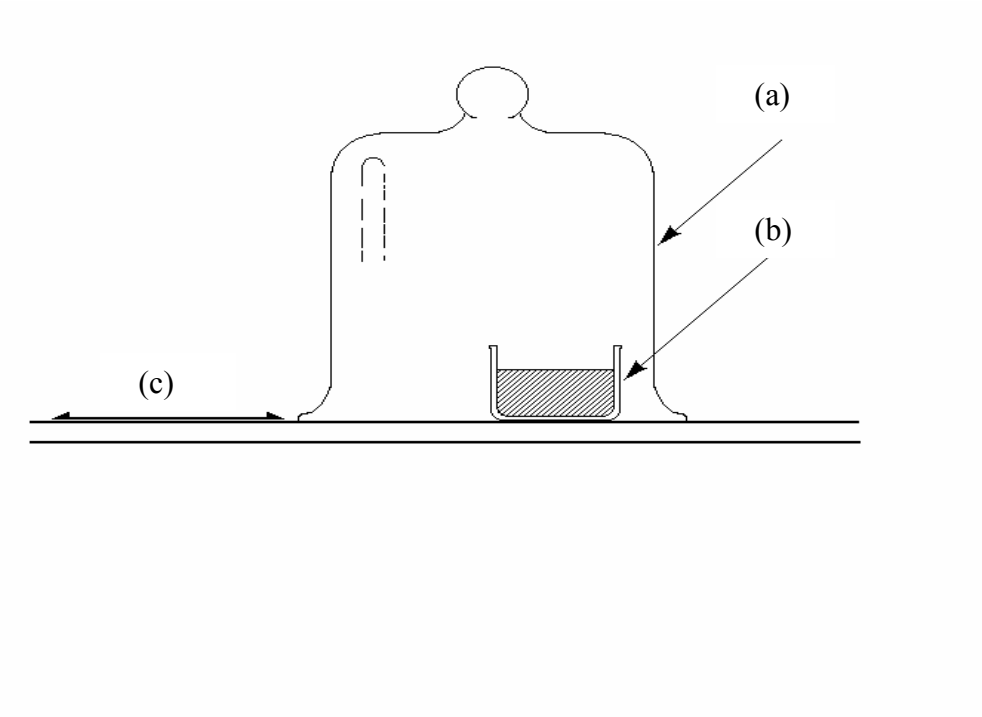

Fig. 2.4. System used for the oxidation studies in various saturated atmospheres. (a) is the glass chamber that contains the saturated environment; (b) is the glass that contains the liquid used for the oxidation; the arrow (c) indicates the movement of the samples in and out of the chamber.

2.2.2 Functionalization

Generally PS samples are first produced by the classical electrochemistry process and then functionalized following various post-treatment procedures. The PS samples are derivatized by the contact with the molecules of pure liquids or present in a solution. The functionalization reaction can develop in various conditions:

- Under white or UV, light Irradiation of variable intensity for times ranging from 30 min to few hours;
- At high temperature, refluxing the PS sample in the liquid;
- In presence of chemical catalyzer e. g. Lewis acids in the liquid for suitable times.

During our activity, we have first tested the above mentioned function procedures, then, we have developed a new in-situ PS formation-functionalization method. This new method consists in putting the molecules to be chemisorbed directly in the solution used for the PS formation reaction. The time duration of the functionalization reaction is that of the PS formation process: from few seconds to several minutes according to the desired thickness of

the porous layer. The percentage of functionalization depends on the concentration of organic substance in the solution.

The method and its peculiarities will be described in details in next chapter.

2.3 SAMPLES CHARACTERIZATION

2.3.1 Gravimetric Analysis

By gravimetric measurements it is possible to determine the porosity and the thickness of a PS layer, although it is a destructive technique.

The porosity is defined as the fraction of void within the PS layer and can be determined easily by weight measurements with an accuracy of about 1%. The virgin wafer is first weighed before anodization (m_1), then just after anodization (m_2) and finally after dissolution of the whole porous layer in a molar NaOH aqueous solution (m_3).

Uniform and rapid stripping in the NaOH solution is obtained when the PS layer is covered with a small amount of ethanol which improves the infiltration of the aqueous NaOH in the pores.

The porosity (q) is given simply by the following equation:

$$q\ (\%) = (m_1 - m_2)/ (m1 - m_3) * 100.$$

From these measured masses, it is also possible to determine the thickness (d) of the layer according to the following formula:

$$d = (m_1 - m_3)/(S * \mathbf{r})$$

where **r** is the density of the bulk Si and Sis the wafer area exposed to HF during anodization.

2.3.2 SEM analysis

The produced PS samples have been analyzed on the surface and on the cross section by scanning electron microscopy, SEM, using an instrument Leica, Cambridge Streoscan 360 having as source of electrons a LaB_6 crystal and Field Emission SEM (FE-SEM, Leo Supra 35). The micrographies have been obtained through collection of secondary electrons using a beam of primary electrons of 20 KeV.

2.3.3 Raman spectroscopy analysis

Raman measurements were performed with a Dilor XY triple spectrometer allowing macro- and micro-Raman measurements, with a liquid nitrogen cooled charge couplet device (CCD) detector and an adapted Olympus microscope. The spectra were excited with an Ar^+ laser (514.5 nm or 488 nm). The laser light was focused onto a spot of 0.2 mm in diameter for macro-Raman, and 1 µm, 2 µm, 10 µm in diameter (depending on the used objective: 100x, 50x, 10x) for micro-Raman. The scattered light was not analyzed in polarization; spectral resolution was 0.5 cm^{-1}; lines of a Ne lamp were used for frequency scale calibration. Care has been taken to avoid the heating of the sample by using a low power density (less than 500 W/cm^2). For theoretical information see the annex B at the end of this thesis.

2.3.4 Fourier Transform Infrared Spectroscopy (FTIR) analysis

The IR spectroscopy is a technique based on absorption or emission of IR radiation caused from the atoms vibrations of a molecule. An IR transmission spectrum is obtained crossing a sample by a radiation and determining what fraction of the incident radiation is absorbed at particular frequency. The frequency to which every peak appears, in an absorption spectrum, corresponds to the vibration or rotation frequency of the molecules of the sample.

The emission or absorption frequency, ν, of the radiation for the transition between the energetic states E_0, fundamental state, and E_1, excited state, is given by the following relation:

$$\nu = (E_1 - E_0)/h$$

where h is the Planck constant.

The interactions between the IR radiation and the matter can be described in terms of changes of the molecule dipole moment associated to the vibrations or rotations.

The IR measurements were performed in reflection mode by a FTIR Biorad Spectrometer FTS-40A with dynamic alignment. The resolution was $2 \div 4$ cm^{-1} in the spectra range $400 \div 4000$ cm^{-1} a gold mirror was used as a reference. The IR spectra of the PS sample has been elaborated by computer to correct the instrumental effects and to obtain spectral information namely the frequency of the various present bands, their FWHM, their intensity, etc, using the "GRAMS/32" (Galactic) software.

Besides, the IR spectra treatment allowed the correction of the IR reflection spectra for the contribution due to the support (see annex C) and for the base line.

The experimental spectra have been finally compared with those calculated by the software Scout, [63, 64] using the Bruggeman model (see annex D). From this comparison the porosity, the thickness and the dielectric function of the measured samples have been obtained.

CHAPTER 3

Research Activity

In this section the original results obtained during the course of the research activity are presented and discussed.

PART I: Effect of the interaction of PS with the environment

First part is devoted to the illustration of some studies (mainly by FTIR and SFG spectroscopy) regarding the effect of the interaction of PS single layers and superstructures with the environment. The controlled oxidation of PS in humid air accelerated by the presence of various organic molecules (Pyridine, Picoline, Lutidine, Ethylamine, Diethylamine, Triethylamine) will be presented. Finally also the case of a dosimeter of urotropin vapors will be discussed. In the second part the functionalization by different procedures of PS layers in view of application of the material as a sensor and biosensor will be illustrated.

3.1 STUDY OF THE INDUCED OXIDATION IN AIR OF PS IN PRESENCE OF PYRIDINE VAPOR

We have studied the interaction of chemical species, from both vapor and liquid phases, with PS because this is of great importance to elucidate several aspects of the surface properties of this material, such as surface adsorption, chemical reactivity, oxidation process, surface functionalization, that are also relevant for all the possible technological applications of PS especially in the sensing field [1, 15, 25].

Recently we have studied the fast oxidation induced in PS layers by the exposure to air with saturated vapors of organic bases. Further work has been carried on to complete an FTIR study of porous silicon layers exposed to humid air with and without pyridine vapors at room temperature**.**

Oxidation processes can strongly influence the properties of porous silicon (PS) material. The oxidation of porous silicon (PS) has been matter of extensive studies in the past years. Intentional oxidation is used to stabilize the PS properties through the formation of passivating surface oxide layers. Moreover, there is a large interest in Si/SiO_2 systems in view of new applications in the field of opto-electronics [2]. In this work, with the aim of a better understanding of this oxidation process, we discuss the results of an FTIR study of PS samples

exposed to humid air with and without pyridine vapor at room temperature in the time range from 0.1 to 10,000 min (300 h). The oxidation has been followed by recording the time evolution of the IR absorption intensities of the main species involved in the process, namely: Si-H_x, O_ySi-H_x, Si-OH and Si-O-Si. We found that in the presence of pyridine the oxidation is much faster.

The PS samples were prepared by partial anodic dissolution of p^+ Si (100) wafers, with a resistivity of 0.01 **W**cm, in an electrochemical cell containing a HF (50%) ethanoic solution (1:2 by volume). The cathode was an Au wire and the current density was 100 mA/cm^2. The produced samples were mesoporous PS layers with 68% porosity and thickness around 0.7 **m**m. They were introduced in a chamber containing air saturated with water vapor or air (relative humidity 25-30%) saturated with pyridine vapors. The temperature was kept at around 24 °C.

After different exposure times ranging from few seconds to 12 days, the FTIR reflection spectra of the PS samples were measured ex-situ. Care was taken to minimize the perturbation of the open atmosphere in getting the samples in and out of the chamber.

The experimental conditions were: angle of incidence 20°, spectral range 500 –4000 cm^{-1} and resolution 4 cm^{-1}.

First we consider the case of PS exposed to air saturated with water vapor at RT. With increasing the exposure time (t_e), the infrared spectrum evolves as exemplified in Fig. 3.1.

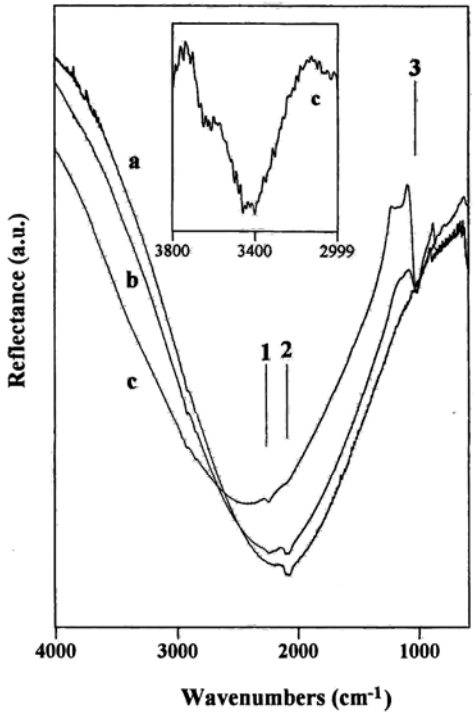

Fig. 3.1. FTIR reflection spectra of a PS sample exposed at RT to air saturated with water vapor for 0 min (a), 3880 min (b) and 12372 min (c). The vertical lines indicate the positions of the main bands: O_ySi-H_x (1), Si-H_x (2) and Si-O-Si (3). The O-H region of spectrum (c), after background correction, is presented in the inset.

For the sample as prepared ($t_e = 0$) the main absorption bands are due to the Si-H vibrations of SiH_x (Si-H stretching in SiH at 2080 cm^{-1} and in SiH_2 at 2106 cm^{-1}), as expected for the hydrogen terminated PS surface. With increasing t_e the reflection minimum due to the interference moves to higher frequency owing to the reduction of the effective refractive index of the PS layer due to the substitution of Si with silicon oxide. Besides, new bands appear and the relative intensities of all the bands change. Strong silicon oxide absorption bands appear in the region 950 – 1250 cm^{-1} (that includes the bulk as well the surface Si-O-Si stretching vibrations [63]) and their intensity increases with the exposure time. In the region 2100 – 2300 cm^{-1}, bands attributable to the Si-H stretching for silicon back-bonded to oxygen atoms, O_ySiH_x (Si-H stretching in $OSiH_3$ at 2136 cm^{-1}, in O_2SiH_2 at 2200 cm^{-1} and in O_3SiH at 2249 cm^{-1} [65]), grow up. In the 3000 – 3700 cm^{-1} region weak and broad bands due to the O-H vibrations also appear (inset in Fig. 3.1). While the intensities of all the above mentioned new bands tend to increase with t_e, the Si-H stretching bands due to the original H terminated PS surface have opposite trend.

A complete set of time dependencies for the mentioned species is summarized in Fig. 3.2 where the total integrated absorption intensities, obtained by spectral treatments and by adding the contributions of all the bands present in the specific spectral regions mentioned above, are reported as a function of t_e.

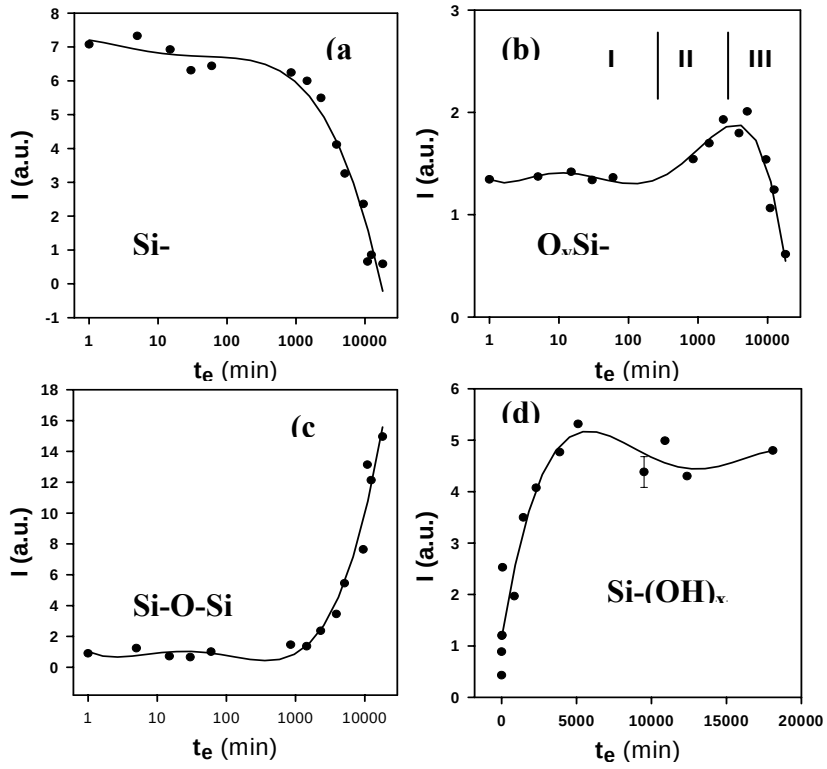

Fig. 3.2. Integrated absorption intensity of Si-H_x (a), O_ySi-H_x (b), Si-O-Si (c) and O-H (d) infrared bands as a function of the time of exposure to air saturated with water vapor at RT. The solid lines are guides to the eye.

All the process can be divided in three stages (see Fig 3.2b). Stage I, the first 1000 min, corresponds to the formation of Si-OH species (the O-H is the only signal increasing during this time) on the surface through the dissociative interaction of water molecules [18] that is slowed down by the H terminations of the PS surface. The Si-OH is a special effective site [66, 67] for the attack of water to silicon back-bonds to form Si-O-Si that gives rise to an increase in intensity of the absorption bands of the silicon oxide and O_ySiH_x species and to a decrease of the SiH_x signal (stage II). After about 5000 min (stage III), the amount of H atoms bonded on the PS surface is significantly reduced because of the formation of Si-OH and surface Si-O-Si bonds. The oxidation process continues: the silicon oxide signal is still growing up while that of the O_ySiH_x species decreases. Fig. 3.3 demonstrates that there is a strong correlation between the reduction of the SiH_x species and the formation of the silicon oxide, thus confirming that the H terminated silicon sites are the places where the oxidation in PS material initiates and develops.

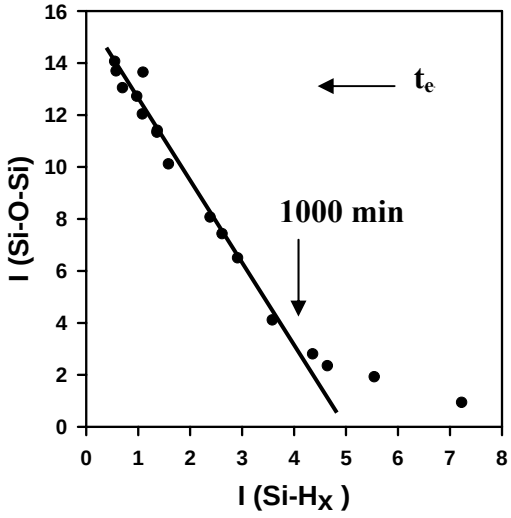

Fig. 3.3. Integrated absorption intensity of Si-O-Si bands versus integrated absorption intensity of Si-H_x bands. The horizontal arrow indicates the direction of increasing exposure time.

The IR spectra of PS sample exposed to humid air saturated with pyridine vapor at RT are very similar to those presented in Fig. 3.1. For sake of brevity, only the main results are summarized in Fig. 3.4.

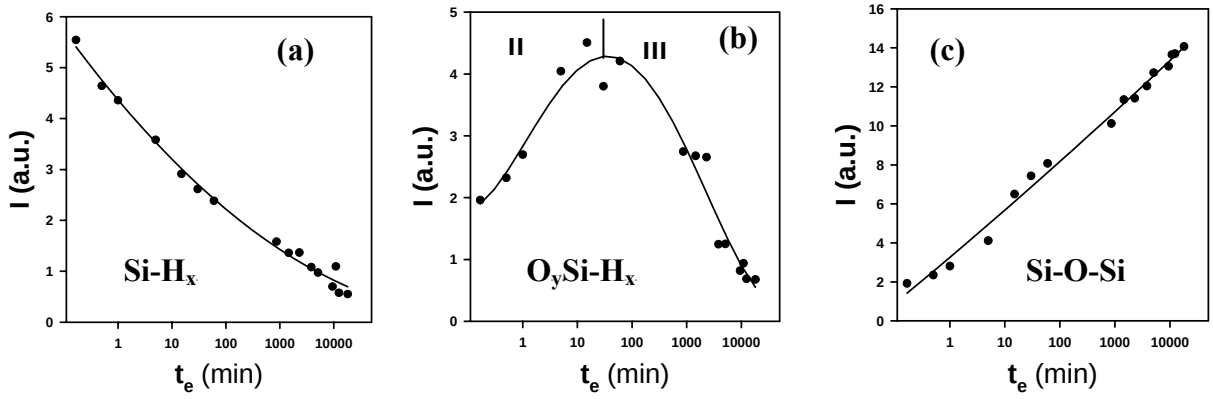

Fig. 3.4. Integrated absorption intensity of Si-H_x (a), O_ySi-H_x (b), and Si-O-Si (c) infrared bands as a function of the time of exposure to humid air saturated with pyridine vapor at RT. The solid lines are guides to the eye.

All the dependencies on t_e, also those here not shown, parallel those above discussed, but in a compressed time scale. After only 10 s of exposure time the process is already in the stage II, Fig. 3.4 (b), and after 20 min there is the transition to the stage III. It can be noted that the SiH_x absorption intensity always decreases with t_e while that of the silicon oxide increases.

To make a further comparison between the two oxidation processes, we have evaluated the oxidation degree, i.e. the percentage of silicon converted into silicon oxide, from the IR spectra through a method described elsewhere [68], for two parts of the same sample exposed to the two different oxidation treatments. These quantities are plotted as a function of the exposure time in Fig. 3.5.

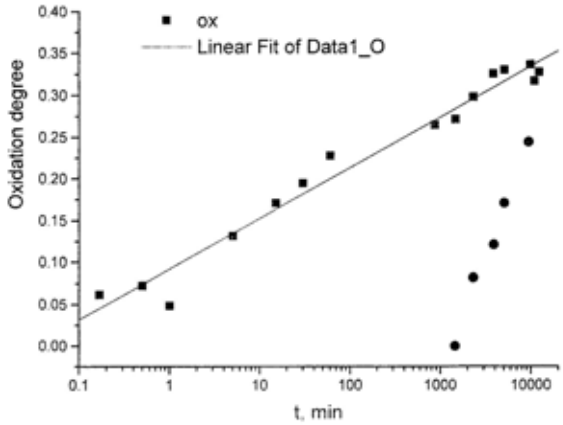

Fig. 3.5. Oxidation degree for two parts of the same PS sample treated in air saturated with water vapor (●) and in humid air saturated with pyridine vapor (■) at RT as a function of the exposure time.

It is quite clear how much more effective is the oxidation in the presence of pyridine considering that, for example, in this case the oxidation degree reaches the value 0.15 (15% conversion) after 5 min with pyridine and after 5000 min in the case of oxidation in humid air alone. We interpret this accelerated oxidation by pyridine vapor in humid air as due to the attractive interaction of the pyridine molecules, through their nitrogen lone pair, with the oxygen and water molecules, the real oxidant agents, that causes the weakening of the Si-H bonds and hence the local Si oxidation. This mechanism, via promotion of the interaction of Si atoms with the oxidant agents (mainly the water molecules), develops and sustains the observed fast oxidation of the PS material. Finally, we note that, in spite of the different rates of the processes, the final oxidation degree is the same in both cases being likely related to the original amount of Si-H species in the PS layer. These results have been published in *Surface Science* [8].

3.2 STUDY OF THE INDUCED OXIDATION IN AIR OF PS IN PRESENCE OF DIFFERENT ORGANIC BASE VAPORS

The oxidative phenomena have been investigated at RT in air saturated also with different organic bases, all having a nitrogen atom with its available lone pair. We have chosen two organic molecules (Lutidine and Picoline) similar to pyridine (that we have already discussed in the previous paragraph), and a family of aliphatic organic bases to compare a primary, secondary and tertiary amine (ethyl-, diethyl-, triethyl-amine). The purpose was to understand which peculiar parameters of the bases influence mainly the PS oxidation process.

The following base parameters, reported in the table 3.1, have been considered:

1. The boiling point, b.p. [69], expressed in Celsius degrees;
2. The basicity constant in liquid phase, K_b [69];
3. The vapor tension (at RT), P, expressed in Torr and calculated through the relation

$$\text{Log } P = A\text{-}B/ (T + C)$$

where A, B, C are constants at a determined temperature for each substance [69], T is the temperature expressed in °C;

4. The concentration, Conc., of the molecules in vapor phase, express in molarity, obtained once known the vapor tension by the following equation:

$$\text{Conc.} = P/RT$$

where R is the constant of the gases, T is the temperature in absolute degrees;

5. Finally the "gas basicity", GB [70] that for a species (molecule, radical, or atom), is defined in terms of the hypothetical gas-phase reaction:

$$M\,(g) + H^+\,(g) \rightarrow MH^+\,(g) \qquad (1)$$

The GB of M at temperature T, GB (M,T), is the negative of the Gibbs free energy change for this reaction:

$$GB\,(M,T) \equiv -\Delta G^0_{Rn1}\,(T).$$

The subscript Rn1 means that the thermochemical quantity is associated with the hypothetical gas-phase reaction indicated above.

The GB represents the basic strength in vapor phase and it is always express in kilocalories per mole.

Table 3.1. *Parameters related to the utilized bases in the oxidative phenomena study*.

NAME	**b.p.** (°C)	K_b	**P**[2] (Torr)	**Conc.** (M)	**GB** (Kcal/mol)
Pyridine	115.5	$15.4*10^{-10}$	16.58	$9.04*10^{-4}$	214.7
2,6-Lutidine	145.7	$1.40*10^{-12}$	4.33	$2.36*10^{-4}$	222.5
Picoline	128.8	$3.02*10^{-8}$	8.84	$4.82*10^{-4}$	219.2
Ethylamine	16.0	$8.51*10^{-4}$	185.60	$4.9425*10^{-2}$	210.0
Diethylamine	56.3	$4.27*10^{-4}$	906.58	$1.0118*10^{-2}$	219.7
Triethylamine	89.3	$5.25*10^{-4}$	46.00	$2.508*10^{-3}$	227.0

The IR spectra of the sample exposed to the various organic bases, for contact times from 1 to 60 min, present the same absorption bands of the samples treated with air saturated with H_2O and Pyridine vapors (see table 3.1). Analyzing the graphs that report the dependence of the integrated intensities of the different bands present in the spectra, we can note for all the bases: i) the intensity of the Si-H stretching of the SiH_x species decrease with the contact time [Fig. 3.6 (a) and (b)] (like that already observed for the sample exposed to the saturated Pyr vapor, although each sample treated with a different base present a different slope); ii) the intensity of the Si-O-Si bonds increase with the contact time [Fig. 3.3 (a) and (b)]. The intensity of the Si-H stretching of the O_ySiH_X species with the contact time shows different trends for each base. Going from Lutidine, to Picoline, to Pyr, the intensity, of the O_ySiH_X species, in the first 60 min of exposure, increases almost linearly with decreasing slope. In Fig. 3.6 the case of Lutidine (a) and Picoline (b) are illustrated, the Pyridine case was shown in Fig. 3.4 (b).

[2] Vapor Pressure

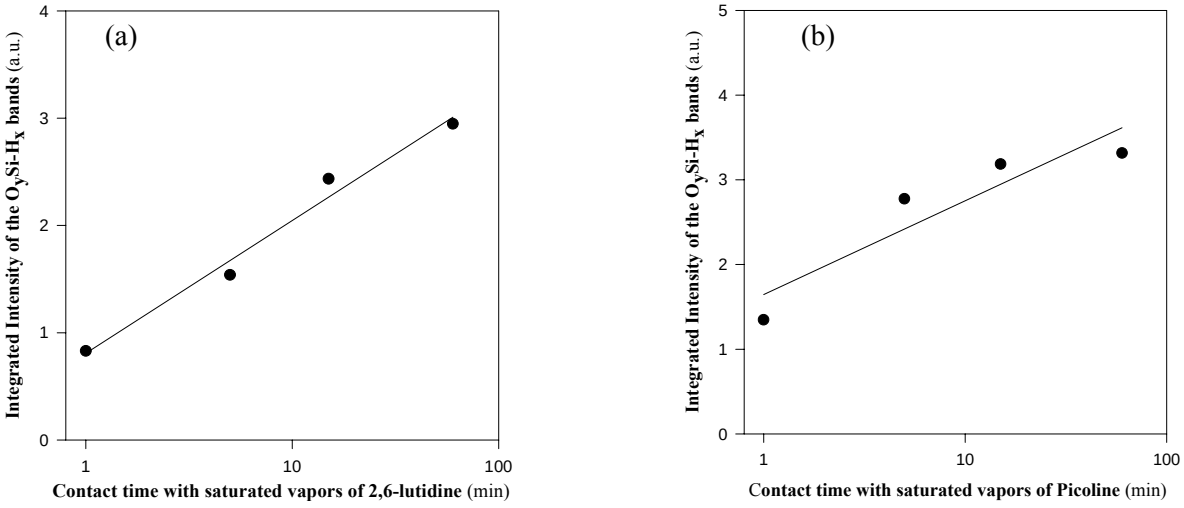

Fig. 3.6. Integrated intensity of the IR absorption bands related to the O_ySiH_x species as a function of the contact time, in logarithmic scale, with the saturated vapors of Lutidine (a) and Picoline (b).

The intensities of the O_ySi-H_x bonds decreases on the contact time for all the three amines (in this case from 0 to 30 min), with decreasing slope going from Triethylamine (Fig. 3.7), to Diethylamine (Fig. 3.8), to Ethylamine (Fig. 3.9).

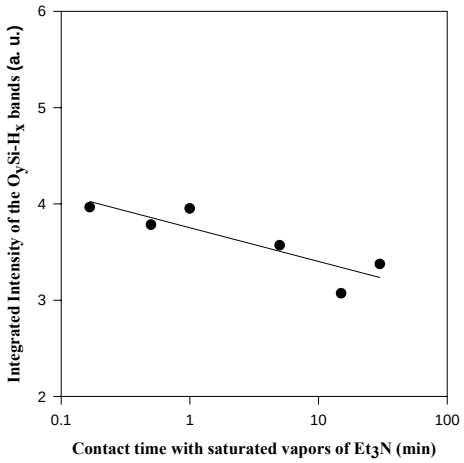

Fig. 3.7. Dependence of the integrated intensity of the IR absorption bands related to the O_ySiH_x species as a function of the contact time with the saturated vapors of Triethylamine, in logarithmic scale.

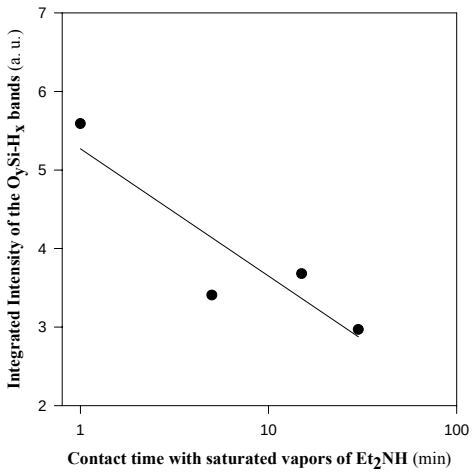

Fig. 3.8. Dependence of the integrated intensity of the IR absorption bands related to the O_ySiH_x species as a function of the contact time with the saturated vapors of Diethylamine, in logarithmic scale.

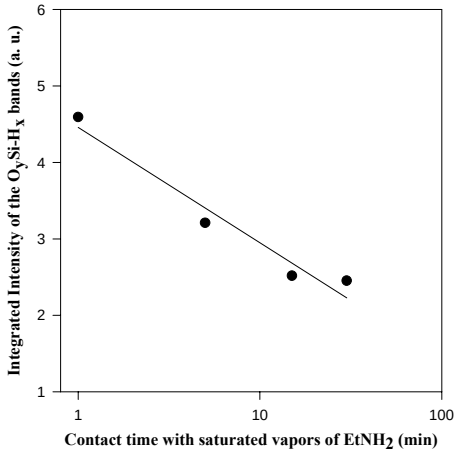

Fig. 3.9. Dependence of the integrated intensity of the IR absorption bands related to the O_ySiH_x species as a function of the contact time with the saturated vapors of Ethylamine, in logarithmic scale.

All these dependences are qualitatively summarized in Table 3.2 according to the order: Lutidine, Picoline, Pyridine, Triethylamine, Diethylamine, Ethylamine.

Table 3.2. *Dependence of the integrated intensity of the bands related to the stretching of the O_ySiH_x bonds as a function of the contact time (1 ÷ 15 min) with the saturated vapors of the different bases*

Lutidine	Picoline	Pyridine	Triethylamine	Diethylamine	Ethylamine
increasing	increasing	increasing / decreasing	decreasing	decreasing	decreasing

Analyzing the data related to the PS oxidation in air saturated with different organic bases we have considered a possible correlation between the strength of the different bases and their capacity to catalyze the oxidation, examining the dependence of the integrated intensities of the IR absorption bands associated to the stretching of the Si-O-Si bonds as a function of the K_b and the basicity constant in gaseous phase (see table 3.1).

The IR absorption bands integrated intensity associated to the stretching of the Si-O-Si bonds are been preliminarily normalized respect to the initial contents of SiH_x species of the as prepared samples because we are not comparing the same sample treated with different bases, but we have three different samples, although very similar among them. This normalization is legitimated by the strict linear relations that exist between the integrated intensity of the bands associated to the stretching of the SiH_x and Si-O-Si species for each sample in contact with the different oxidizing atmospheres (see for example Fig. 3.3). Indeed the Si-O-Si species are directly correlated to the oxidation degree of the samples (see par. 3.1) and hence the relation between the oxidation degree of the sample and their initial contents of SiH_x species is justified.

A possible correlation between the basicity constant and the oxidation effect suggests some interaction in gaseous phase between the base and the H_2O present in the air, which can influence the oxidation process. Instead, a correlation with the K_b suggests that the interaction between the catalyzers and the oxidizings occurs after the absorption phase. However, correlations are not found in each of the two cases.

From the comparison of the results obtained for each base, on the contrary, a clear correlation has been demonstrated between the concentration in gaseous phase of the different bases and the normalized integrated intensity of the IR absorption bands associated to the stretching of the Si-O-Si bonds, measured after the same contact time with the different oxidizing atmospheres. This correlation for a contact time of 15 min is illustrated in Fig. 3.10 (a) and (b).

The absence of correlations between the K_b or the G. B. and the oxidation degree of the different samples (also after the normalization for the concentrations of the organic bases in gaseous phase) suggests that the catalyzing action for the oxidation does not occur by a dissociative action on the H_2O or O_2, neither in vapor phase nor after the adsorption. As in the case of pyridine, we attribute to the presence of the nitrogen lone pair of the organic base the main role in the promotion of the PS oxidation in presence of the water vapor of the air. Whereas a direct action on the hydrogen atom (slightly negatively charged) terminating the Si surface (slightly positively charged) appears unlikely, an important intermediate step could be the formation of an organic base-water adduct characterized by a more negative charge oxygen

atom, because of the charge redistribution. This adduct might interact more strongly than the water molecule with the silicon hydrides on the PS surface thus starting reactions that finally end with the formation of silicon oxide species. This means a larger contribute of the water and oxygen etch reaction to the surface Si-H bond and to the Si-Si back-bonds.

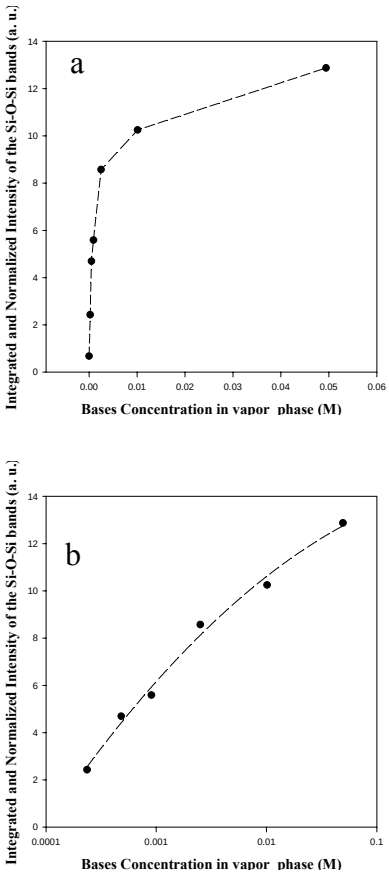

Fig. 3.10. Dependence of the normalized integrated intensity of the bands associated to the O-Si-O species as a function of the concentration of the different bases used for the study of the PS oxidation, in linear scale, (a), and in logarithmic scale, (b).

The role here proposed for the bases in the oxidizing phenomena explains also the correlation found between the oxidation and the concentration in vapor phase of the different bases (see Fig. 3.10). More molecules of the base are available and more are the real oxidizing agents presents on the PS surface able to trigger the oxidation reaction.

Finally, we can note that as a function of the effectiveness of the oxidation process catalyzed by the bases under consideration, we can see, in the first 60 min of exposure, various stages of the oxidizing process. Following the increasing order of the concentration in gaseous phase from the Lutidine to the Ethylamine we can observe: for the sample treated with the saturated vapor of Lutidine a smaller amount of O_ySiH_x formed species that is reflected in an increasing trend with the contact time with the saturated vapor (Fig. 3.6 (a)); a larger amount, but always

in the growth stage, for the sample treated with the saturated vapor of Picoline (Fig. 3.6 (b)); the last growth stage for the sample in saturated vapor of Pyr and the beginning of the decreasing stage (Fig. 3.4). In the case of the ethylamine we are in a more advanced stage of the oxidizing process, so we can see: a first decreasing stage for the sample treated with the saturated vapor of Triethylamine (Fig. 3.7); a second decreasing stage less steep of the first for the sample in saturated vapors of Diethylamine (Fig. 3.8) and the last decreasing stage for the sample treated with the saturated vapors of Ethylamine (Fig. 3.9). These finding have a practical application indeed they demonstrate that it is possible to realize a fast and controlled oxidation of PS samples by exposing the material to air with well defined concentration of selected organic bases.

3.3 STUDY OF THE INTERACTION BETWEEN PS AND UROTROPIN VAPOR: POSSIBLE DOSIMETER

We have studied by FTIR reflection spectroscopy the adsorption in PS films and PS Fabry-Perot structures of hexamethylenetetramine, $N_4C_6H_{12}$ (urotropin), a molecule of remarkable interest in several application areas (e. g. rubber, explosives, fuel, pharmaceutical industries, etc) and that also can manifest some toxicity. The aim was to investigate the effects of the interaction of this molecule with the PS materials also in view of a possible application of PS systems to the detection of the urotropin vapor. The adsorption has been studied recording the time evolution (from 4 to 266 hours, about 11 days) of the IR absorption intensities of all the strongest urotropin bands in the case of PS single layer and of the C-H stretching bands (2870-2960 cm^{-1}) in the case of PS Fabry-Perot systems.

We used a FP system because it allows us to amplify signals of adsorbed organic molecules as was emphasized in previous works of our group. The samples have been prepared by our standard electrochemical procedure on p^+-type Si (100) wafers with resistivity 0.01 Ω cm. The IR reflection spectra, measured before and after the urotropin treatments, were recorded in the range 400 ÷ 5000 cm^{-1} with a resolution of 4 cm^{-1}. For the experiments a set of mesoporous PS films of different porosity (64 ÷ 79%) and thickness (0.6 ÷ 0.7 μm) and a FPMC centered around 2900 cm^{-1} were prepared. The angle of incidence was fixed at 20° in the case of PS films and it varied from 10° to 50° in the case of FPMC.

The PS exposure to urotropin vapor had done by putting the urotropin powder in a closed box with air (relative humidity 25 ÷ 35%) at RT. Once prepared, the PS sample was measured by IR

spectroscopy and then immediately inserted in the adsorption chamber. After a predefined exposure time it was extracted and measured again by IR spectroscopy. The exposure time to this urotropin saturated atmosphere ($1.4*10^{-7}$ M) varied from minutes to several days.

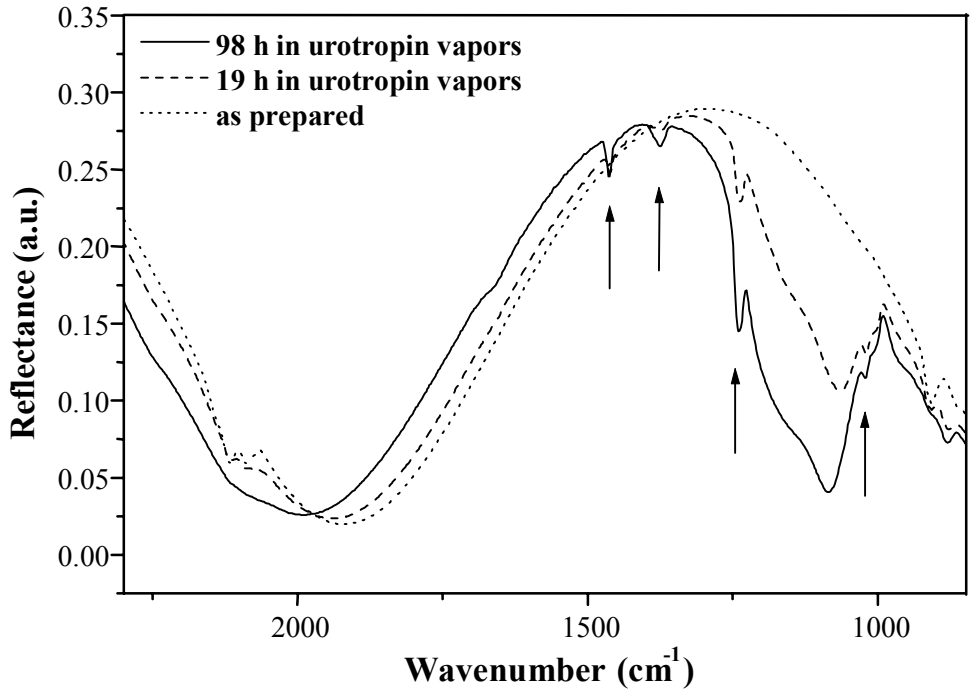

Fig. 3.6. FTIR reflection spectra of a PS film exposed at RT to air with saturated urotropin vapor for different exposure times. The arrows indicate the positions of the main urotropin bands observed in the plotted frequency region.

In Fig. 3.6 the IR reflection spectra of a sample of PS single layer, as prepared, after 19h and after 98h in urotropin vapors, are shown. We can see typical interference fringes of PS thin films and we can also follow the time evolution of the IR absorption intensities of the strongest urotropin bands centered at 1020, 1240, 1370 and 1460 cm^{-1} (the arrows indicate the positions).

- The intensities of all these bands increase with the exposure time. As an example we can see, in the Fig. 3.7, the dependence on the exposure time of the integrated intensity of the absorption band at 1240 cm^{-1}.

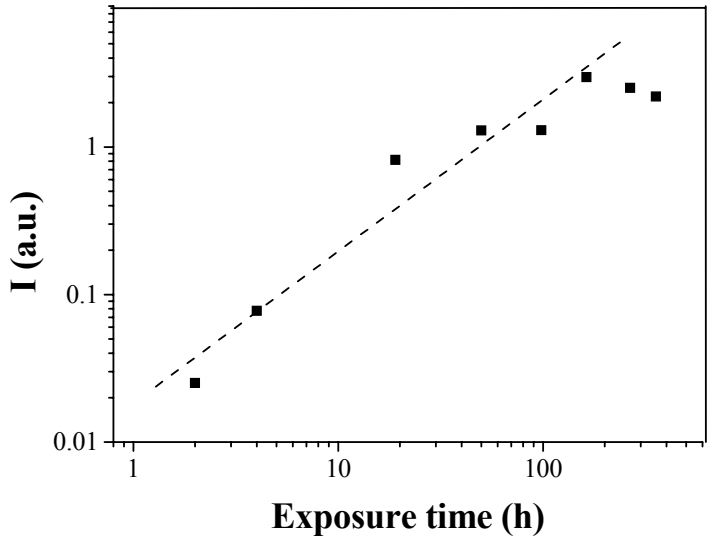

Fig. 3.7. Integrated absorption intensity of the urotropin band at 1240 cm^{-1} as a function of the time of exposure to air saturated with urotropin vapor at RT. The dashed line is a guide to the eye.

- The interaction with the urotropin provokes modification in the PS spectra as well as the appearance of bands attributed to silicon oxide around 1100 cm^{-1}.
- Fig. 3.8 presents the case of a PS FPMC designed to work in the IR region around 2900 cm^{-1}, exposed for 14h to the air saturated with urotropin vapor. The IR spectrum measured at an angle of incidence of 10° shows the cavity mode (the sharp dip in reflectivity) centered at 2770 cm^{-1} and the absorption bands due to the C-H stretching vibrations of the urotropin at higher frequencies (2870, 2930 and 2960 cm^{-1}). By increasing the angle of incidence the cavity mode moves to higher frequency and hence it crosses the C-H bands.

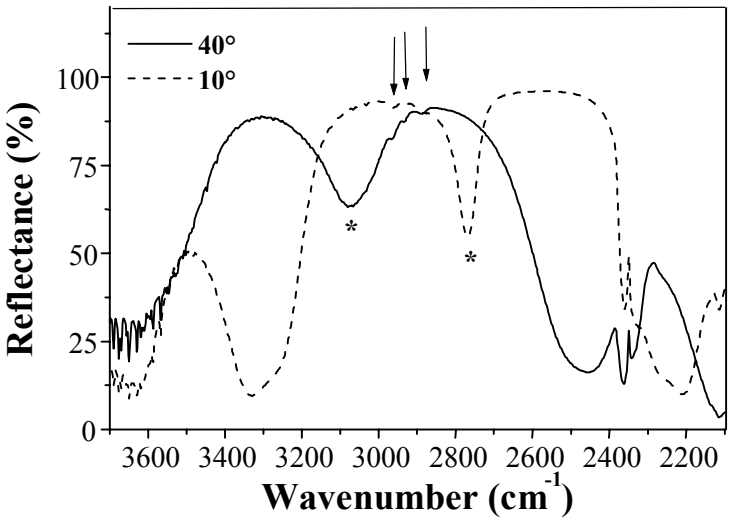

Fig. 3.8. FTIR reflection spectra measured at two angles of incidence of a PS FPMC exposed at RT to air with saturated urotropin vapor for 14 hours. The asterisks indicate the positions of the cavity mode whereas the arrows indicate the frequencies of the C-H vibrations of the urotropin.

In this case an enhancement up to two orders of magnitude has been obtained thus demonstrating the possibility of increasing the detection sensitivity of the PS systems to IR urotropin signal. Improved quality of PS FP systems should exhibit even higher enhancement factors.

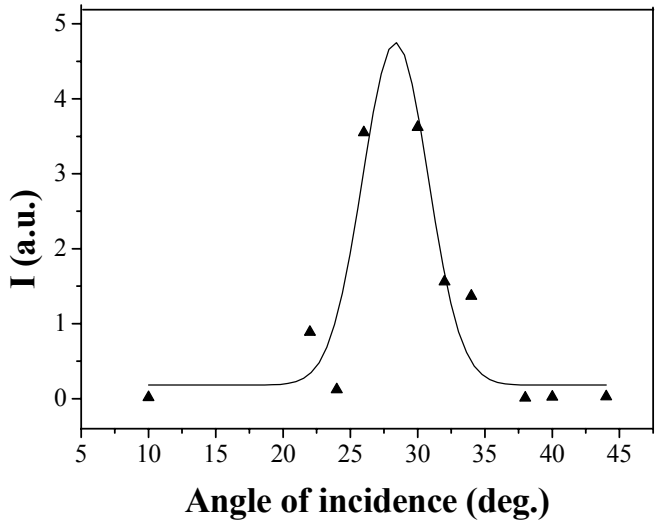

Fig. 3.9. Dependence on the angle of incidence of the integrated absorption intensity of the urotropin band at 2870 cm^{-1} for the FPMC of Fig. 3.8.

In conclusion the IR reflection spectra of PS single layer exposed to urotropin vapors show the increase with the exposure time of the intensity of the bands of the adsorbed molecules;

Urotropin is a catalyst of the oxidation of the PS in air as other organic bases;
The interaction between the C-H absorption bands and the cavity mode is a demonstration that the urotropin adsorption involves the whole PS superstructure;
The coupling between the C-H absorption bands and the cavity mode causes the enhancement of the absorption band intensity. This effect is due to the electric field enhancement caused by multireflection in the cavity at resonance condition (i.e. around the cavity mode frequency).
The possibility of accumulating the urotropin in PS material with the increase of the exposure time and the very low desorption rate of the adsorbed species suggest a possible use of PS systems for the detection (e.g. as dosimeters) of urotropin vapor in industrial environment. The results of this work have been presented in the 3rd. International Conference "Porous Semiconductors-Science and Technology" and then published in Physica Status Solidi [72].

3.4 SUM FREQUENCY GENERATION SPECTROSCOPY OF PS LAYERS

PS samples as prepared and exposed in air to urotropin vapors have studied also by SFG spectroscopy. Even if the first theoretical studies are dated 1962 [73], it needs to wait the 1987 to have laser and assemblages able to experimentally put in evidence a sum frequency generation, SFG, created by an interface [74]. The non linear optics brought a decisive solution to the problem of detecting only the adsorbed molecules and not the bulk. Actually the non linear optical processes of the second order are forbidden in a bulk material that has inversion symmetry. Only the interface between two materials breaks the symmetry and produces a signal. The optical techniques as those not linear perturb very little the studied system and they are "in situ" measures.
In the SFG technique, a pulsed visible laser beam (in our case green light λ = 532 nm) is overlapped on a surface with a tunable, pulsed infrared (IR) laser beam (λ = 2 - 15 μm). The two laser pulses combine to produce light at the sum of their frequencies (440 to 500 nm) by a nonlinear process. Since the interface is the only not central-symmetrical system, it is also varying only the frequency of the source of SFG signal (IR or visible), some resonances of the interface components can be excited. For example the vibrational levels of the adsorbates can be investigated by varying the frequencies of the incident IR light. Indeed this non linear spectroscopy of the interface is a very direct tool to identify the adsorbed species through their vibrational imprint. The light emitted at the sum frequency is detected by a photomultiplier and

the spectrum is obtained by tuning the IR beam over the frequency range of interest (see Fig. 3.10).

An amorphous medium, such as a polymer, does not generate a sum frequency signal because the bulk is randomly oriented, and second-order mixing is thus forbidden. However, polar ordering can occur at the surface of a polymer to reduce interfacial energy, resulting in a net orientation of molecules, and allowing a sum frequency response. Therefore, SFG is intrinsically surface specific.

Stronger SFG signal occurs when either the IR or visible beam is in resonance with a vibrational mode or electronic state, respectively. Molecular-level information about the interfacial species can be derived from the vibrational spectrum obtained by tuning the IR beam. This allows both the identity and orientation of surface groups or molecules to be determined.

More information about the non linear optics theory can be found in the annex at the end of this thesis.

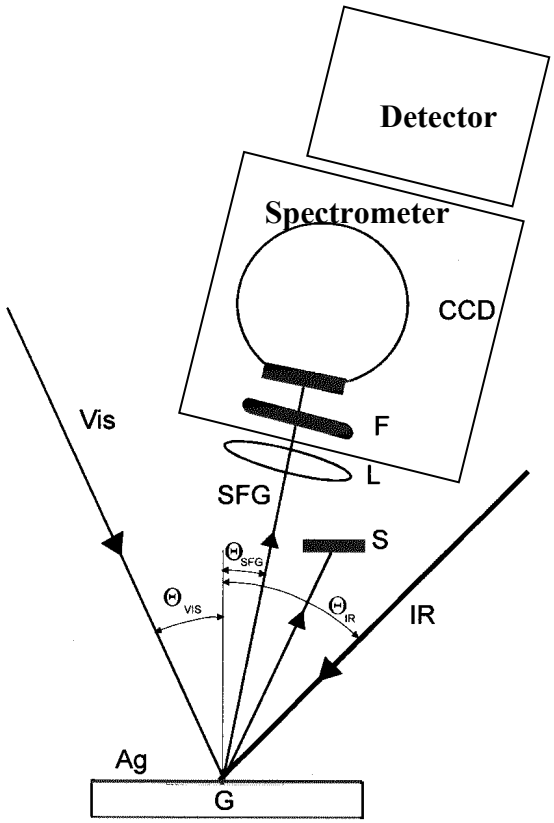

Fig. 3.10. Optical scheme of the SFG experiment. The angles Θ_{VIS}, Θ_{IR} and Θ_{SFG} correspond to the visible and infrared radiation incidence and the SFG radiation emission, respectively. The specularly reflected visible beam is stopped by a black screen S.

The interaction of an electromagnetic wave with electric field $\underline{E}$ with matter produces, through the action of its charges (free or bonded) a polarization $\underline{P} = f(\underline{E})$. This polarization, $\underline{P}$, produces an additional electric field that modifies the global field E_T. The relation $\underline{P} = f(\underline{E_T})$ can be developed in series of powers of E_T, following the Taylor's formula, usually stopping to the first order, getting $P^{(1)} = \chi^{(1)} E$. Nevertheless when the field E amplitude increases this linear approximation it is not correct. The sample does not respond linearly any more but quadratic terms appear. Si introduces therefore a corrective term to the polarization: $P^{(2)} = b E^2$. We enter into the domain of the non linear optics.

We now suppose that the considered material is radiated by two monochromatic waves sufficiently intense (pulsations ω_1 and ω_2) to generate the non linear effects. The irradiated electric field oscillates with the same pulsations of the dipolar moment. In the case of the SFG the aim is that to identify some molecular vibrations that fall in the infrared region, typically from 2 to 15 μm. A classical linear vibrational spectroscopy like the absorption spectroscopy (for example FTIR), operate in the infrared region, instead, the SFG radiation is situated in a more favorable spectral domain, namely the visible, where a simple photomultiplier in "photons counts" can be used to analyze the signal.

The IR-Visible sum-frequency generation (SFG) spectroscopy is a promising tool to study porous materials with a strongly developed internal surface by identifying the surface species adsorbed on the pores walls. Moreover a strong enhancement of an electric field in PS layers can be achieved both for linear [47, 71] and for non linear [75] spectral measurements if we create a Fabry-Perot (FP) structure based on alternating layers of different porosity (and hence of different refractive index). Such structures had been already used to increase the intensity of second harmonic generation in PS structures [76].

While second harmonic generation, SHG, has been already studied in PS systems, no SFG investigation on PS has been so far presented. In our recent paper (accepted for publication on Physica Status Solidi 2005 [77]), we report for the first time on the SFG measurements of the H-terminated surface of PS single layers and PS photonic crystals.

Several PS samples were prepared: single layers of various porosity and thickness, and photonic crystal structures. The SFG spectra were measured at LURE (Orsay, Paris-France) and LASMOS (Namur, Belgium). For most measurements the experimental angles with respect to the normal to the surface were: 55° for the incident visible light (wavelength 532 nm), 65° for the infrared incident light and 56° for the SFG radiation. Most experiments were performed with p (TM) polarization for the infrared incident beam and with s (TE) polarization for both the visible incident beam and the SFG beam. The preliminary optical characterizations of the PS

films and structures have been performed by reflectivity measurements in visible and infrared spectral regions (a CARY5 spectrometer for measurements in the visible range and a FTS-40 BIORAD Fourier-transform IR spectrometer have been used). These spectra were fitted by suitable model and software treatment to obtain film thickness, porosity and dielectric function.
Moreover, although the origin of the nonlinear optical properties in PS material is still matter of debate, previous works demonstrated that SHG signal can be generated inside PS layers and superstructures. On this base, in the SFG experiments on PS layers, not only the top interface at the air side is expected to contribute to the signal but the whole illuminated PS volume. Indeed, species present on the inner surface (e.g. on the pores walls) of the material should be the main source of the SFG radiation trough the resonant part of the second order susceptibility of the PS layer. The intensity of the detected SFG signal, in the case of the studied samples, is the result of various optical processes that include multiple-reflection interference of the incident visible and infrared radiation as well as of the sum-frequency radiation generated in the PS sample along the phase matching direction and transmitted along the direction θ_{SFG} in the air. According to the Wave vector conservation law, the emission angle θ_{SFG}, with respect to the normal to the sample surface, of the SFG beam can be expressed by:

$$\theta_{SFG} = Arc\sin\frac{\omega_{vis}\sin\theta_{vis} + \omega_{IR}\sin\theta_{IR}}{\omega_{vis} + \omega_{IR}}$$

where ω_{vis} and ω_{IR}, θ_{vis} and θ_{IR}, are the frequency and the incident angle of the visible and the infrared radiation, respectively.
The current and the anodization time were controlled to prepare different PS samples: three kind of single layers, at high porosity (180mA, 38.5s), at medium porosity (100mA, 100s) and at low porosity (85mA, 62s); and FP structures utilizing this parameters: 180mA, 6.47; 4 x (85mA, 2.5s; 180mA, 3.43s); 85mA, 2.5s; 180mA, 7.06s; 5 x (85mA, 2.5s; 180mA, 3.43s). Figures 3.11 and 3.12 show the visible and infrared spectrum of one of this FP.

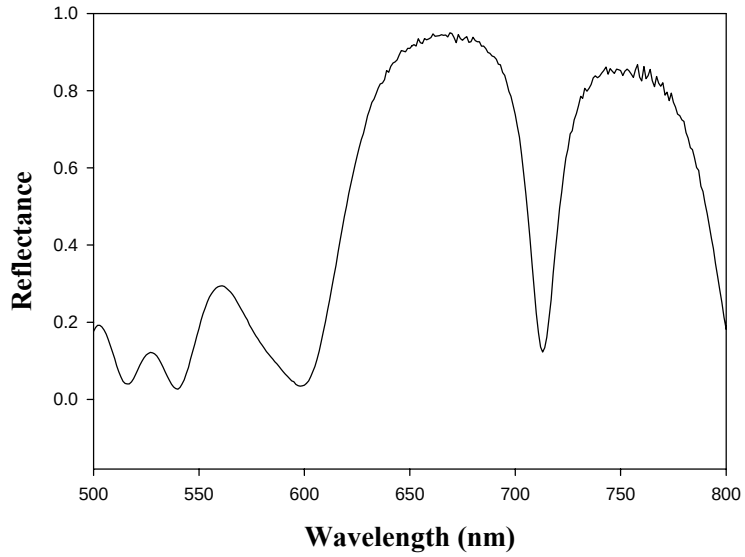

Fig. 3.11. Visible spectrum of a PSFP sample.

In the visible spectrum we can note the cavity mode centered at 713 nm, in the infrared spectrum we can recognize the typical interferential fringes and Si-H stretching absorption bands around 2100 cm^{-1}.

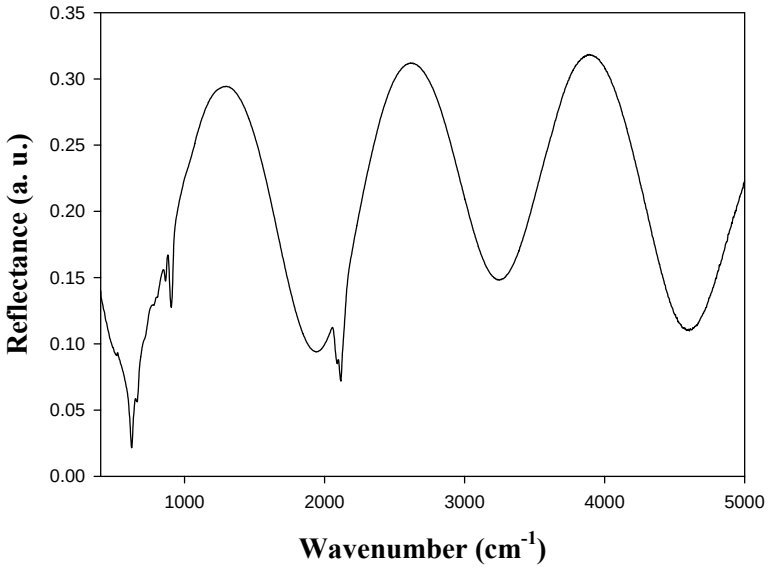

Fig. 3.12. IR spectrum of the same PSFP sample in Fig. 3.11.

To measure SFG spectra we have used the setup [78] with 2 optical parametric oscillators (OPO) pumped by YAG laser.

One of them, based on BBO crystal, produces visible light. We have used the wavelengths. Another OPO, using an $AgGaS_2$ crystal, and produces ~4-5 μm IR tunable beam. The sum-frequency (SF) spectra are obtained by overlapping the visible and IR beams on the PS sample surface at incident angles of 55° and 65°, respectively. The SF signal from the polymer surface is collected by a photomultiplier tube (PMT) and processed using gated integrator. Surface vibrational spectra are obtained by measuring the SF signal as a function of the input IR frequency. A schematic of the experimental setup is shown in Fig. 3.10.

To obtain surface specificity, the analysis is only performed in reflection mode. We were able to detect, for the first time, a quite good SFG signal in the chosen spectral range of the $Si\text{-}H_x$ stretching modes that were due to the native hydrogen present on the PS surface (see Fig. 3.13a). All the samples used in the experiments were designed to maximize the SFG throughput.

The SFG spectra in the $Si\text{-}H_x$ region of three layers of different thickness and porosity: (1) 0.47 μm, 61%, (2) 0.57 μm, 71% and (3) 0.81 μm, 82%, are shown in Fig. 3.13(a).

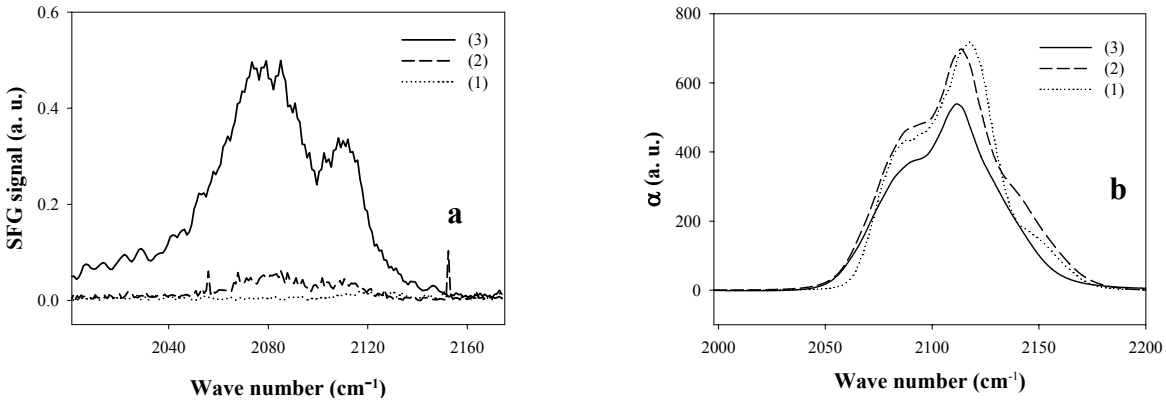

Fig. 3.13. SFG (a) and IR absorption coefficient (b) spectra of 3 single layers PS samples of various thickness and porosity: (1) 0.47 μm, 61%, (2) 0.57 μm, 71% and (3) 0.81 μm, 82%.

Two main broad bands are present in the spectra: the first one around 2080 cm^{-1} and the second one in the range 2110-2120 cm^{-1}, attributable to the ≡Si-H and to the =$Si\text{-}H_2$ stretching vibrations, respectively. The spectra are clearly quite different, the resonant signal being almost null for sample (1) and strong and well defined for sample (3). First of all, these results indicate that the outer air/PS interface is not the main source of the observed SFG signal. Indeed, in this case the signal, independent of the thickness, should decrease, since the number of hydrides species at the interface reduces with the increase of the porosity, see Fig. 3.13 (b), where the measured absorption coefficient, α, in the frequency region of the SiHx vibration, for the same samples is presented. This quantity, that represents the amount of normally incident radiant energy adsorbed by unit distance of the adsorbing medium, decreases slightly with the increase

of the porosity in agreement with the already reported decrease of the surface area per unit volume for this kind of PS materials [1 (a)]. The dependence of the observed signal on the thickness is expected to be quite complicated. When the SFG radiation is generated in the bulk of a layer its intensity should increase with the square of the thickness if the optical absorption can be ignored [78]. Of course, absorption attenuates the SFG intensity. Although the absorption is lower for the most porous material, the observed increase of a factor ten of the SFG intensity between sample (2) and (3) can not be attributed to the increase of the thickness of a factor 1.4. A more dramatic evidence is offered from the comparison between sample (1) and (3), where the thickness increases of a factor 1.7 while the intensity change is much bigger, the SFG signal being almost undetectable for sample (1). This finding suggests that a complete explanation of the results should include many effects: optical and structural as well. In any case, the results suggest that only a fraction of the surface hydrides species, likely located in special sites or pores of the PS material are SFG active and contribute to the resonant part of the second order susceptibility. Besides, the kind of active species and their number should modify and increase with the change in the local morphology (e.g. pores enlargement, changes in the pore shape, thinning of the Si skeleton, etc.) associated with the increase of the porosity. Further work is necessary to better clarify this point.

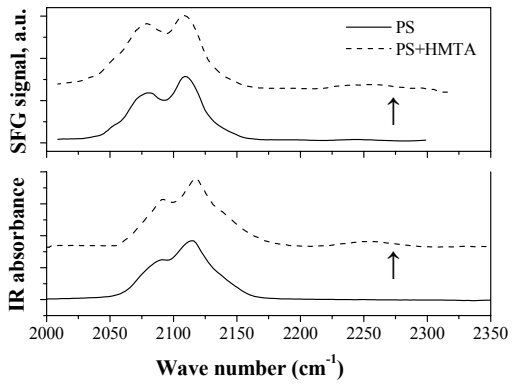

Fig. 3.14. The SFG spectrum for a single PS layer before (full line) and after (dashed line) hexamethylenetetramine vapor treatment (upper part). Si-H modes IR absorbance (lower part). The arrow indicates the band due to the O_3Si-H vibration.

The PS oxidation induced by the exposure to air saturated by hexamethylenetetramine (HMTA) vapor, previously studied by infrared spectroscopy [72], has been also detected by SFG spectroscopy. Indeed, in agreement with IR measurements, a new band near 2250 cm^{-1}, attributable to the O_3Si-H vibration, appears in the sample (1.9 μm thick, 80 % porosity) treated with HMTA vapor for 12 hours. These results are illustrated in Fig. 3.14, where the SFG and IR spectra of a PS layer, before and after the oxidation procedure, are presented.

The SFG signal of the hydrides surface species has been studied also in a PS one-dimensional photonic crystal structure with a defect producing an energy level in the photonic band gap, namely a Fabry-Perot microcavity structure. This structure was made of alternating layers of low and high porosity, according to the scheme: 2x (L, H), L, 2xH, 4x (L, H), with L ≡ (0.078 μm, 73%) and H ≡ (0.141 μm, 86%).

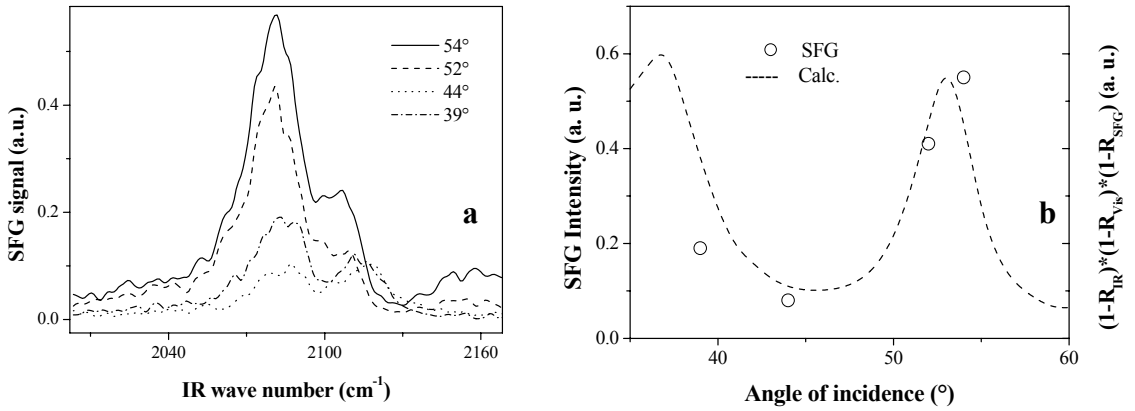

Fig. 3.15. (a) Smoothed SFG spectra for a PS Fabry-Perot structure at different angles of incidence of the visible beam. (b) Angular dependence of the total integrated intensity of the SFG signal for a PS Fabry-Perot structure: exp. (o) and calc. (-) $(1-R_{IR})^*$ $(1-R_{vis})^*(1-R_{SFG})$.

At 38° the cavity mode is in resonance with the visible laser beam. At 55° it coincides with the SF emission. Experimental SFG spectra for four angles of incidence of the visible laser beam are presented in Fig. 3.15(a). In the present case, to correctly calculate the angular dependence of the SFG signal, the nonlinear transfer-matrix formalism should be used, as it has been already shown for the SHG in a similar PS one-dimensional photonic crystal. Here, in approximate way, the SFG angular dependence is described by the product of the transmittivity factors [1-R (ω)], evaluated for both input and output radiation. Indeed, the points in Fig. 3.15(b) show that the angular dependence of the SFG integrated intensity (the total band area) is in quite good agreement with the dashed curve representing the angular dependence for the product $(1-R_{IR})^*$ $(1-R_{vis})^*(1-R_{SFG})$. Moreover, the data show that the SFG intensity can span one order of magnitude for the measured PS photonic crystal. Finally, a much higher enhancement (more than two orders of magnitude) could be expected for a suitable PS structure, as a one dimensional photonic crystal with two defect levels in the optical gap, that could allow a simultaneous resonance with both the visible and SFG radiation.
In summary, for the first time, the SFG spectra of surface species in PS layers and structures have been reported. Also the species associated to the oxidation induced by exposure of urotropin vapors have been studied. Besides, it has been shown that not all the species present on the inner surface of

the PS material do contribute to the SFG radiation. Enhancement of one order of magnitude of the SFG signal from a Fabry-Perot microcavity has been measured.

These results open the way to the possibility of studying by SFG spectroscopy the adsorbates produced by functionalization processes and more generally the chemistry of PS surface that are of wide importance both in fundamental studies and in view of many possible applications of this material.

PART II: Functionalization of PS layers in view of application as environmental and biological sensor

3.5 SYSTEMS REALIZZATION FOR SENSORISTIC APPLICATIONS

We have studied the functionalization of PS using various techniques and considering several organic molecules of interest for applications in the environmental sensing. The aim is to chemisorb at the inner PS surface (of the order of hundreds of m^2/g) the molecules of interest to provide new properties or to stabilize the material. The tested procedures are the followings ones:

Standard functionalization procedures

We have tested various functionalization methods:

3.5.1 Electrochemical Reaction

In text experiments we have studied surface functionalization of our PS samples with different organic molecules by an electrochemical method, widely documented in literature [79 ÷ 83]. All samples, once prepared through the usual procedure already described, cut in four parts (all measured by IR spectroscopy) were moved to a Schlenk tube, connected to a vacuum line for ~3h at 80ºC to desorb water and other air contaminants. Finally the samples were moved to dry-box for the electrochemical reactions in reduction, Anodic Electro grafting (AEG), or in oxidation, Cathodic Electro Grafting (CEG). The used organic molecules were: Chloromethyl isomenthyl ether (a chiral molecule), Iodohexene, Chlorohexene, L-pentine[3]. The signals of the absorbed molecules are present in the IR spectra but the prevailing effect is a strong oxidation besides sometimes the samples were partially destroyed.

[3] L = 2-(5-amino-3,4-dicyano-2H-pyrrol-2-ylidene)-1,1,2-tricyanoethanide.

In conclusion this technique is not optimal for our PS samples that are fragile if submitted to these electrochemical treatments and the efficiency of the PS surface coverage is always quite weak**.**

3.5.2 Photochemical Reaction

A second tested functionalization method has been the photochemical technique also widely documented in literature [84 ÷ 87].

A PS sample has been prepared beginning from n-type crystalline Si, doped with P, 0.5 Ωcm which has been submitted for 180 s to an anodic dissolution constant current equal to 80 mA in an electrolytic solution 1:1 = HF:EtOH and with an illumination on the sample of 25 mW/cm^2 realized through lamp of W.

This sample has been submitted to the photochemical functionalization reaction with 1-heptene, using a W lamp and a focusing lens to get on the sample an intensity of illumination equal to ~300 mW/cm^2. The photo-assisted functionalization reaction has already been performed according to the procedure note in literature for different alkenes [5].

The as prepared PS sample has been measured with the FTIR spectrometer, one half of its has been screened to avoiding the illumination, it has been put in a glassy container, it has covered with the 1-heptene and submitted to illumination for 30 min and it has again been measured finally through FTIR spectroscopy.

As above, once prepared through the usual procedure already described, the sample was cut in four parts (all measured by IR spectroscopy) that were then moved to a Schlenk tube, connected to a vacuum line for ~3h at 80ºC to desorb water and other air contaminants. Finally the samples were moved to dry-box in a quartz container and filled with the liquid organic molecule of interest and submitted to illumination of varying intensity and duration. We used 1-(N-5-hexenyl)-amino-9-fluorenone (a fluorescent molecule) exposed for one hour to illumination with white light (intensity around 50mW/cm^2). After the treatment the samples were washed with the solvent that was used for the synthesis of the molecule (mesitylene). Then we measured the samples by IR spectroscopy before and after washing by acetone. In the IR spectra there were the characteristics bands of this molecule. We also measured the samples by fluorescence and UV-VIS spectroscopy without obtaining significant signals. In conclusions this functionalization technique is not enough efficient for our PS samples and as the previous one the efficiency is quite low**.**

3.5.3 Thermal Reaction

Considering the non optimal results obtained with the two previous techniques we also tried the thermal functionalization [87 ÷ 91]. Samples as prepared, were subsequently treated according to the above described procedure (vacuum thermal treatment, etc) were heated from 80°C to 180°C for suitable times according to the different used organic molecules. We used: 1-aminofluorohexenone (in mesitylene 2h at 180ºC), hexenaminofluorenone (2h at 180°C), hexen-7-amino-4-methylcumarine (2h at 180°C)(three fluorescent molecules), C_6H_6MgCl (80ºC for three days) (a Grignard reagent), heptyne (at 80°C for 100 s, 1000 s, 1 h and 2 h). We measured the samples by IR spectroscopy before and after washing with acetone and ethanol. Also in this case the efficiency of this method was low. Indeed for the fluorescent molecules visible and fluorescence spectra did not show significant signals of the absorbed species.

3.5.4 Chemical Reaction

A second PS sample has been prepared using a p-type crystalline Si substrate, doped with the B, 0.01 Ωcm submitted to an anodization current of 100 mA for 20 s. This sample has been submitted to a chemical functionalization reaction with 6-I-1-hexene using as catalyst $EtAlCl_2$ (1 M in hexane) according to the following procedure showed in literature [92].

The as prepared sample has been measured through FTIR spectroscopy, kept under vacuum (5 * 10^{-5} mmHg) for 4 hours, absorbed, under current of N_2, in a mixture of 6-iodine-1-esene (0.5 ml) and $EtAlCl_2$ (0.1 ml) and kept for 16 hours in atmosphere of N_2. Then the sample has washed with THF, CH_2Cl_2 and in last with EtOH, dried in current of N_2 and finally, again measured through FTIR spectroscopy.

3.6 A NEW FUNCTIONALIZATION METHOD

3.6.1 The Method

Considering the scarce results (low level of functionalization and usually a quite strong oxidation) obtained with the previously tested methods and by analyzing the PS electrochemical formation processes we have developed a new “in situ” PS functionalization method.

The basic idea (see Fig. 3.16) is that of dissolving the acid-compatible organic molecules of interest directly inside the HF ethanoic solution to be used for the electrochemical preparation of

the PS layers. During the partial anodic dissolution of silicon to form the PS layer the presence of the organic molecules at the Si sites where the Si-H bonds are attacked and Si atoms are dissolved can allow an efficient interaction with the Si atoms to form the Si-C bonds and hence to realize the functionalization reaction in optimal conditions. The oxidation should be limited by the presence of HF that normally leaves an oxide deprived Si surface covered by Si-H bonds.

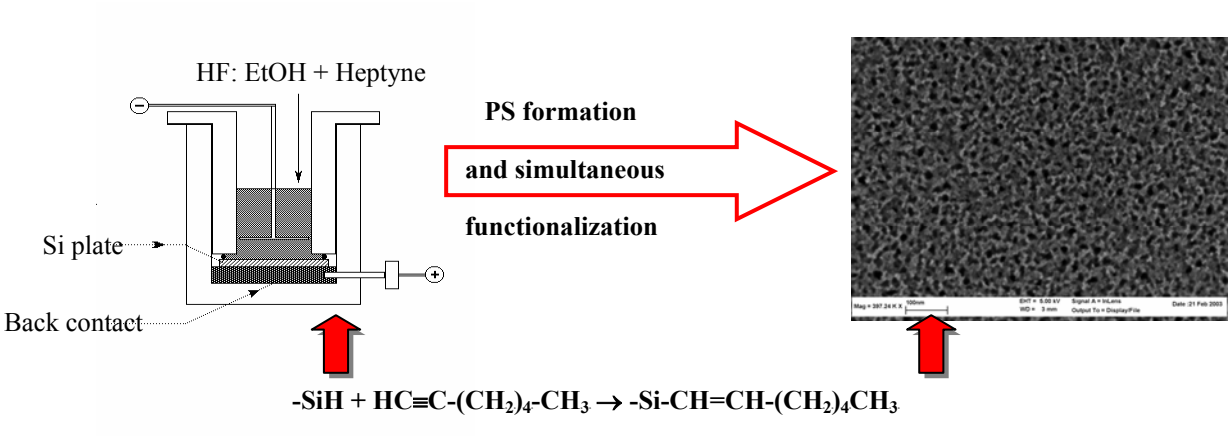

Fig. 3.16. Scheme of the new "in situ" functionalization reaction of heptyne on a PS sample.

The duration of the process is that of the normal formation of the PS layer, of the order of seconds or minutes. In this case, the functionalization occurs together with the PS formation in a single step process ("in situ" functionalization) without the necessity of subsequent and longer procedures in controlled environments (e.g. vacuum treatments, dry box, etc.).

To prove this idea a series of samples and experiments have been carried out. The selected organic molecules were acid resistant and with a triple Carbon-Carbon terminal bond, although molecules with internal triple Carbon-Carbon bonds and with different conjugated double Carbon-Carbon bonds have been also considered.

Going into detail we studied by FTIR reflection spectroscopy the covalent functionalization of some PS sample with 1-Heptyne. The samples have been prepared by the partial anodic etching procedure on p^+-type Si (100) wafers with resistivity 0.01 Ω cm in an electrochemical cell containing an HF (50%). EtOH solution (1:2 by volume) added with a variable amount of 1-Heptyne. The current and the anodization-functionalization time were controlled by a galvanostat interfaced to a PC computer. The IR reflection spectra were measured after the formation reaction and again after washing with EtOH and Acetone. They were recorded in the range 400 - 5000 cm^{-1} with a resolution of 4 cm^{-1} using a Fourier transform infrared spectrometer. The angle of incidence was fixed at 20°.

For the experiments a set of mesoporous PS films of different porosity (66 - 74%) and thickness (0.3 - 0.4 μm) were prepared with the same current density and etching time (60 mA/cm^2, 100 s) and different concentration of heptyne from 0 to 0.9 M.

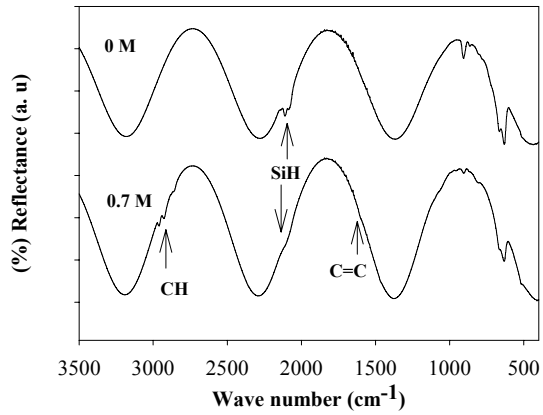

Fig. 3.17. FTIR reflection spectra of a PS film prepared without 1-heptyne and with 1-heptyne 0.7 M. The arrows indicate the frequencies of the ν SiH_x bands and of the main 1-heptyne bands.

The results reported in Fig. 3.17 demonstrate the effectiveness of the new "in situ" functionalization method. In this figure the IR reflection spectra of two as prepared PS sample without 1-heptyne (0 M) and with 1-heptyne (0.7 M), are shown. We can note the typical modulation due to interference present in PS thin films. The spectra reveal the presence of clear features attributable to Si bonded 1-heptyne species. Indeed: i) the absence of the terminal $\nu_{\equiv C-H}$ at 3300 cm^{-1} excludes physisorbed heptyne; ii) all the other bands due to the C-H_x vibrations are recognizable (ν_{C-Hx} 2960, 2928, 2876, and 2860 cm^{-1}, CH_2 and CH_3 bending (δ) at 1464 and 1376 cm^{-1}); iii) the $\nu_{C\equiv C}$ triple bond stretching (around 2200 cm^{-1}) is totally absent and it is replaced by of the $\nu_{C=C}$ double bond stretching (around 1600 cm^{-1}) and the vinyl stretching =C-H (around 3050 cm^{-1}) as it is expected for molecules chemisorbed on silicon through the terminal C atom of the original triple bond; iv) some weak bands, attributable to Si-O-Si vibrations, are present in both the spectra in the 1000 – 1100 cm^{-1} range; v) the strong reduction of the signal due to the Si-H_x species (2109-2074 cm^{-1}), without appreciable oxidation, is a clear evidence and in the functionalized PS layer the chemisorbed species have replaced the hydrogen in a large fraction of the surface sites of the PS surface normally occupied by silicon hydride species.

The comparison of the two spectra in Fig. 3.17 indicates that the presence of 1-heptyne in the solution modify only slightly the structure (i.e. the thickness and the porosity) of the PS layer, being the two interference patterns almost equal. For more quantitative analysis the IR spectra of all the measured samples have been mattered to data reduction and compared with model spectra obtained by suitable software (e. g. SCOUT). Through this analysis the absorption coefficient (α) for the main absorption bands present in the reflection spectra was obtained. In Fig. 3.18 this quantity is presented as a function of the frequency for the vibrations C-H, Si-H_x and C=C for samples obtained with different heptyne concentration (0 ÷ 0.8 M) in the preparation solution.

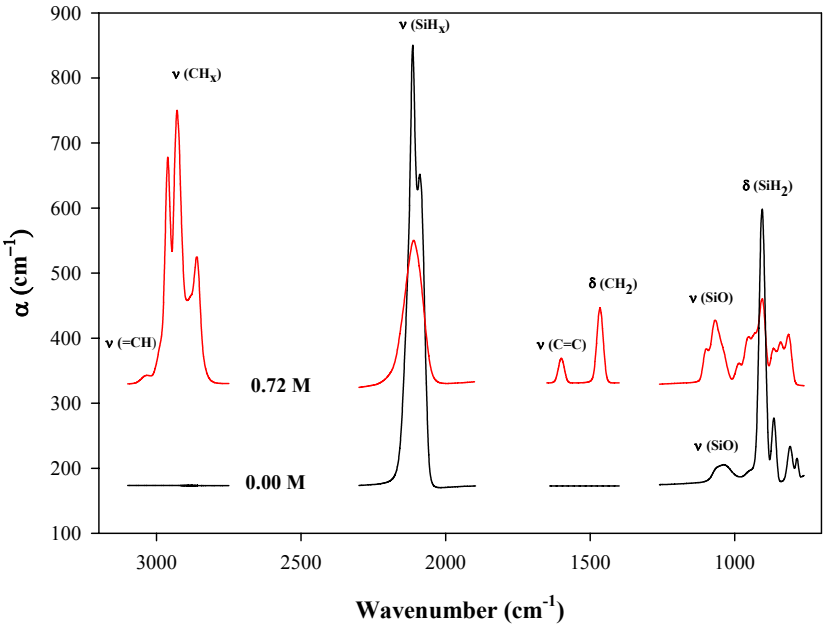

Fig. 3.18. Absorption coefficient, α, of two samples, produced without 1-heptyne (black line) and with 1-heptyne 0.72 M (red line), in preparation HF/EtOH solution, in the frequency ranges of CH_x, Si-H_x, C=C and SiO vibrations. The spectra are represented in the correct scale of absorption intensity but, for sake of clarity, they have been shifted along the ordinate axes.

As we can see in Fig. 3.18 the signal of superficial species Si-H decreases whereas strong signals of adsorbed 1-heptyne appear.

The integrated intensities of all the 1-heptyne characteristic bands increase with the increase of the 1-heptyne concentration in the anodic solution. As an example, we can see in Fig. 3.19(a) the dependence on the 1-heptyne concentration (from 0 to 0.8 M) of the absorption coefficient in the C-H stretching region (at 2927 cm^{-1}) and in the Si-H stretching region (at 2113 cm^{-1}).

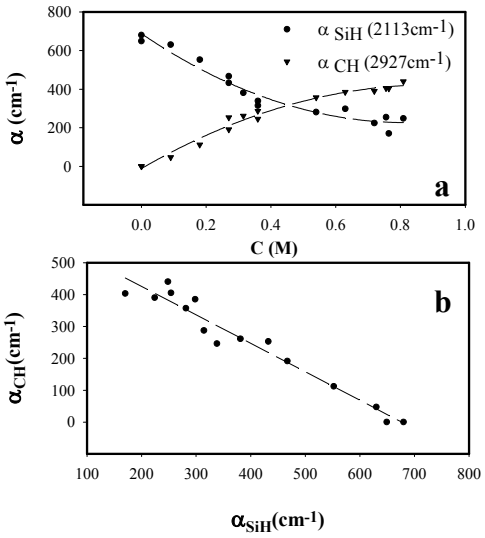

Fig. 3.19. (a) Absorption coefficient, α_{CH}, in the νC-H_x region (at 2927 cm^{-1}) and α_{SiH}, in the νSi-H_x region (at 2113 cm^{-1}) as a function of the 1-heptyne concentration, C, in the anodic solution; (b) α_{CH} (2927 cm^{-1}) vs. α_{SiH} (2113 cm^{-1}). The dashed lines are a guide to the eye.

These results indicate an evident inverse correlation, clearly illustrated in Fig. 3.19(b), between the surface abundance of the chemisorbed molecules and that of the silicon hydride species. From the relative decrease of the integrated intensities of the Si-H absorption signal the average efficiency of the functionalization process can be evaluated [93]. In this case we found values as high as 50-60%.

To further study the effects induced on the PS material by the presence of the organic molecules in the preparation solution, we have also measured the dependence of thickness and porosity on the heptyne concentration.

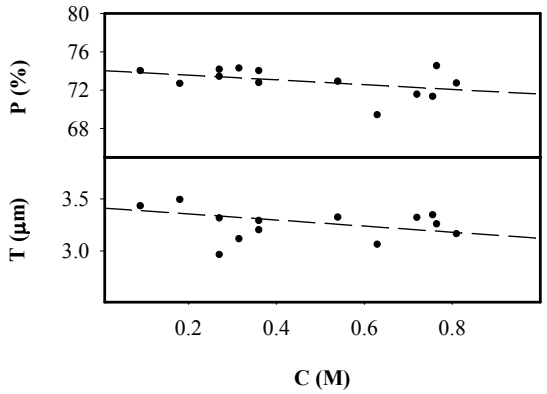

Fig. 3.20. Porosity, P, and thickness, T, of PS samples as a function of the 1-heptyne concentration, C, in the anodic preparation solution.

These parameters slowly decrease with the increase of the 1-heptyne concentration, as illustrated in Fig. 3.20, thus indicating that the chemical species interact with the Si atoms on the sample surface and modify slightly the PS morphology. These little variations of porosity and thickness are not a problem for the sample preparation since it is possible to use "calibration" curves, similar to those of Fig. 3.20, to design and prepare PS layers having the desired morphological properties and amount of functionalization.

Similar dependencies have been obtained also for sample prepared with different current densities as we can see in Fig 3.21.

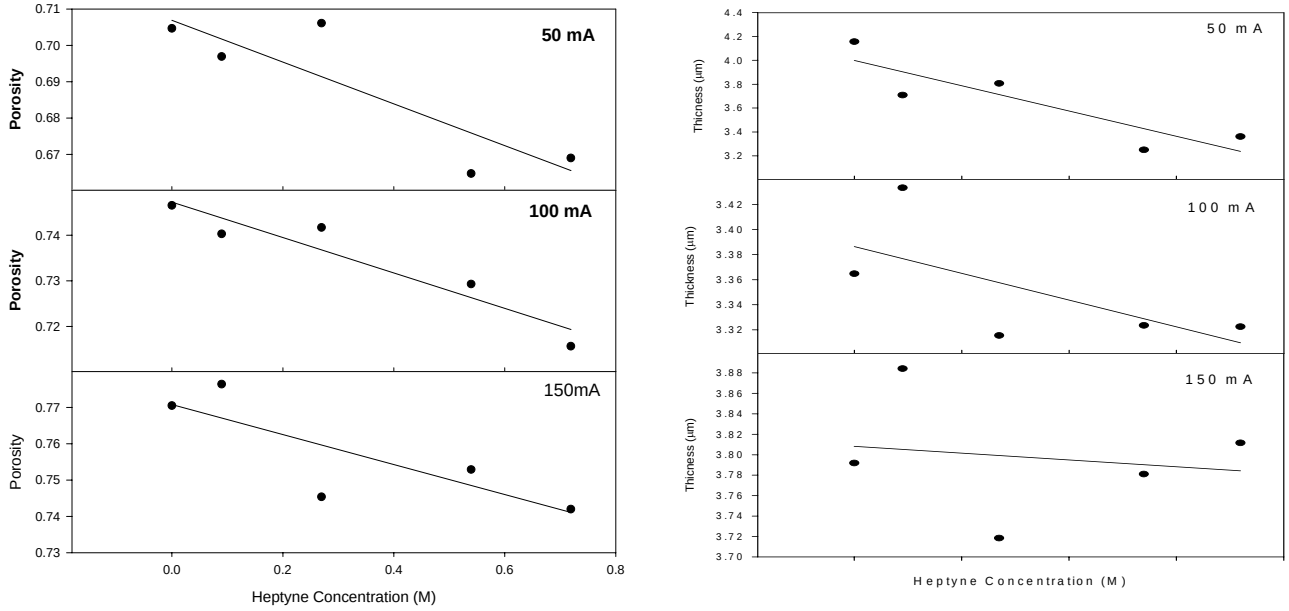

Fig. 3.21. Thickness and Porosity of PS samples as a function of the 1-heptyne concentration in the anodic preparation solution at different current density.

3.6.2 Functionalization by Contact in the etching solution

It is important to stress that if an unfunctionalized PS sample is kept in contact with the same (0.7M) 1-heptyne HF ethanoic solution, for a time as long as 1000 s, not significant functionalization, only 2%, of functionalization related to a 100s-100mA sample prepared by our method, is achieved (see Fig. 3.22).

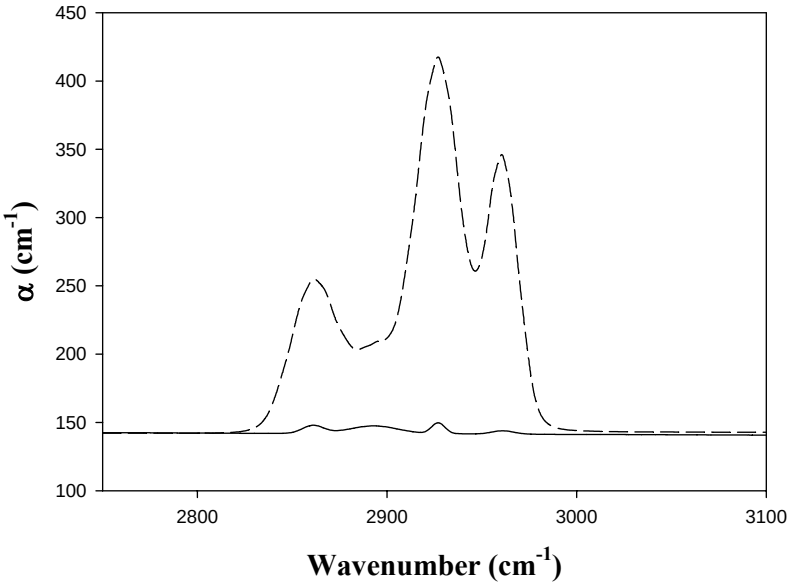

Fig. 3.22. Absorption coefficient, α, of the electrochemically functionalized (with 1-heptyne 0.72 M) PS sample (dotted line) and of a similar sample (solid line) functionalized only by contact with the same solution with 1-heptyne 0.72 M, in the frequency ranges of CH_x vibrations. The spectra are represented in the correct scale of absorption intensity but, for sake of clarity, they have been shifted along the ordinate axes.

This fact also demonstrates that it is essential the presence of the organic molecules in the solution during the electrochemical formation of the PS material for the effectiveness of this functionalization method.

3.6.3 Comparison of the functionalization by contact in the etching solution of oxidized and fresh PS samples

The idea was to compare the effectiveness of the substitution of the Si oxide, instead of hydrides species (as normally occur in HF solution) with functionalized ones.

We have prepared three PS single layers using the same parameters in the preparation, two of these were oxidized by exposure for 1 hour at air saturated with Et_2NH, which we know to be a catalyzer for PS oxidation in air (see paragraph 3.2). Then we treated the unoxidized and one of the oxidized samples for 300 s in the HF: EtOH (1:2), 0.7 M in 1-heptyne solution. The last oxidized sample were treated with the same HF: EtOH (1:2) solution but without 1-heptyne. It is known that in absence of organics the presence of HF substitute the oxide leaving hydrogen covered surface. The idea to be verified was that if in presence of organics some silicon oxide could be substituted by the organic itself instead than by the hydrogen.

The scheme below summarizes the whole experiments:

I. 20 s, 100 mA → → (5') HF:EtOH (1:2) + 1-heptyne 0.7 M

II. 20 s, 100 mA → 1h oxidized by Et_2NH → (5') HF:EtOH (1:2) + 1-heptyne 0.7 M

III. 20 s, 100 mA → 1h oxidized by Et2NH → (5') HF:EtOH (1:2)

In Fig. 3.23 we can see the spectra correspondent to the situation II of the scheme. We can note the oxidation in the spectrum (b), due to the exposure of the diethylamine vapors, mainly in the big band near 1100 cm^{-1} and the decreasing of the ν_{SiHx} bands centered at 2100 cm^{-1}. In the spectra (c), after 300 s of contact with the hydrofluoric solution of 1-heptyne, we have again the ν_{Si-Hx} bands, we do not have oxidation bands near 1100 cm^{-1} but we can not see also ν_{C-Hx} bands, in substitution of oxide sites.

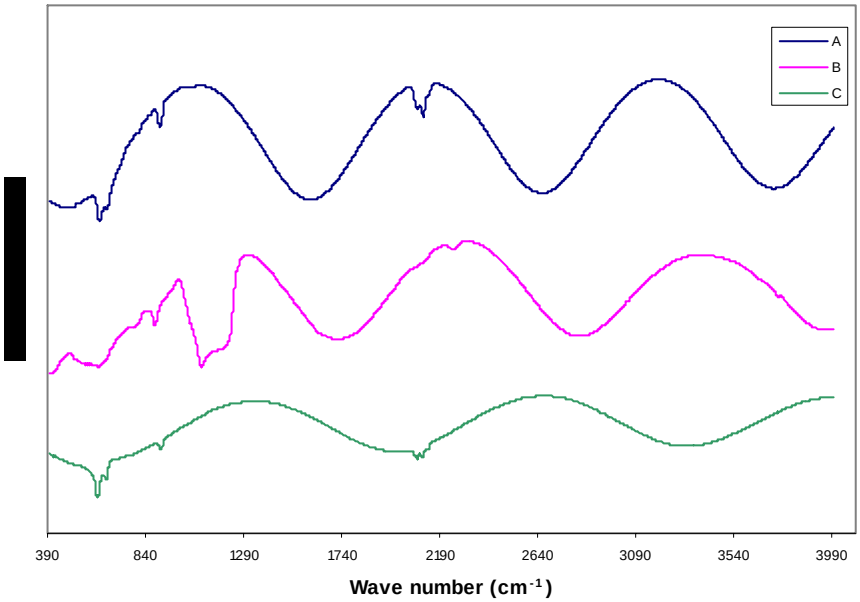

Fig. 3.23. IR spectra of the same PS sample: (a) as prepared, unfunctionalized; (b) after oxidation and (c) after 300 s in contact with the HF: EtOH (1:2), 0.7 M in 1-heptyne solution. The spectra have been shifted along the ordinate axes for sake of clarity.

Finally we have not appreciated any significant differences in the amount of CH_x or SiH_x species between the as prepared and the oxidized PS sample treated with the same contact solution, we found an amount of CH_x species in agreement with the time of contact with the 1-heptyne (Fig. 3.22). This confirms that the passage of the current plays a fundamental role in the functionalization process.

3.6.4 Ageing Study

The sample oxidation is naturally limited during the formation for the presence of HF in the anodic solution; after the functionalization because of the partial coverage of the PS surface with

bounded organic molecules. In fact one method to significantly reduce the natural PS oxidation in air is the coverage of the surface by capping. Also our functionalization process with organic molecules forms a protective capping against the oxidation in air. In fact a FTIR study (Fig. 3.24) carried out on our samples, produced with the same parameters but with a different functionalization degree (from 0 to 0.7 M), confirmed this further positive quality of functionalized PS surfaces, that is to be partially protected towards the natural oxidation in air.

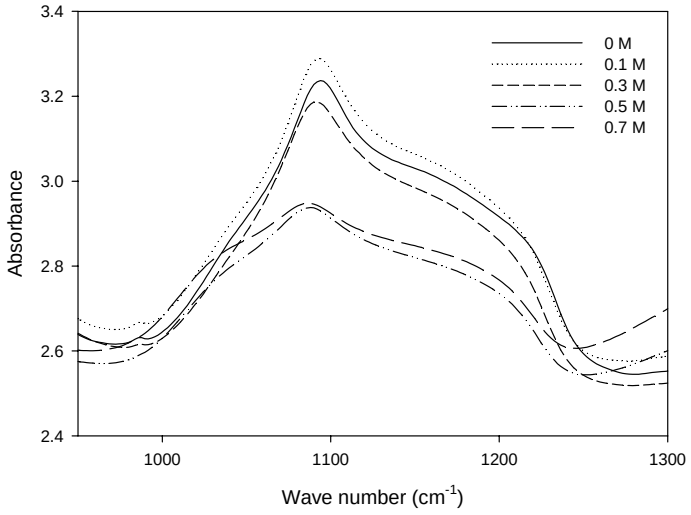

Fig. 3.24. Absorption bands in the silicon oxidation region after 14 months of aging in air of PS single layer functionalized with different 1-heptyne concentrations, from 0 to 0.7M.

Seen the graph (Fig. 3.25) of the IR absorption band integrated intensities of the Si-O-Si bond stretching typical of the oxidized samples we can note that after 14 months of permanence in air, the sample functionalized with 0.7 M concentration of 1-heptyne in the anodic solution presents 58% less oxidation respect to the unfunctionalized sample.

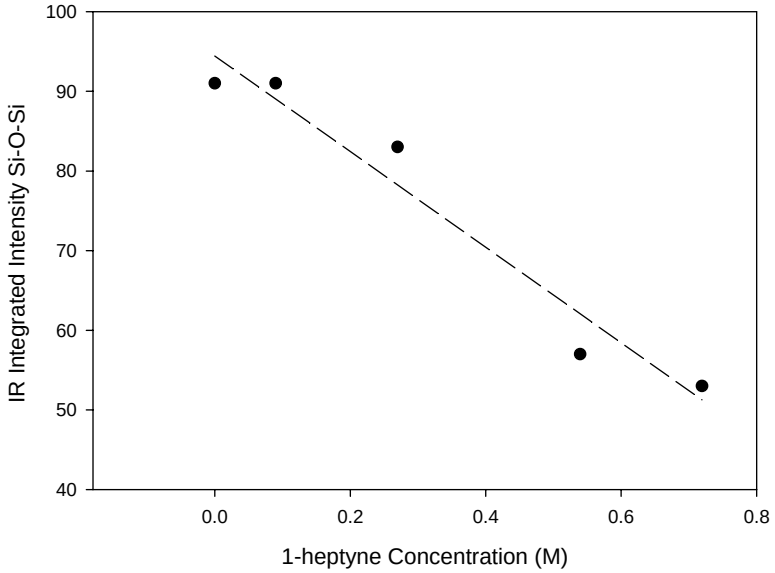

Fig. 3.25. IR integrated intensity of the principal band of the oxidation as a function of the 1-heptyne concentration.

Hence, the oxidation of functionalized PS is naturally limited and it is consistent with the "previously estimated" 50 ÷ 60% surface coverage with the 1-heptyne organic molecule.

3.6.5 Spatially Confined PS Functionalization

Finally, our new method has a unique and very appealing feature, namely the possibility to confine the adsorbed species in selected layers in a PS stack (or multi-layer PS system), i.e. e. only in those prepared in presence of the organic molecules.

Preliminary results indicate that selective functionalization of single layers in a stack of PS can really be achieved by this method.

First, we have prepared a PS Fabry-Perot structure [4*(85mA, 18.5s; 180mA, 14.3s); 85mA, 18.5s; 180mA, 28s; 4*(85mA, 18.5s; 180mA, 14.3s)], by functionalizing only the cavity layer, with 1-heptyne (i.e. e. the 1-heptyne was present in the solution only during the electrochemical formation of the cavity layer). IR spectra of these FP systems of course show signals relatives to the functionalized molecules but also evidence an amplification of the signals that are in resonance with the optical cavity of the generated systems. This finding demonstrates that the molecules are not covalently bonded only on the external surface of our sample but that they are chemisorbed deeply in the structure, otherwise we would not have been able to see any amplification.

We have, successively, generated a series of three samples: i) a functionalized single layer of thickness **d** (180mA, 28s; T 1.4 μm, C 0.6M); ii) a three layer sample of the same thickness **d**,

prepared with the organic molecule present in the electrochemical solution only during the formation of the intermediate layer (180mA, 27.7s, T 1.5 μm; 180mA, 28s, T 1.4 μm, C 0.6M; 180mA, 27.7s, T 1.3 μm) and, finally, iii) a sample like the second but with the first layer of thickness 2**d** (180mA, 55.4s T 2.9 μm; 180mA, 28s T 1.5 μm, C 0.6M; 180mA, 27.7s T 1.0 μm). After processing with appropriate software the obtained IR data, in Fig. 3.26, we have seen that the amount of functionalized organic molecule was equal for all the three samples, demonstrating the absolute uninfluence of the upper layer on the functionalized lower one, see Fig. 3.27.

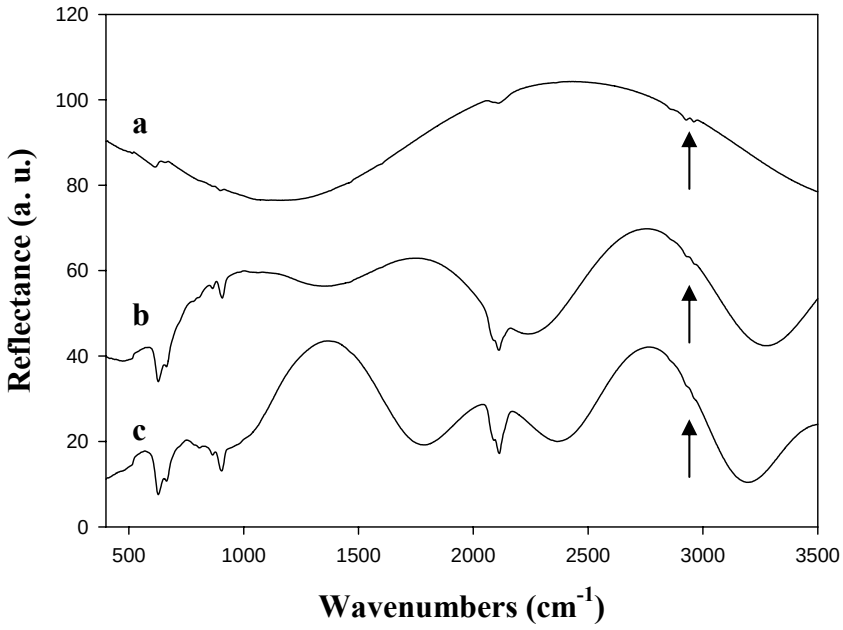

Fig.3.26. FTIR reflection spectra of (a) the functionalized (with 1-heptyne 0.72 M) monolayer of thickness d; (b) three layer sample of the same thickness d, the central one functionalized; (c) a three layer sample like (b) but with the first layer of thickness 2d. The arrows indicate the frequencies of the ν CH_x bands of 1-heptyne.

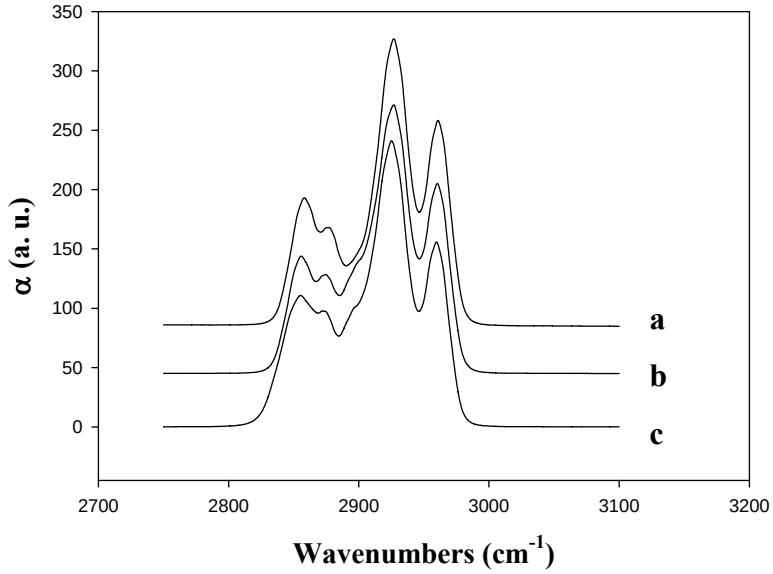

Fig. 3.27. Absorption coefficient, α, of the functionalized (with 1-heptyne 0.72 M) monolayer of thickness d (a); three layer sample d, d functionalized, d (b); three layer sample 2d, d functionalized, d (c) in the frequency ranges of CH_x vibrations. The spectra are represented in the correct scale of absorption intensity but, for sake of clarity, they have been shifted along the ordinate axes.

Further information was obtained producing two identical FP having as unique difference the Silicon functionalization only in the cavity of one of the two samples.

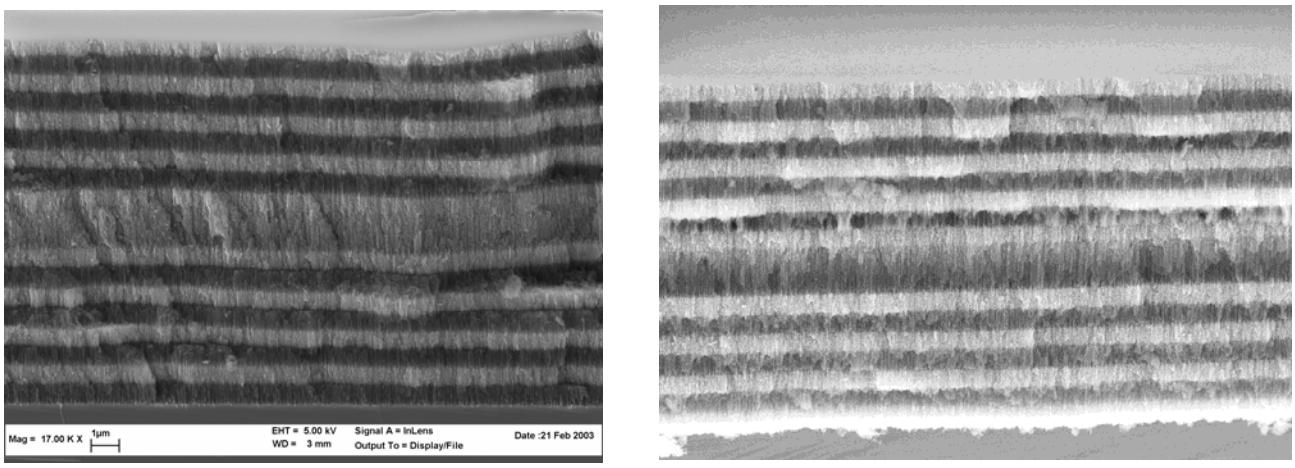

Fig. 3.28. SEM image of two equal PSFP samples but on the left we have the functionalized only in the cavity with 1-heptyne and on the right the unfunctionalized one.

To completely explain the meaning of this last sentence we can consider the Fig. 3.28 (left) that is a SEM image of a structure Fabry-Perot, functionalized only in the cavity with 1-heptyne [4*(85mA, 18.5s; 180mA, 14.3s); 85mA, 18.5s; 180mA, 28s; 4*(85mA, 18.5s; 180mA, 14.3s)]. We have generated the two Bragg without the organic molecule in the electrodic solution but the

cavity in the presence of 1-heptyne 0.7 M. We can see in the figure three different kinds of layers: of high porosity (darker), of low porosity (lighter) and a central zone of double thickness, of an intermediate color that is the functionalized zone. Without the presence of the organic molecule this zone should be dark like the other layers at the same high porosity, as it is the case in Fig. 3.28 (right); but the presence of the organic molecule modifies the porosity in this zone as we have seen in Fig. 3.20.

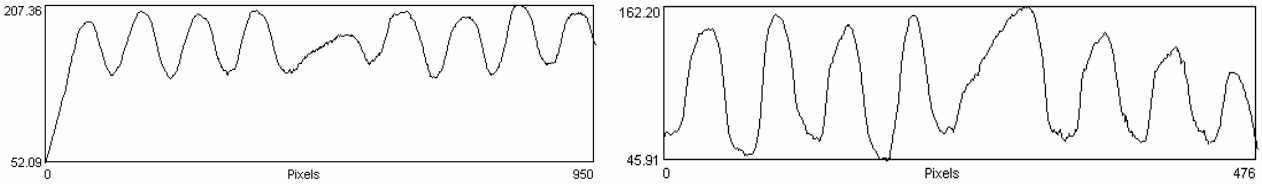

Fig. 3.29. Gray density of the PSFP in Fig. 3.28. On the left we have the functionalized only in the cavity with 1-heptyne and on the right the unfunctionalized one.

As we can appreciate from the gray density of these two samples (in Fig. 3.29) the porosity of the functionalized cavity has an intermediate value as we can expect looking at Fig. 3.28. We can know the porosity values of the high porosity layers (84.45%), and of the low porosity layers (66.36%) elaborating the IR spectra through the software Scout. The values of the porosities being known, high porosity (dark layers) and of the low one (clear layers) and associating to the gray density the correspondent porosity value, we can extrapolate from the figure 3.29 the porosity value for the cavity, associated to its gray density, equal to 76.9% that is in good agreement with 77.8%, value determined through the elaboration of the IR spectra of a functionalized PS layer. All the two profiles show the presence of a porosity gradient in the cavity that we will further investigate as future works.

We finally had a more direct confirm of the confinement of the organic molecules come trough the results of the following last experiment. A particular two layers system was prepared with the same current density and anodization time but with the presence of 1-heptyne molecules only during the formation of the second layer. The presence of a very thin high porosity intermediate layer (100mA, 400s; 300mA, 1s; 100mA, 400s, C 0.6M) allowed us to remove the first layer, after the preparation of the system, and to measure separately its IR spectrum (see the scheme in Fig. 3.30.

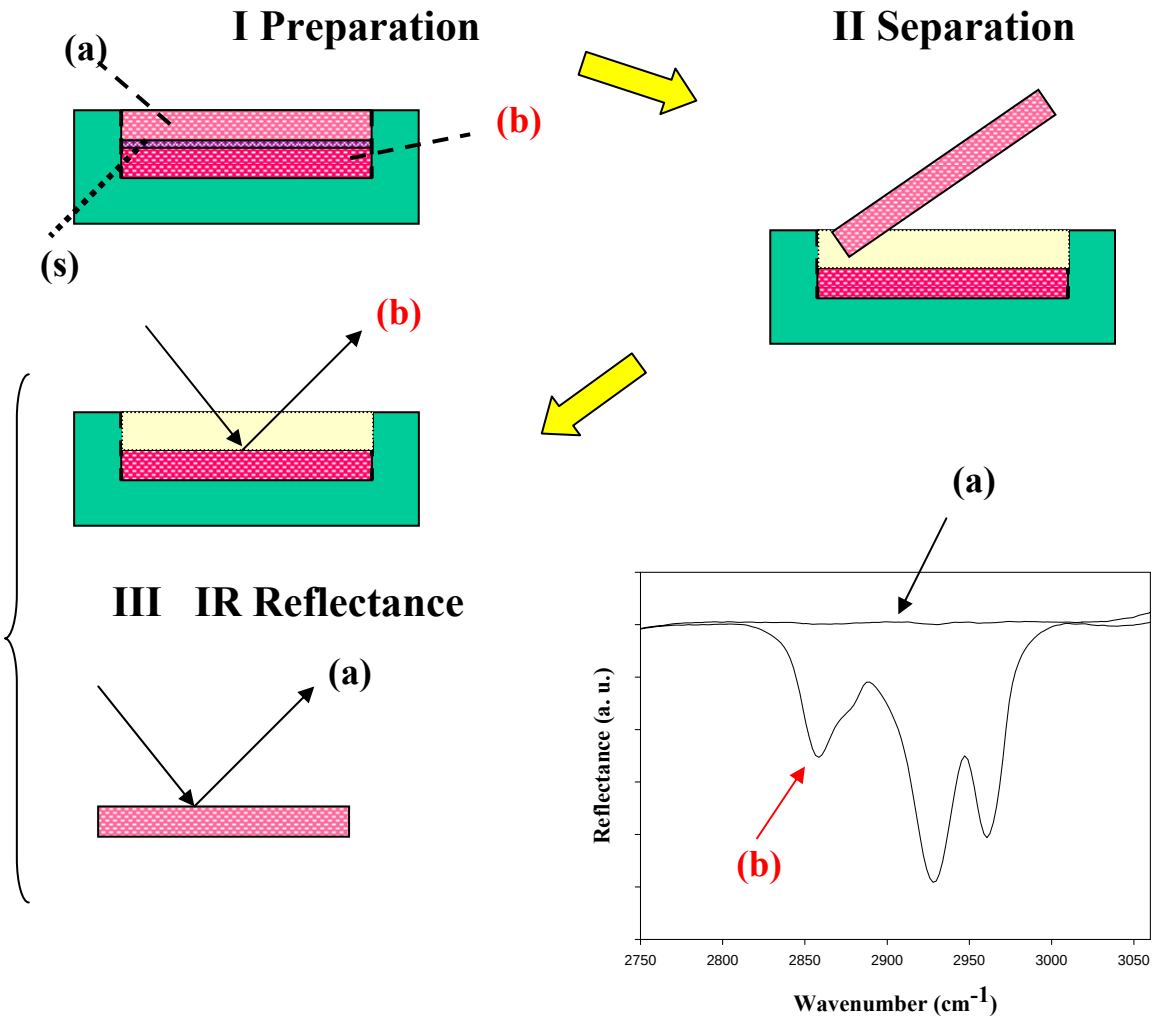

Fig.3.30. Scheme of the particular two layers system preparation and Zoom in the ν_{CH} zone of the two IR spectra. The upper line (a) is the IR spectra of the unfunctionalized layer and the lower one (b) the correspondent IR spectra of the functionalized layer

According with the aim of this experiment the IR spectra (see Fig. 3.30) confirm that the functionalization is spatially located only in the layer formed in presence of 1-heptyne in the electrochemical etching solution (the third layer in our sample).

IR spectra showed the almost total concentration of the organic substance on the second layer and few substance percentage (0.7% of functionalization related to the amount of CH_x founded in the third layer) founded on the second layer can be attributed to a partial imperfection of the

two layers separation or to the effect of the contact functionalization that we know to occur (2% in 1000s).

Recently we have applied the field emission SEM microanalysis technique on one of our three layers PS sample, where the layers were all prepared with the same parameters but the central one was formed in presence of 1-heptyne (0.7 M) in the preparation solution.

Microanalysis measurements, specifically for silicon and carbon, was collected on a vertical line along the cut freshly section starting from the air-PS surface every 2 μm down to the bulk silicon substrate.

Fig. 3.31 clearly shows the carbon localization in the central layer with an amount consistent with the expected surface functionalization degree of 40 % (evaluated from the infrared spectra as indicated in a previous paragraph, page 12).

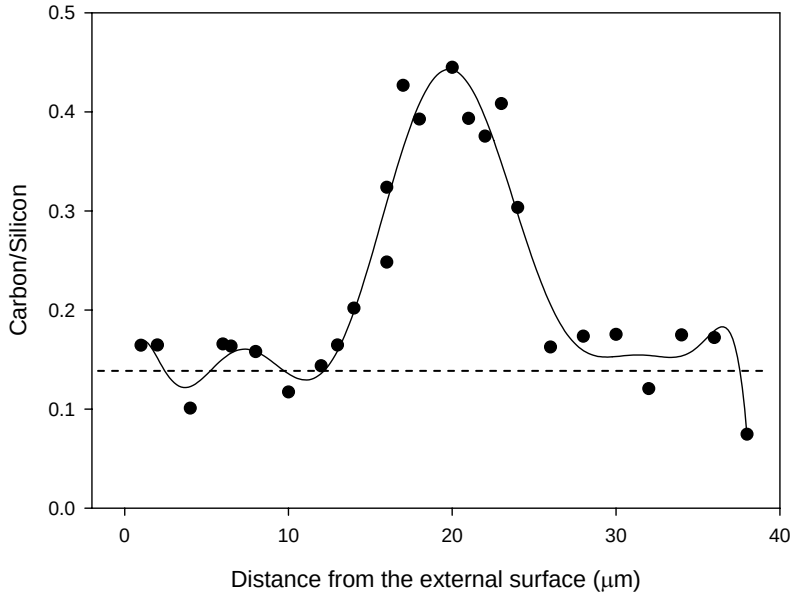

Fig. 3.31. Carbon- Silicon (atomic) ratio as a function of the distance of points from the external surface as obtained by field emission SEM microanalysis. The dashed line corresponds to the carbon content due to the atmospheric contamination during the break up of the sample.

Furthers deepening would be necessary to better exploit the potentiality of the technique on our PS samples functionalized or not.

3.6.6 Other Organic Molecules

Another important goal is to extend the method to other kinds of organic molecules of interest, also in view of applications in the environment sensing field. We have already completed the

study of various molecules (see tab. 1) that confirmed the possibility to utilize "calibration" curves and indicated that different molecules can differently influence porosity and thickness.

Table 2. *Various molecule types tested with the new PS functionalization method.*

Molecule	Formula	Conc. (M)	Functionalization
1-Heptyne	$HC{\equiv}C\text{-}(CH_2)_4CH_3$	0.1 – 1	**YES**
Styrene	$H_2C{=}CH\text{-}C_6H_5$	1.1- 1.4	**YES**
Phenylacetylene	$HC{\equiv}C\text{-}C_6H_5$	0.1 - 1.6	**YES**
Ethylcinnamate	$C_6H_5CH{=}CHC{=}OOCH_2CH_3$	1.0	NO
Propargylchloroformate	$HC{\equiv}CCH_2OC{=}OCl$	1.8	**YES**
Methyl-2-octynoate	$CH_3(CH_2)_4C{\equiv}CC{=}OOCH_3$	1.0	NO
Methylenebisacrilamide	$(_2HC{=}CHC{=}ONHCH_2\text{-})_2$	1.4	NO
Phenylpropiolic acid	$C_6H_5C{\equiv}CC{=}OOH$	0.7	NO
6-Heptynoic acid	$HC{\equiv}C\text{-}(CH_2)_4C{=}OOH$	0.75	**YES**
Caffeic acid	$(HO)_{2m,p}C_6H_5CH{=}CHC{=}OOH$	0.4	NO
Methylvinylketone	$CH_3C{=}OCH{=}CH_2$	0.1 – 1.6	**YES**
1-Hexene	$HC{=}C\text{-}(CH_2)_3CH_3$	0.5 - 0.75	**YES**
1-Pentene	$HC{=}C\text{-}(CH_2)_2CH_3$	0.75	**YES**

From these preliminary tested molecules we knew: i) molecules with triple C≡C bonds are more efficient than molecule with double C=C bonds; ii) Internal triple and double bonds do not work; iii) Terminal double bonds work better if conjugated. Probably, the steric parameters and the geometry of the molecules that we want functionalize strongly influence their functionalization ability. A deeper understanding of these results will be achieved only once that the microscopic mechanism at the base of this formation-functionalization process will be clarified. This will be one of the goals of the future work.

As an example we report with some detail the functionalization of two of the molecules reported in the table: Methylvinylketone (MVK) and Phenylacetylene. We can see in Fig. 3.32 the dependence on the MVK (on the left) and Phenylacetylene (on the right) concentration (from 0 to 1.6 M) of the absorption coefficient in the C-H stretching region (at 2925 cm^{-1} for MVK), in the CH bending region (at 1956, 1491, 1446 cm^{-1} for Phenylacetylene) and in the Si-H stretching region (at 2114 cm^{-1}).

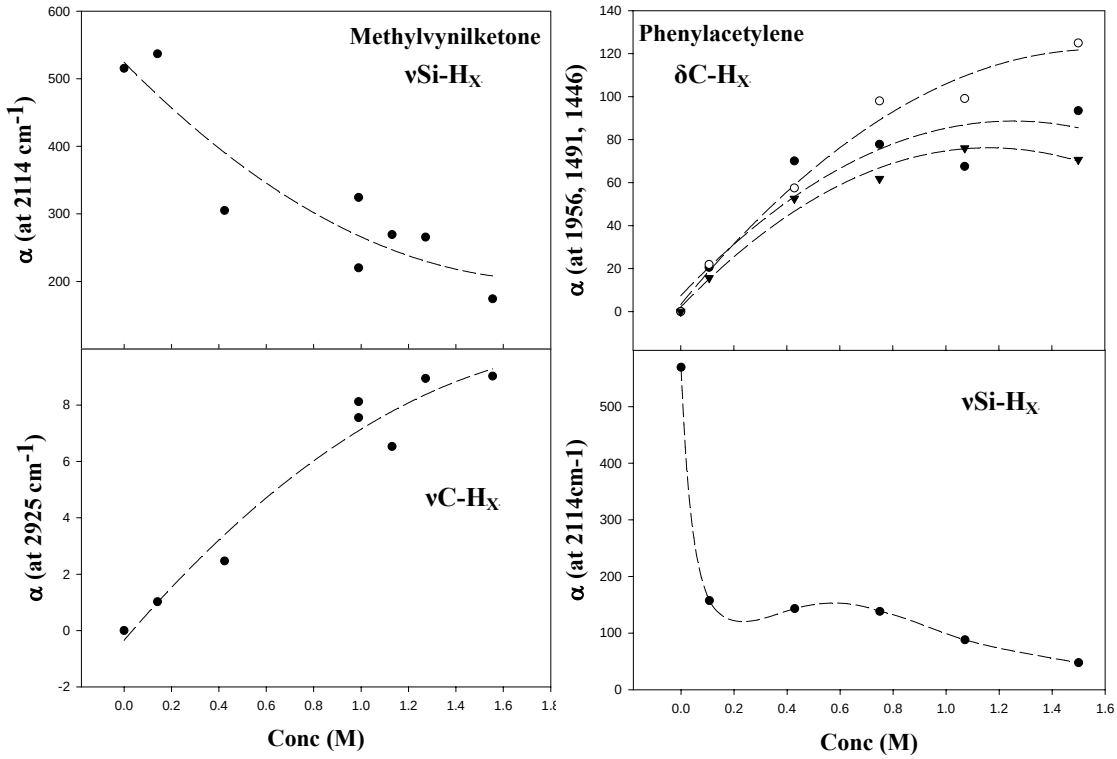

Fig. 3.32. Absorption coefficient, α_{CH}, in the C-H stretching region (at 2925 cm^{-1} down on the left), α_{CH}, in the C-H bending region (at 1956, 1491, 1446 cm^{-1} up on the right) and α_{SiH}, in the Si-H region (at 2114 cm^{-1}) as a function of the MVK (on the left) and Phenylacetylene (on the right) concentration, in the anodic solution. The dashed lines are a guide to the eye.

The adsorption coefficient related with the presence of functionalized organic molecules increases with the organic molecules concentration to the detriment of superficial Si-H species absorbing around 2114 cm^{-1} as in the 1-heptyne case (see Fig. 3.32a). We can also see in Fig. 3.33 porosity and thickness as a function of the concentration in the preparation solution of the methylvinylketone (MVK) and phenylacetylene.

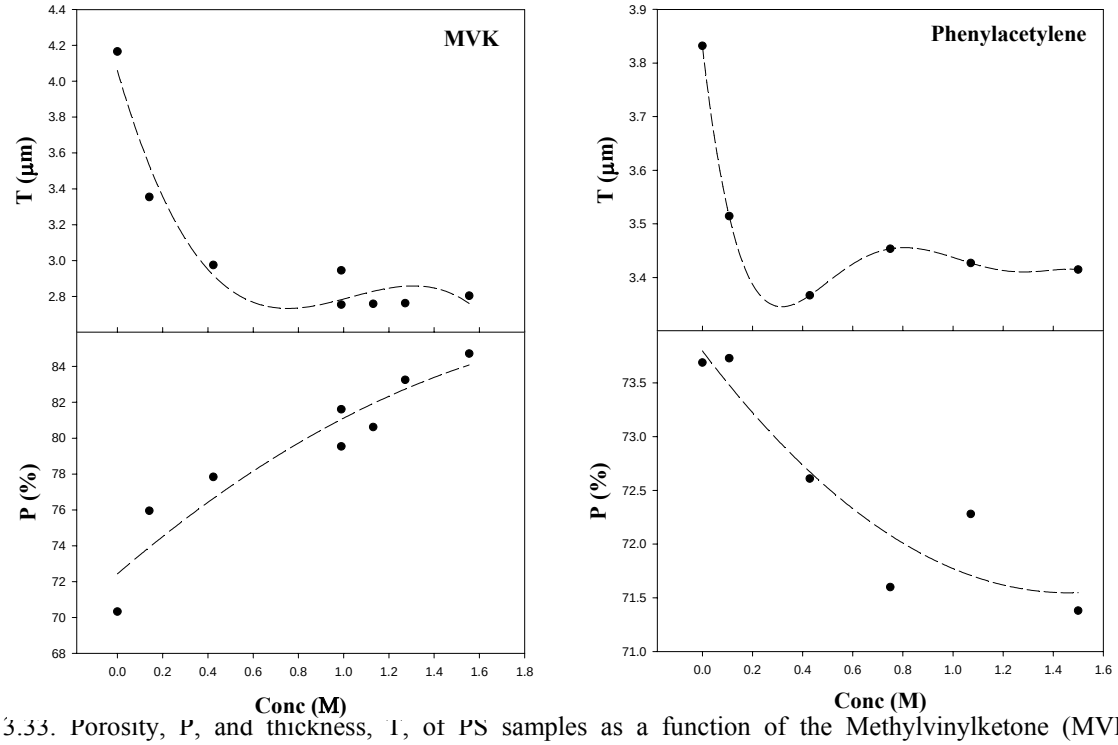

Fig. 3.33. Porosity, P, and thickness, T, of PS samples as a function of the Methylvinylketone (MVK) and phenylacetylene concentration, C, in the anodic preparation solution

These two molecules differently influence porosity and thickness of samples. In fact, in the case of phenylacetylene, thickness and porosity have a dependence on the organic molecule concentration like 1-heptyne, although with stronger effects, instead MVK has the same dependence of thickness on the organic molecule concentration but an inverse dependence of the porosity.

3.7 TWO STEPS FUNCTIONALIZATION OF PS SAMPLES

Our new functionalization method can functionalize the PS surface only using hydrofluoric acid resistant molecules with a carbon-carbon triple or double terminal bond but further studies have shown us that it is possible to extend the method to different organic molecules utilizing a two- or more-step process. The basic idea is to modify the organic molecule previously functionalized with our *in situ* method of preparation-functionalization of PS layers [94] in a different one of interest directly through a simple chemical reaction well known in solution, in order to make layers with predefined unique chemical and interfacial properties.

Modifications of covalently attached organic molecules on crystalline silicon [95 ÷ 99] and PS [43, 100, 101] are already known. Our two steps functionalization method of PS layers has a unique and very appealing feature: namely the possibility to confine the adsorbed species in

selected layers in a PS stack (or multi-layer PS system), i.e. only in those prepared in presence of the organic molecules and selectively modified by the second step chemical process.

As an example we report the case, studied by FTIR spectroscopy, of the modification of a methyl-6-heptynoate ($C_8H_{12}O_2$) chemisorbed in a PS single layer (first step *in situ* functionalization) to the corresponding tertiary alcohol by a thermal reaction with methyllitium in THF (second step). The results are here reported and discussed in detail.

The samples were prepared by the partial anodic dissolution of p^+ Si (100) wafers with resistivity 0.01 Ω cm in an electrochemical cell containing an HF(50%) – EtOH solution (1:2 by volume) and methyl-6-heptynoate (synthesized from the corresponding acid [102]) 1.5 M (first step). The current density (60mA/cm^2) and the etching time (100 s) were controlled by an AMEL model 549 galvanostat interfaced to a PC computer. For the experiments a set of mesoporous PS films of porosity (75%) and thickness (2.8 μm) were prepared. After this first step the functionalized samples were putted in contact with methyllitium (CH_3Li) 1 M in dry tetrahydrofurane (THF) for 15 minutes at RT. The samples after the anodization-functionalization were washed in water and ethanol, after the second step with ammonium chloride and pure ethanol.

The FTIR reflection spectra, measured after each step, were recorded in the range 400 - 5000 cm^{-1} with a resolution of 4 cm^{-1} using a BIORAD FTS – 40A spectrometer. The angle of incidence was fixed at 20°. To obtain more quantitative data all the measured spectra have been submitted to data reduction [103].

The IR reflection spectra of the same PS single layer, as prepared with the ester (full line) and after the transformation to the corresponding tertiary alcohol (dashed line) are shown in Figure 3.34.

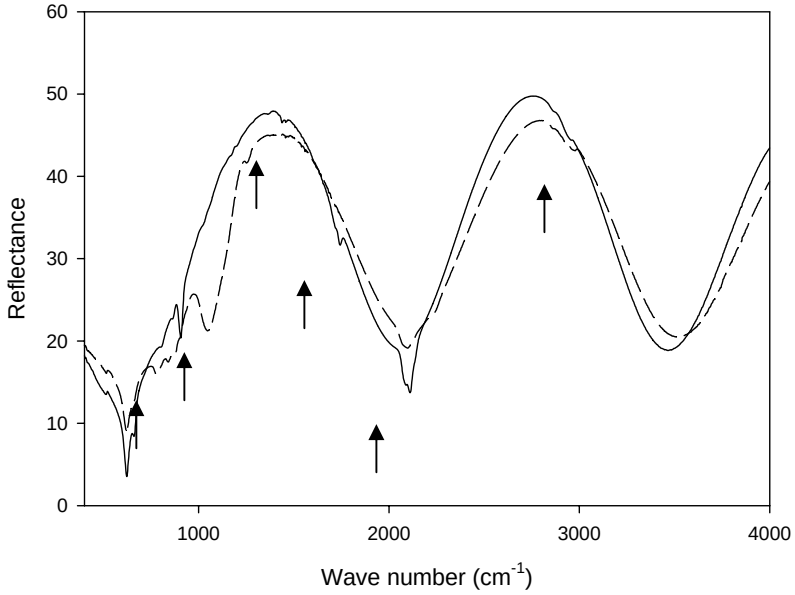

Fig. 3.34. FTIR reflection spectra of a PS film prepared with methyl-6-heptynoate (1.5 M) and after the reaction to the correspondent tertiary alcohol. The arrows indicate the frequencies of the Si-H_x bands and of the main methyl-6-heptenoate (full line) and dimethyl hepten alcohol bands (dashed line).

Apart from some oxidation, that will be discussed later, we can see the modifications in the νC-H_x, νC=O, νC=C, δC-H_x, δC-C regions: some bands disappear and some new bands appear in the spectra dominated by the interference. The arrows indicate the main bands in the spectra (3026, 2995, 2936, 2860 cm^{-1} νC-H_x; 1742, 1716 cm^{-1} νC=O, 1603 cm^{-1} νC=C, 1459, 1439, 1364, 1286 cm^{-1} δC-H_x, 865, 806, 773, 719 cm^{-1} δC-C) due to the presence of the ester in the first step and of the tertiary alcohol in the second one (2979, 2964, 2934, 2912, 2859 cm^{-1} νC-H_x; 1701 cm^{-1} νC=O, 1617 cm^{-1} νC=C, 1459, 1410, 1377, δC-H_x, 877, 843, 795, 777 cm^{-1} δC-C). The variations in the νC-H_x region are more clear in Fig. 3.35, where we can see that the νC-H_2 of the chain correctly remains also after the second step (2936-2934 cm^{-1} ν_{as} and 2860-2859 cm^{-1} ν_s) and two new bands due to the alcoholic C-H_3 stretching (2964 cm^{-1} ν_{as}, 2912 cm^{-1} ν_s) appear.

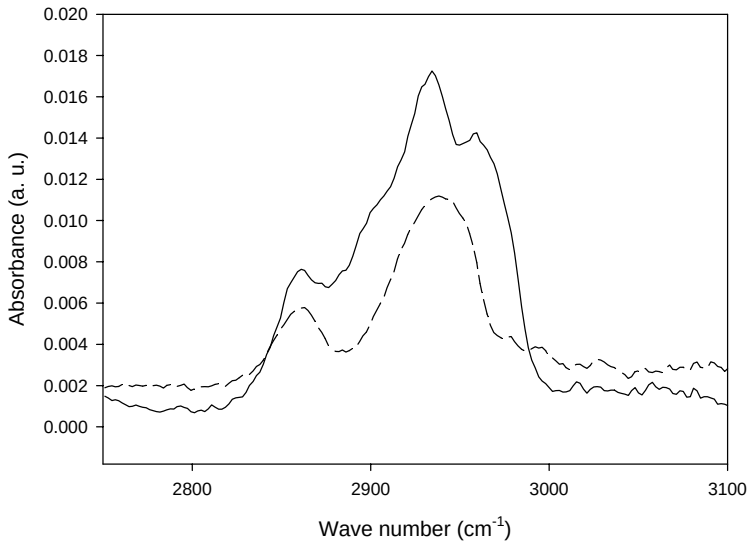

Fig. 3.35. FTIR spectra in the stretching region of the C-H_x species. The full line refers to the tertiary alcohol and the dashed line refers to the original ester.

In Fig. 3.36 we can note the disappearing of the C=O stretching of the ester (at 1742 cm^{-1}) and just a residue at low frequency (1701cm^{-1} due to a residual acidic portion generated during the anodization or to a portion of ester bonded to the surface trough hydrogen bond). The C=C stretching (1603 cm-1) remains but a little shifted at higher frequency (1617 cm^{-1}) for the oxidation of the silicon surface. Finally, in this figure we can see also the bending of the alcoholic O-H and C-H_3 (1410, 1377 cm^{-1}) characteristic of the transformation of the initial ester to the final tertiary alcohol.

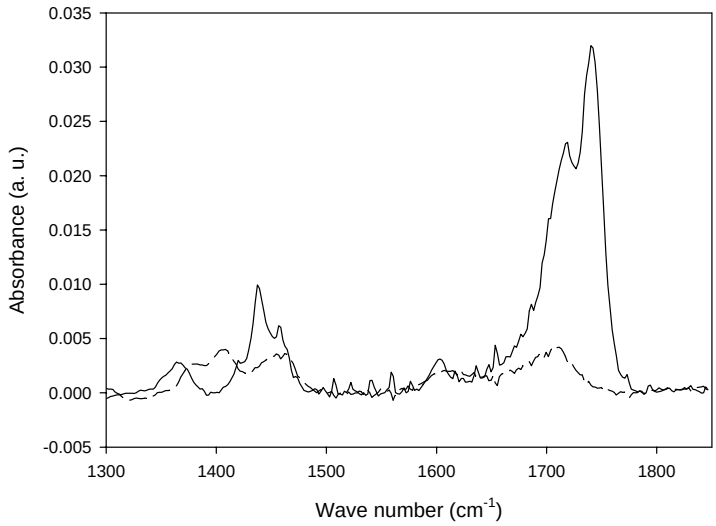

Fig. 3.36. FTIR spectra measured in the region of the C=O, C=C stretching and of the C-H_x bending. The full line represents the original ester and the dashed line the transformed alcohol.

Fig. 3.37 shows other two characteristic bands of the new bonded alcohol: the C-C stretching of the C $(CH_3)_2$ portion (at 843 cm^{-1}) and the O-H bending out of plane (773 cm^{-1}).

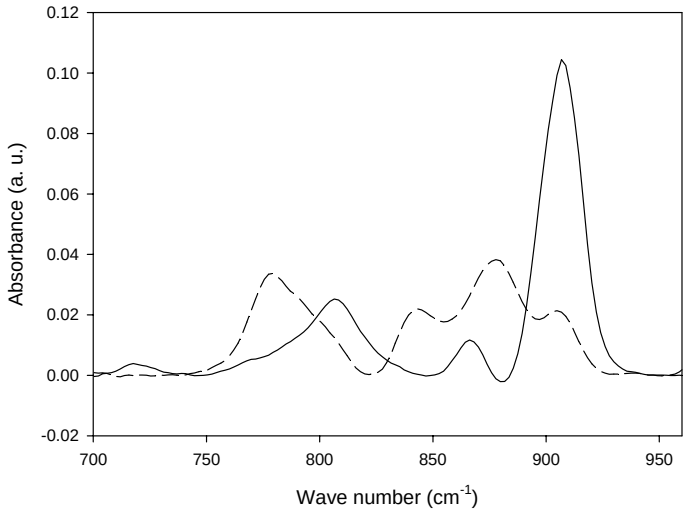

Fig. 3.37. Zoom in the bending region of the C-H_x species. The full line represents the original ester and the dashed line the just formed tertiary alcohol.

The frequency and the assignment of all the IR bands are summarized in Table 3.

Table 3. *.Assignements of the main IR bands related to the methyl-6-heptynoate (1st step) and the corresponding alcohol.*

Frequencies 1st step	**Frequencies 2nd step**	**Assignment**
3026	2979	
2995	2964	
2936	2934	$\nu C\text{-}H_x$
2860	2912	
	2859	
1742		$\nu C{=}O$
1716	1701	$\nu C{=}O$
1603	1617	$\nu C{=}C$
1459	1459	$\delta C\text{-}H_2$
1439	1410	$\delta O\text{-}H$
1364	1377	$\delta C\text{-}H_3$
1286		
	877	$\delta_{=}C\text{-}H$
865		$\delta_{=}C\text{-}H$
	843	$\nu C\text{-}C$ of $C(CH_3)_2$
806		$\nu C\text{-}C$
	795	$\nu C\text{-}C$
777	773	$\delta O\text{-Hoop}$
	719	$\delta_{=}C\text{-Hoop}$

Finally, the PS oxidation process accompanying the adsorbed organic molecules transformation deserves some discussion, considering that oxidation is always in competition with the functionalization process. As indicated in Fig.3.36, the oxidation manifests itself, after the second step (even if a little is already present after the first step) through the growth of a broad asymmetric band near 1100 cm^{-1}, due to the Si-O-Si vibrations. Further effects are the changes in the Si-H bands near 2100 cm^{-1}, the appearance of the $O_ySi\text{-}H_x$ stretching band at 2250 cm^{-1} and Si- H_x scissor band at 907 cm^{-1} that are done to the PS oxidation. The exposure of PS to air normally provokes a slow oxidation of the material [104, 105]. But the presence of a 20 % of

initial ester coverage avoids the complete surface oxidation process of PS sample. We attribute to the presence of the oxygen lone pair of the THF the main role in the promotion of the PS oxidation in presence of the water vapor and O_2 of the air (or some residual water on the PS pores). We cannot quantify all the bands around 1100 cm^{-1} because in this zone we have also the νC-O of the generated alcohol.

In conclusion this functionalization procedure, is simple, fast and quite effective indicated by the IR spectra, which showed species covalently functionalized and resist aut to washing with several solvents. This functionalization methodproved to be fast, being its duration shorter than few minutes, or even seconds, in contrast with other methods that need strictly several hours (i.e. the photochemical way). Another advantage of this method is that is not necessary to control the reaction ambient. Further advantage is the control of the sample oxidation, which is the main competitor in all the PS functionalization reactions. In fact, the presence of HF in the anodic solution allows to reduce the sample oxidation. The most important care to take is the use of anhydrous solvent during the washing procedure because the washing treatments increase a little the weak bands (e.g. around 1100 –1200 cm^{-1}) attributable to a little silicon oxidation.

The work is still in progress and is aimed to a better understanding of the mechanism of this new way of PS functionalization. Another important goal is to extend the method to other kind of organic molecules of interest, also in view of applications in the environment sensing field.

In summary, in this last part we have shown that functionalized PS films can be used as first step to derive an organic molecule with specific action ability.

There are also a number of chemical transformations on c-Si surface [95] that could be adapted for PS surfaces that will be the object of future investigations.

Conclusions

We have prepared under controlled conditions, good quality PS single layers and superstructures. On these systems different research topics strongly related to the subject of the theses, namely, the development and applications of PS materials in environmental sensing have been studied. The main subjects of research have been: i) the effect of the interaction between PS systems and the environment; ii) the functionalization of PS systems in view of application of PS in sensor technology. In conclusion, the main scientific results are summarized here:

Interaction of PS with the environment

- We have stressed the importance to know the behavior of our PS sensor in the ambient to be monitored and especially its ability to maintain unchanged these peculiar characteristics that determine its applicability. From here, being already known in literature the possibility of PS stabilization by the controlled oxidation, our study of the effects of the interaction, e. g. the consequent oxidation, of PS with various oxidizing atmospheres. We have prepared some mesoporous PS samples and then exposed at RT for predetermined times, to various oxidizing atmospheres, i.e. ambient air with saturated vapors of H_2O, Pyridine, Lutidine, Picoline, Ethylamine, Diethylamine and Triethylamine. The effects of the oxidizing process have been studied by reflectance FTIR "ex-situ" measurements. All the PS samples exposed to the various oxidizing atmospheres show a similar evolution also if with different time scales. Besides, the rate of the oxidizing process seems mostly influenced from the concentration in gaseous phase of the organic bases that catalyze the oxidative reactions in air in presence of H_2O rather than from their basic strength. These results can constitute the base of a work aimed to the fine control of the oxidative processes of PS layers obtaining in predefined times the desired oxidation degree and hence the desired factor of stabilization of the materials.
- We have verified that exists the real possibility of PS practical applications in the environmental sensor field by studying the PS interaction with saturated vapor of Urotropin. In fact, the experimental results showed us that our PS materials can be used as "dosimeter" for this toxic organic molecule commonly used in several application areas (e.g. rubber, explosives, fuel, pharmaceutical industries, etc.). The adsorption has been studied recording the time evolution of the IR absorption intensities of all the strongest urotropin bands in the case of PS single layer and of PS Fabry-Perot systems. The IR reflection spectra of PS single layer exposed to urotropin vapors show the increase with

the exposure time of the intensity of the bands of the adsorbed molecules. The enhancement of the absorption band intensity up to two orders of magnitude measured on one PS FP demonstrates that the urotropin adsorption involves the whole PS superstructure. Finally, the possibility of accumulating the urotropin in PS material with the increase of the exposure time and the very low desorption rate of the adsorbed species suggests a possible use of PS systems for the detection (e.g. as dosimeters) of urotropin vapor.

- We were able to detect, for the first time, a quite clear SFG signal in the spectral range of the Si-H_x stretching modes due to the native hydrogen present on the PS surface. The SFG signal due to the stretching of the OSi-H_x species, generated by the oxidation induced in air by the exposure to urotropin vapors, was also measured. From the measurements carried out we have seen a dependence of the signal related to the Si-H_x species as a function of the sample porosity showing a complex relation between the amount of the Si-H_x species presents on the whole surface of the sample and the intensity of the SFG related signal. Our results indicate that the outer air/PS interface is not the main source of the observed SFG signal. This finding indicates that a complete explanation of the results should include many effects: optical and structural as well. In any case, the results suggest that only a fraction of the surface hydrides species, likely located in special sites or pores of the PS material, are SFG active and contribute to the resonant part of the second order susceptibility. Besides, the kind of active species and their number should modify and increase with the change in the local morphology (e.g. pores enlargement, changes in the pore shape, thinning of the Si skeleton, etc.) associated with the increase of the porosity. Further work is necessary to better clarify this point. Moreover, using multilayer systems as FP, the data show that the SFG intensity can span one order of magnitude (an enhancement of the signal was already obtained in other optical spectroscopies: IR, Raman, SHG). Finally, a much higher enhancement (more than two orders of magnitude) could be expected for a suitable PS structure, as a FP, that could allow a simultaneous resonance with both the visible and SFG radiation.

PS Functionalization

- In literature the use of functionalized PS with biological organic species is known for applications in the biosensor field. Since the functionalization of PS systems with suitable organic molecules can provide new properties useful for application of PS in sensor

technology several standard procedures for the derivatization of PS have been preliminarily tested.

- With the aim to improve the effectiveness of these procedures a new method has been then devised and tested. This new method of "in-situ" formation with the simultaneous functionalization of PS layers, being the molecules to be chemisorbed presents in the preparation solution, is simple, fast and effective. We have first tested the method with a simple organic molecule such as the 1-heptyne highlighting the characteristics of this new methodology and of the samples functionalized by thi procedure. These results indicate an evident inverse correlation, between the surface abundance of the chemisorbed molecules and that of the silicon hydride species. From the relative decrease of the integrated intensities of the Si-H absorption signal the average efficiency of the functionalization process can be evaluated. In this case we found values as high as 50-60%. The chemical species interact with the Si atoms on the sample surface and modify slightly the PS morphology. These little variations of porosity and thickness are not a problem for the sample preparation since it is possible to use "calibration" curves to design and prepare PS layers having the desired morphological properties and amount of functionalization. Experiments demonstrate that it is essential the presence of the organic molecules in the solution and the current flow occurring during the electrochemical formation of the PS material for the effectiveness of this functionalization method. The sample oxidation is naturally limited during the formation for the presence of HF in the anodic solution; and after the functionalization because of the partial coverage of the PS surface with bounded organic molecules. In fact one method to limit the natural PS oxidation in air is the coverage of the surface by capping. Indeed our ageing measurements demonstrate a strong reduction (up to 60 %) of the oxidation in air for the functionalized PS samples.
- We have shown that our method has a unique and very appealing feature, namely the possibility to confine the adsorbed species in selected layers in a PS stack (or multi-layer PS system), i.e. e. only in those prepared in presence of the organic molecules. The results of several experiments demonstrate directly or indirectly this property. Among them we can enumerate: FTIR reflectance spectra of PS structures; gray-scale analysis of SEM pictures of the cross section of single layers and FP PS systems; and finally by field emission SEM microanalysis of some three layers PS structures. The confinement of the chemisorbed species in a layer inside a stack of PS layers can be achieved with very low contamination of the other layers ($\leq$ 1-2 % of the coverage in the functionalized layer).

- Our PS functionalization method has been then applied also to other organic molecules obtaining clear indications of applicability. In general, molecules with triple C≡C bonds are more efficient than molecule with double C=C bonds. Internal triple and double bonds do not work. Terminal double bonds work better if conjugated. Probably, the steric parameters and the geometry of the molecules that we want functionalize strongly influence their functionalization ability. As an example, we have reported with some detail the functionalization of Methylvinylketone (MVK) and Phenylacetylene.
- Further work made us able to extend the functionalization process to different organic molecules (even not fluoridic acid resistant and/or without a triple or double carbon-carbon terminal bond), utilizing a two or more steps process. As an example we reported the case, studied by FTIR spectroscopy, of the modification of a methyl-6-heptynoate ($C_8H_{12}O_2$) chemisorbed in a PS single layer (first step *in situ* functionalization) to the correspondent tertiary alcohol by a thermal reaction with methyllitium in THF (second step). In conclusion this new PS functionalization method allows to exploit its localization peculiarity to generate PS sensors of new design and even new PS multisensor devices.

In conclusion, we have verified that PS material could match the main requirements of a good sensor, i.e.: i) response reproducibility, that implies also the material time stability; indeed the controlled oxidation or the protection by chemisorbed species against the oxidation provide a tool towards a better stability of the material; ii) sensibility: we demonstrated that with PS FP systems the response signal obtained increase of two or more orders of magnitude; iii) specificity: the functionalization of PS systems with suitable organic molecules could provide some specificity to the sensor (e. g. using the interaction antigen/antibody).

Finally, we have proposed a practical application of our PS samples in the environmental sensor field, namely, as a dosimeter for urotropin (a toxic molecule used in several application areas, e.g. rubber, explosives, fuel, pharmaceutical industries, etc.) vapors.

References

[1] *Property of Porous Silicon*, Edited by Canham, EMIS Data reviews series N°18:

(a) CAP. 2.2, R. Hérino, **1997**, 89 **π** 96.

(b) CAP. 2.1, L. T. Canham, **1997**, 83 **π** 88.

(c) CAP. 1.2, A. Halimaoui, **1997**, 12 **π** 22.

(d) CAP. 1.5, D. Bellet, **1997**, 38 **π** 43.

(e) CAP. 1.6, L. T. Canham, **1997**, 44 **π** 49.

(f) CAP. 1.7, A. Loni, **1997**, 51 **π** 58.

(g) CAP. 1.1, P. Allongue, **1997**, 3 ÷ 11.

(h) CAP. 1.8. J.-N. Chazalviel and F. Ozanam, **1997**, 59 **π** 65.

(i) CAP. 1.9. R. Hérino, **1997**, 66 **π** 76.

(j) CAP. 12.7, P. Menna and S. Tsuo, **1997**, 384 **π** 389.

(k) CAP. 12.5, L. T. Canham, **1997**, 371 **π** 376.

[2] L. Pavesi, L. Dal Negro, C. Mazzoleni, G. Franzò and F. Priolo, *Nature*, 408, 440 **π** 444, **2000**.

[3] J. M. Buriak, *Chem. Commun*., **1999**, 1051 **π** 1060.

[4] J. M. Buriak, *Advanced Materials*, 11 (3), **1999**, 265 **π** 267.

[5] M. P. Stewart and J. M. Buriak, *Angew. Chem. Int. Ed*., 37 (23), **1998**, 3257 **π** 3260.

[6] M. Born and E. Wolf, "*Principles of Optics*" Electromagnetic Theory of Propagation, Interference and Diffraction of Light, fifth edition **1975**, Pergamon Press, CAP. 7.

[7] V. Mulloni, Z. Gaburro and L. Pavesi, *Phys. Stat. Sol.* (a) 182 (**2000**), 479.

[8] G. Mattei, V. Valentini, V. A. Yakovlev, *Surf. Sci.* 502-503 (**2002**), 58-62.

[9] D. R. Turner, *J. Electrochem. Soc*. 105 (**1958)**, 402.

[10] H. Gerischer, P. Allongue and V. Costa Kieling, *Ber. Bunseuges Phys. Chem.* 97 (**1993**) 753-757.

[11] C. Pickering, M. I. J. Beale, D. J. Robbins, P. J. Pearson and R. Geef, *J. Appl. Phys.* 17 (**1984**), 6535.

[12] L. T. Canham, *Appl. Phys. Lett.* 57 (**1990**), 1046.

[13] J.C . Vial and J. Derrien (Editors), *Porous Silicon Science and Technology*, Springer-Verlag, Berlin Heidelberg and Les Editions de Paris, Les Ulis, **1995**.

[14] *Advances in Microcrystalline and Nanocrystalline Semiconductors*, Materials research society symposium proceedings, volume 452, **1996**.

[15] Z.C. Feng and R. Tsu (Editors), *Porous Silicon*, World Scientific, Singapore, **1994**.

[16] *Surface/Interface and Stress Effects in Electronic Material Nanostructures*, Materials research society symposium proceedings, volume 405, **1995**.

[17] *Porous Semiconductors Science and Technology*, Materials of the 2nd International Conference, Madrid 12 ÷ 17 March **2000**.

[18] R. L. Smith and S. D. Collins, *J. Appl. Phys.* 71 (**1992**) R 1.

[19] V. P. Parkhutik, 301-328, Z.C. Feng and R. Tsu (Editors), *Porous Silicon*, World Scientific, Singapore, **1994.**

[20] G. C. Lohn and V. A. Singh, *Physical Review B* 52 (15), **1995**, 11125-11130.

[21] V. Lehmann and U. Gösele, *Appl. Phys. Lett.* 58 (8), 25 February **1991**,856-858.

[22] A. Valance, *Physical Review B* 52 (11), **1995**, 8323-8336.

[23] A. Valance, *Physical Review B* 55 (15), **1997**, 9706-9715.

[24] L. N. Aleksandrov and P. L. Novikov, JETP Lett. 65 (9), 1997, 714-719.

[25] M. I. J. Beale, J. D. Benjamin, J. Uren, N. G. Chew, A. G. Cullis, *J. Cry. Growth (Netherlands)*, vol. 73, **1985**, 622.

[26] A. Halimaoui, *Appl. Phys. Lett.* (USA) 63 (**1993**), 1264.

[27] A. Halimaoui, *Surf. Sci. Lett.* (Netherlands) 306 (**1994**), L550-4.

[28] M. Thönissen, M. G. Berger, W. Thei**b**, S. Hilbrich, M. Krüger, R. Arens-Fischer, S. Billat, G. Lerondel and H. Lüth, 431-436, *Advances in Microcrystalline and Nanocrystalline Semiconductors*, Materials research society symposium proceedings, Vol. 452.

[29] L. T. Canham, A. G. Cullis, C. Pickering, O. D. Dosser, T. I. Cox, T. P. Lynch, *Nature (UK)*, vol. 368 (**1994**), 133.

[30] St. Frohnhoff, R. Arens-Fischer, T. Heinrich, J. Fricke, M. Arntzen, W. Theiss, *Thin Solid Films (Switzerland)*, vol. 255 (**1995)**, 115.

[31] J. Von Behren, P. M. Fauchet, E. H. Chimowitz, C. T. Lira, *Mater. Res. Soc. Symp. Proc. (USA)*, vol 452, **1997**, 565.

[32] U. Grüning, A. Yenon, *Thin Solid Films(Switzerland)*, vol. 255, **1995**, 135.

[33] G. Amato, V. Bullara, N. Brunetto, L. Boarino, *Thin Solid Films(Switzerland)*, vol. 276, **1996**, 204; G. Amato, N. Brunetto, *Mater. Lett. (Netherlands)*, vol. 26, **1996**, 295.

[34] D. Bellet, G. Dolino, *Phys. Rev. B (USA)*, vol. 50 (**1994)**, 17162.

[35] V. Pellegrini et al., *Appl. Phys. Lett. (USA)*, vol. 67 (**1995**), 1084.

[36] F. Ozanam, J. N. Chazalviel, *J. Electroanal. Chem. Interfacial Electrochem. (Swtzerland)*, vol. 269 (2), **1988**, 251 ÷ 266.

[37] K. H. Li, C. Tsai, J. C. Campbell, M. Kovar, J. M. White, *J. Electron. Mater. (USA)*, vol. 23 (**1994**), 409.

[38] S. Letant, J. C. Vial, *J. Appl. Phys. (USA)*, vol. 80 (12), **1996**, 7018-7022.

[39] F. Ozanam, J. N. Chazalviel, R. B. Wehrspohn, *Thin Solid Films(Switzerland)*, vol. 297 (**1997**), 53 ÷ 60.

[40] L. G. Earwaker, M. C. Briggs, M. I. Nasir, J. P. G. Farr, J. M. Keen, *Nucl. Instrum. Methods B (Netherlands)*, vol. 56/57 (**1991**), 855 ÷ 859.

[41] A. Loni, A. J. Simons, P. D. J. Calcott, J. P. Newey, T. I. Cox, L. T. Canham, *Appl. Phys. Lett. (USA)*, 71 (1), **1997**, 107 **π** 109.

[42] A. Halimaoui, Lecture 3, 33-52, *Porous Silicon Science and Technology*, Editors J-C.Vial & J.Derrien, Centre de Physique Les Houches.

[43] S. Chan, P. M. Fauchet, Y. Li, L. J. Rothberg, B. L. Miller, *Phys. Stat. Sol. (a)* 182 (**2000**), 541.

[44] O. Bisi, S. Ossicini, L. Pavesi, *Surf. Sci. Rep.*, **264**, 1-126 (2000).

[45] A. G. Cullis, L. T. Canham and P. D. J. Calcott, *Appl. Phys. Rev*. **82** (3), 909-965 (1997)

[46] G. Mattei, A. Marucci, V. A. Yakovlev, *Mat. Sci. And Engineering* B 51 (**1998**), 158 **π** 161.

[47] L.A.Kuzik, V.A.Yakovlev, G.Mattei. *Appl. Phys. Lett.* 75(13),1830-1832, **1999**.

[48] I. Schechter, M. Ben-Chorin and A. Kux, *Anal. Chem*., 67 (**1995**), 3727 **π** 3732.

[49] L. Boarino, C. Baratto, E. Garrone, F. Geobaldo, G. Amato, E. Comini, A. M. Rossi, G. Faglia, G. Sberveglieri, *Porous Semicondactors Science and Technology*, Materials of the 2-nd International Conference Madrid, 12-17 March, O-35 (**2000**), 96 **π** 98.

[50] L. Quercia, F. Cerullo, V. La Ferrara, G. Di Francia, C. Baratto and G. Faglia, *Phys. Stat. Sol*. (a) 182 (**2000**), 473.

[51] H. Arwin, M. Gavutis, J. Gustafsson, M. Schultzberg, S. Zangooie and P. Tengvall, *Phys Stat. Sol*. (a) 182 (**2000**), 515.

[52] A. Rosengren, L. Wallman, M. Bengtsson, Th. Laurell, N. Danielsen and L. M. Bjursten, *Phys. Stat. Sol*. (a) 182 (**2000**), 527.

[53] A. H. Mayne, S. C. Bayliss, P. Barr, M. Tobin and L. D. Buckberry, *Phys. Stat. Sol*. (a) 182 (**2000**), 505.

[54] S. Uehara, K. Kurose and T. Matsubara, *Phys. Stat. Sol*. (a) 182 (**2000**), 461.

[55] S. P. Duttagupta, S. K. Kurinec and P. M. Fauchet, *Advances in Microcrystalline and Nanocrystalline Semiconductors*, Mat. Res. Soc. Symp. Proc., vol. 452 (**1997**), 625 **π** 630.

[56] P. Menna, G. Di Francia, V. La Ferrara, *Sol. Energy Mater. Sol. Cells (Netherlands)*, vol. 37 (**1995**), 13 **π** 24.

[57] S. Hasegawa, K. Maehashi, H. Nakashima, T. Ito, A. Hiraki, *J. Cryst. Growth (Netherlands),* vol. 95 (**1989**), 113 **π** 116.

[58] K. Maehashi, M. Sato, S. Hasegawa, H. Nakashima, T. Ito, A. Hiraki, *Jpn. J. Appl. Phys. (Japan)*, vol. 30 (**1991**), L683 **π**L685.

[59] A. Prasad, S. Balakrishnan, S. K. Jain, G. C. Jain, *J. Electrochem. Soc. (USA)*, vol. 129 (**1982**), 596 **π** 599.

[60] S. Strehle, D. sarti, A. Kotkus, K. Grigoras, C. Lévy-Clément, *Thin Solid Films (Switzerland)*, vol. 297 (**1997**), 291 **π** 295.

[61] L. Schirone, G. Sotgiu, F. P. Califano, *Thin Solid Films (Switzerland)*, vol. 297 (**1997)**, 296 **π** 298.

[62] G. Sun, Y. Li, Y. Lu, B. Khan, G. S. Tompa, *Mat. Res. Soc. Symp. Proc. (USA)*, vol. 358 (**1995**), 593 **π** 598.

[63] D. B. Mawhinney, J. A. Glass, Jr., and J. T. Yates,Jr., *J. Phys. Chem. B* 101 (**1997**) 1202.

[64] W. Theiss, *The SCOUT Through CHAOS*, Manual of the Windows application SCOUT, Hard and Software for Optical Spectroscopy, Aachen (Germany) **1998**.

[65] Y. Ogata, H. Niki, T.Sakka and M. Iwasaki*, J. Electrochem. Soc*. 142 (**1995**) 1595.

[66] D. Gräf, M. Grundner and R. Schulz, *J. Vac. Sci. Technol.. A* 7 (**1989**) 808.

[67] E. P. Boonekamp, J. J. Kelly, J. Van de Ven and A. H. M. Sondag, *J. Appl. Phys*. 75 (**1994**) 8121.

[68] G. Mattei, E. V. Alieva, J. E. Petrov, and V. A. Yakovlev, *Phys. Stat. Sol. (a)* 182 (**2000**) 139.

[69] *Handbook of Chemistry and Physics*, 58th edition **1977-1978**, crc press.

[70] E. P. Hunter and S. G. Lias, Evaluated Gas Phase Basicities and Proton Affinities of Molecules: An Update, *J. Phys. Chem. Ref. Data*, **1998**, 27, 3, 413.

[71] G. Mattei, E.V. Alieva, J.E. Petrov and V.A. Yakovlev, *Surf. Sci*. 427-428, 235 (**1999**).

[72] V.A. Yakovlev, V. Valentini and G. Mattei, *Phys. Stat. Sol*. 197 (1), 158-162, **2003**.

[73] N. Bloembergen and P. S. Pershan, *Phys. Rev.* 128, 606 – 622, **1962**.

[74] P. Guyot-Sionnest, J. H. Hunt and Y. R. Shen, *Phys. Rev. Lett.* 59, 1597 – 1600, **1987**.

[75] T. V. Dolgova, A. I. Maidykovski, M. G. Martemyenov, A. A. Fedyanin, O. A. Aktsipetrov, G. Marowsky, V. A. Yakovlev, G. Mattei, *Appl. Phys. Lett.* 81 (15), 2725-2727, **2002**.

[76] A. A. Mani, L. Dreesen, Ph. Hollander, C. Humbert, Y. Caudano, P. A. Thiry, A. Peremans, *Appl. Phys. Lett.* 79, 1945, **2001**.

[77] G. Mattei, V. Valentini, V. A. Yakovlev, A. A. Mani, Y. Sartenaer, P. A. Thiry, A. Peremans, Y. Caudano, L. Dreesen, B. Busson, F. Vidal, C. Humbert and A. Tadjeddine, accepted for publication on *Phys. Stat. Sol.* (2005).

[78] Y. R. Shen, *The Principles of Nonlinear Optics* (John Wiley & Sons, USA, 1984), chap. 6.

[79] C. H. de Villeneuve, J. Pinson, M. C. Bernard, P. M. Allongue, *J. Phys. Chem. B.* 101 (**1997**) 2415.

[80] Allongue, P.; de Villeneuve, C. H.; Pinson, J.; Ozanam, F.; Chazaviel, J. N.; Wallart, X. *Electrochim. Acta* **1998**, 43, 2791 – 2798.

[81] Robins, E. G.; Stewart, M. P.; Buriak, J. M. *Chem. Com.* **1999**, 2479 – 2480.

[82] Gurtner, C.; Wun, A. W.; Sailor, M. J. *Angew. Chem. Int. Ed.* 38 (13-14), **1999**, 1966 - 1968.

[83] F. Ozanam, C. Vieillard, M. Warntjes, T. Dubois, M. Pauly, J.-N. Chazalviel, *The Can. J. Chem. Eng.* 76, **1998**, 1020 – 1026.

[84] M. R. Linford, C. E. D. Chidsey, *J. Am. Chem. Soc.* 115 (**1993**) 1263.

[85] M. R. Linford, P. Fenter, P. M. Eisenberger, C. E. D. Chidsey, *J. Am. Chem. Soc.* 117 (**1995**) 3145.

[86] F. Effenberger, G. Gotz, B. Bidlingmaier, M. Wezstein, *Angew. Chem. Int. Ed. Engl.* 37 (**1998**) 2462.

[87] A. B. Sieval, A. L. Demirel, J. W. M. Nissink, M. R. Linford, J. H. van der Maas, W. H. de Jeu, H. Zuilhof, E. J. R. Sudhölter, *Langmuir* 14 (**1998**) 1759.

[88] Bansal, A.; Li, X.; Lauerman, I.; Lewis, N. S. *J. Am. Chem. Soc.* **1996**, 118, 7225 – 7226.

[89] A. B. Sieval, V. Vleeming, H. Zuilhof, E. J. R. Sudhölter, *Langmuir* 15 (**1999**) 8288 - 8291.

[90] Bateman, J.E.; Eagling, R. D.; Worall, D. R.; Horrocks, B. R.; Houlton, A. *Angew. Chem., Int. Ed.* **1998**, 37, 2683 – 2685.

[91] A. B. Sieval, R. Opitz, J. H. van der Maas, M. G. Schoeman, G. Meiler,. F. J. Vergeldt, H. Zuilhof, E. J. R. Sudhölter, *Langmuir* 16 (**2000**) 10359 - 10368.

[92] J. M. Holland, M. S. Stewart, M. J. Allen and J. M. Buriak, *J. of Solid State Cemistry* 147, **1999**, 251.

[93] Buriak, J. M.; Stewart, M. P.; Geders, T. W.; Allen, M. J.; Choi, H. C.; Smith, J.; Raftery, D.; Canham, L. T. *J. Am. Chem. Soc. 121*, 11491, **1999.**

[94] G. Mattei, V. Valentini, *J. Am. Chem. Soc.* **125**, 9608-9609 (2003**)**.

[95] P. Wagner, S. Nock, J. Spudich, W. D. Volkmuth, S. Chu, R. L. Cicero, C. P. Wade, M. R. Linford, C. E. D. Chidsey, *J. Struct. Biol.* **119**, 189 (1997).

[96] R. Boukherroub, D. M. Wayner, *J. Am. Chem. Soc.* **121**, 11513 (1999).

[97] A. B. Sieval, R. Linke, H. Zuilhof, E. J. R. Sudhölter, *Adv. Mater.* **12**, 1457 (2000).

[98] T. Strother, R. J. Hamers, L. M. Smith, *Nucleic Acids Research* **28**(18), 3535 (2000).

[99] B. Fabre, G. P. Lopinski, D. M. Wayner, *Chem. Comm.* 2904 (2002).

[100] Buriak, J. M. *Chem. Rev*. **102**, 1272 (2002).

[101] K.-P. S. Dancil, D. P. Greiner, M. J. Sailor, *J. Am. Chem. Soc.* **121**, 7925 (1999).

[102] A. B. Sieval, A. L. Demirel, J. W. M. Nissink, M. R. Linford, J. H. van der Maas, W. H. de Jeu, H. Zuilhof, E. J. R. Sudhölter, *Langmuir* **14**, 1759 (1998).

[103] W. Theis, *Surf. Sci. Rep.* **29**, 91 (1997).

[104] J. Salonen, V.P. Lehto and E. Laine, *Appl. Surf. Sci.* **120**, 191 (1997).

[105] Y.H. Ogata T. Tsuboi, T. Sakka and S. Naito, *J. Por. Mater.* **7**, 63 (2000).

ANNEXES

A. Crystalline Si: general information and properties

In the A part of this annex we report some general information and properties of the crystalline Si.

Chemical Formula	Si
Crystal Class	Cubic
Dielectric Constant for $9.37*10^{9}$ Hz	13
Melting Point, K	1690
Thermal Conductivity, W/(m K) at 125 K at 313 K At 400 K	 598.6 163 105.1
Thermal Expansion, l/K at 75 K at 293 K At 1400 K	 $-0.5*10^{-6}$ $2.6*10^{-6}$ $4.6*10^{-6}$
Specific Heat, cal/(g K) at 298 K At 1800 K	 0.18 0.253
Debye Temperature, K	640
Band gap, eV	1.1
Solubility in water	None
Knoop Hardness, Kg/mm^2	1100
Mohs Hardness	7
Young's Modulus, GPa	130.91
Shear Modulus, GPa	79.92
Bulk Modulus, GPa	101.97
Poisson's Ratio	0.28

Refractive Index

Silicon is commonly used as substrate material for infrared reflectors and windows in the 1.5-8 micron region. The strong absorption band at 9 microns makes it unsuitable for CO_2 laser transmission application, but it is frequently used for laser mirrors because of its high thermal conductivity and low density. Silicon is also useful as a transmitter in the 20 micron range.

Wavelength, μm	Refractive Index
1.40	3.49
1.50	3.48
1.66	3.47
1.82	3.46
2.05	3.45
2.50	3.44
3.50-5.00	3.43
6.00-25.00	3.42

Crystalline Si Chemical Properties

Atomic Weight	28.0855
Isotopes 28 29 30	 92.23% 4.67% 3.10%
Atomic Number	14
Atomic Radius	177 pm (covalent bond)
Ionic Radius	40 pm
Density (solid)	2.33 g/cm^3
Density (liquid)	2.53 g/cm^3
Atomic Density	4.995e22 atoms/cm^3
Atoms per unit cell	8
Crystal Structure	Diamond
Density of surface atoms	

(100) (110) (111)	6.78e14/cm^2 9.59e14/cm^2 7.83e14/cm^2
Lattice Constant	5.431 Å
Bond Length	2.36 Å

Crystalline Si Mechanical Properties

Coefficient of Thermal Linear Expansion	2.6e-6/K
C11	165.7 GPa
C12	63.9 GPa
C44	79.6 GPa
Thermal Conductivity (solid)	1.412 W/cm-K
Thermal Conductivity (liquid)	4.3 W/cm-K
Specific Heat	0.70 J/g-K
Thermal Diffusivity	0.9 cm^2/s
Melting Point	1683 K
Boiling Point	2628 K
Critical Temperature	5159 K
Vapor Pressure at 1050 °C at 1250 °C	 1e-7 Torr 1e-5 Torr
Molar Heat Capacity	20.00 J/mol-K
Average Energy Loss per phonon scattering	0.063 eV
Optical phonon free path Electrons Holes	 6.2 nm 4.5 nm

A good reference paper on the elastic constants for some semiconductors is the following: W. A. Brantley, J. Appl. Phys. 44 (1), 534, 1973.

Crystalline Si Electrical Properties

Relative Permittivity	11.7
Permittivity	1.04e-10 F/m
Band Gap at 0 K	1.124 eV 1.170 eV
Temperature Dependence of band gap	-2.3e-4 eV/K
n Mobility	1350 (cm/s)/(V/cm)
p Mobility	480 (cm/s)/(V/cm)
Field breakdown	3e7 V/m
Work function (intrinsic)	4.15 eV
Intrinsic carrier concentration (rt)	1.45e10 carriers/cm^3
Effective Density of States, conduction band	3.22e19/cm^3
Effective Density of States, valence band	1.83e19/cm^3
Effective mass (electrons)	0.26 M0
Effective mass (holes)	0.38 M0
Atomic density	4.995e22 atoms/cm^3
Intrinsic Debye length	24 μm
density of surface atoms (100) (110) (111)	 6.78e14/cm^2 9.59e14/cm^2 7.83e14/cm^2
Intrinsic Resistivity	2.3e5 **W**-cm

Ionization Energies for Various Dopants

Donors	**Acceptors**
Sb 0.039 eV	B 0.45 eV
P 0.045 eV	Al 0.067 eV
As 0.054 eV	Ga 0.072 eV
	In 0.16 eV

Solutions for Polishing Etches

80 μm/min

- 3 ml HF
- 5 ml HNO_3
- 3 ml Glacial Acetic Acid

Planar Etch 3 μm/min

- 2 ml HF
- 15 ml HNO_3
- 3 ml Glacial Acetic Acid

Almost neutral etch 0.7 μm/ min

- 10 ml H_2O_2
- 3.7 g NH_4F
- 2 ml HF
- 1 ml $KMnO_4$

0.3-0.4 μm/min

- 50 ml HF
- 100 ml HNO_3
- 150 ml Glacial Acetic Acid
- 3 g Iodine

Buffered Etches for SiO_2

Buffered oxide etch (BHF) 1000-2500 Å/min at 25 °C

- 28 ml HF
- 113g NH_4F
- 170 ml deionized H_2O

Slow BHF 800 Å/min at 25 °C

- 1 ml BHF
- 7 ml deionized H_2O

P-etch 128 Å/min at 25 °C

- 15 ml HF
- 10 ml HNO_3
- 300 ml deionized H_2O

Crystallographic Etches for Si

Dash Etch, 8h

Sirtl Etch for Si (111)

- 1 ml HF
- 1 ml HNO_3

1 ml HF

1 ml Chromium Trioxide (5 molar in water)

- 10 ml Glacial Acetic Acid

Secco etch for (100) and (111) Si, 5 min

- 2 ml HF
- 1 ml K Chromate (0.15 molar in water)

Wright Etch for (100) and (111) Si, 5 min, long shelf life

- 60 ml HF
- 30 ml HNO_3
- 60 ml Glacial Acetic Acid
- 60 ml deionized H_2O
- 30 ml of solution of 1 g K Chromate in 2 ml of H_2O
- 2 g $(CuNO_3)_2$*$3H_2O$

Silver Etch, for faults in Epitaxial layers

- 2 ml HF
- 1 ml HNO_3
- 2 ml $AgNO_3$ (0.65 molar in water)

For p-n junction delineation, 1 min

- 200 ml HF
- 1 ml HNO_3

Cleaning Solutions

Organic Cleaning

- Hot Trichloroethylene or Xylene
- Mechanical Scrubbing, ultrasonic, gas jets

Rinse in hot deionized water

Solution1; 10-20 min at 80 °C agitated (N_2)

- 1 ml NH_4OH
- 1 ml H_2O_2
- 5-7 ml deionized water

Solution 2; 10-20 min at 80 °C agitated (N_2)

- 1 ml HCl
- 1-2 ml H_2O_2
- 6-8 ml deionized water

Silicon Dioxide (SiO_2)

Properties

Crystal structure	Amorphous
Atomic Weight	60.08
Thermal Conductivity	0.014 W/cm-K
Thermal Diffusivity	0.006 cm^2/s
Relative Dielectric Constant	3.9
Index of Refraction	1.46
Dielectric Constant	3.45e-11 F/m
Breakdown field	6e8 V/m
Atomic Density	2.27e22 molecules/cm^3
Density (dry oxide)	2.27 g/cm^3
Energy Gap	~9 eV
Specific Heat	1.0 J/g-K
Melting Point	~1700 °C
Coefficient of Thermal Expansion	5e-7/K
Electronic affinity	1.0 eV

Etchants

Buffered HF

- 49% HF
- NH_4F
- Deionized H_2O

B. Raman Spectroscopy

The quantum theory considers the monochromatic electromagnetic radiation of frequency ν_0 as constituted by a flow of particles called photons having energy $h\nu_0$, where h is the Planck constant. When a light beam passes through a surface inside a medium, part of the photons will be subjected to elastic collisions with the matter (Rayleight scattering) and a part to inelastic collisions (Raman scattering), Fig. B1.

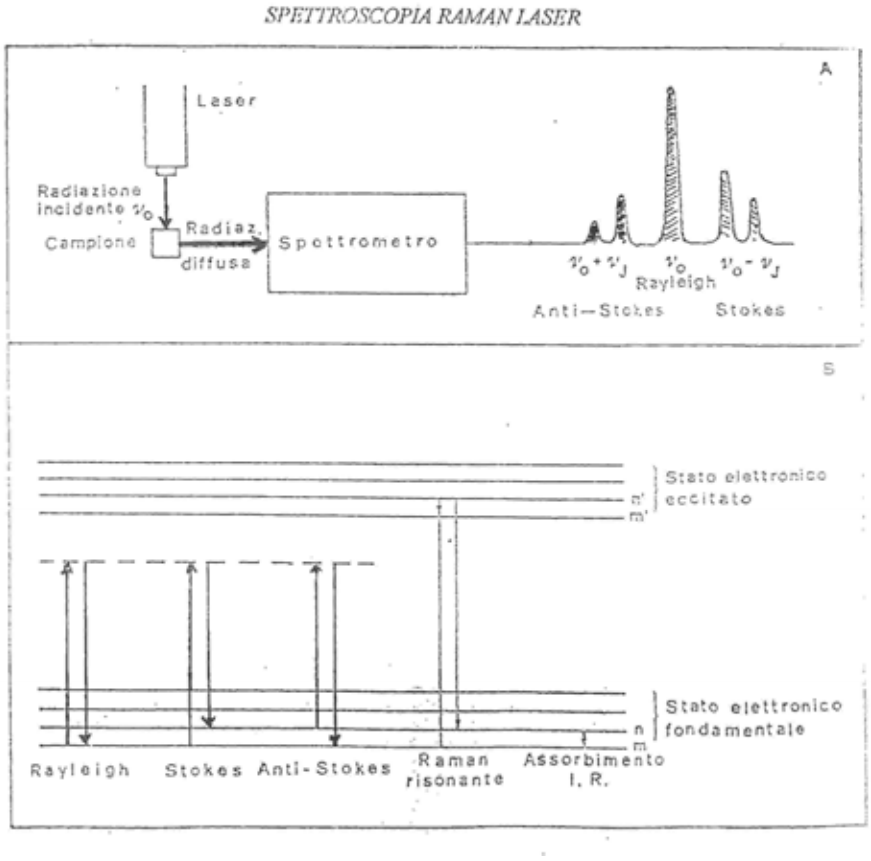

Fig. B1. (A) Scheme of Raman experiment (90° geometry); (B) scheme of the transitions that produces a Raman spectrum.

As a consequence of inelastic collision the matter can lose energy producing, in spectrum of the scattered light, the appearance of lines called anti-Stokes ($\nu_0 + \nu_1$), or gain energy, giving rice to Stokes lines ($\nu_0 - \nu_1$), where ν_1 is the frequency corresponding to the transition energy $h(\nu_0 - \nu_1)$ in the material involved in the process. Since a loss of energy can happen only if the molecule is found originally in an excited vibrational or rotational state, while an energetic gain can always happen, the Stokes radiation is generally more intense than the anti-Stokes one, which has a minor statistic probability to happen.

From the point of view of the classical physics when a molecule is put in a static electric field it undergoes a partial charge separation that produces an induced electric dipole moment and the molecule results polarized. The value of the induced dipole (μ) depends on the intensity of the applied electric field (E) and on the polarizability (α) of the molecule:

$$\boldsymbol{\mu} = \boldsymbol{\alpha}\, E$$

When some molecules are exposed to an electromagnetic radiation of frequency ν_0 the electric field felt by every molecule changes in agreement with the equation:

$$E = E_0 \operatorname{sen} (2\pi\nu_0 t)$$

and the induced dipole becames:

$$\boldsymbol{\mu} = \boldsymbol{\alpha}\, E = \boldsymbol{\alpha}\, E_0 \operatorname{sen} (2\pi\nu_0 t)$$

This is the classical explanation of the elastic (Rayleight) scattering.

If the molecule carries out some internal motion, vibration or rotation, its polarizability will not be constant in the time, but it will vary according to the relation:

$$\boldsymbol{\alpha}(t) = \boldsymbol{\alpha}_0 + (\partial\boldsymbol{\alpha}/\partial x)_{x = x0}\, x\,(t)$$

where α_0 is the static polarization and the expansion in series of $\alpha(t)$ is stopped at the first term because the extent of the vibration (x) is generally very small.

The external motion, e.g. a vibration, ca be expressed by a harmonic oscillator given by:

$$x = x_0 \operatorname{sen} (2\pi\nu_1 t)$$

where x_0 is the equilibrium distance.

Replacing these two last expressions in that of the electric dipole moment μ, the fundamental relation of the Raman spectroscopy is obtained:

$$\boldsymbol{\mu} = \boldsymbol{\alpha}_0 E_0 \operatorname{sen} (2\pi\nu_0 t) + (\partial\boldsymbol{\alpha}/\partial x)_{x = x0}\, x_0 E_0 \operatorname{sen} (2\pi\nu_1 t) \operatorname{sen} (2\pi\nu_0 t) \qquad (1)$$

The first term of the equation (1) corresponds to the Rayleight scattering, the second one to the real Raman scattering. The last term, if expressed in a different mathematical form:

$$\operatorname{sen} (2\pi\nu_1 t) \operatorname{sen} (2\pi\nu_0 t) = \tfrac{1}{2} [\cos 2\pi(\nu_0 + \nu_1)\, t + \cos 2\pi(\nu_0 - \nu_1)\, t]$$

shows two evident contributions to the scattered light, namely the Stokes ($\nu_0 - \nu_1$) and anti-Stokes ($\nu_0 + \nu_1$) radiations.

In the Raman scattering hold the laws of energy conservation, $\nu_s = \nu_i - \nu_j$, and of the wave vectors conservation, $k_s = k_i - k_j$; besides the scattered power dP_j at frequency, ν_s (Stokes), is

$$dP_j \propto (\nu_s)^4 \, f(T) \, I_i \, S_j(k_i, k_s) \, d\Omega \, d\nu$$

with:

ν_i and ν_j frequencies of the incident radiation and of the vibration j;

$f(T) = 1 + 1/(\exp(h\nu_j/KT)-1)$ (Stokes), factor of statistic occupation related to the temperature T (K is the Boltzman constant);

I_i intensity of the incident radiation;

S_j Raman cross section for the vibration j;

k_i and k_s are the wave vectors of the incident radiation and of the diffused one (it is: $k = 2\pi/\lambda$);

$d\nu$ is an elemental interval of frequency;

$d\Omega$ is the elemental solid angle of collection.

This general formula is valid whether indicates the vibration of a molecule or phonon, namely the collective elastic vibration of a crystalline solid (e.g. Si).

The conservation of the wave vector in the process of Raman scattering (at first order) in crystalline Si allows only the observation of the optic phonons at the center of the Brillouin zone (see left side of Fig. B 2) ($q \sim 0$) and its frequency is around 520 cm^{-1} [62].

In the case of a nanostructured sample with particles of nanometric dimensions, the translational symmetry of the ideal crystal is disturbed and the wave vector conservation law is weakened. If a phonon is confined in a space ΔL, the uncertainty of the moment is given by $\Delta q \Delta L \approx 1$[*]. Then the phonons included in the uncertainty interval of the wave vector around the Brillouin zone become Raman-active (see right side of the Fig. B 2). Since the phonon dispersion curve has a negative curvature, the Raman signal shifts to lower energies and widens. Simple considerations show that for structures of smaller dimensions (the smaller ΔL, the larger Δq) we can expect a shift to lower energy and a larger broadening. Indeed, the shape and the size of the nanocrystals has a great influence on the Raman spectrum. The PS Raman spectrum is very similar to that of the polycrystalline Si of nanometric dimensions.

[*] From the uncertainty principle $\Delta p \Delta x = \hbar$ and $p = \hbar q$; p = momentum, x = position, q = wave vector.

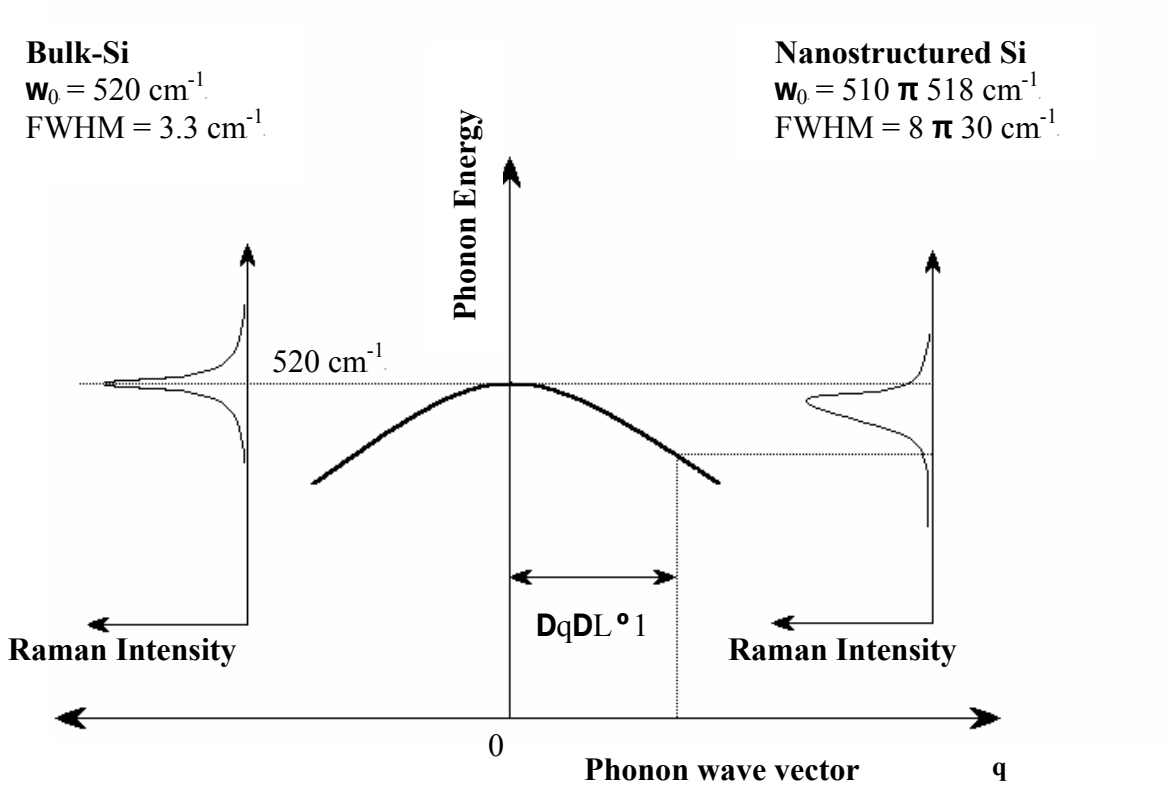

Fig. B 2. Scheme of the phononic dispersion. In a Si single crystal only the phonon with the wave vector q = 0 is active in the Raman spectroscopy (left side). In the nanocrystalline Si the small dimensions produce uncertainty in the moment such that the phonons with wave vector Δq become active in the Raman spectroscopy. Accordingly the Raman peak moves to lower energies and widens.

The Raman band observed for the crystalline Si has a lorentzian shape with a full width at half maximum (FWHM) around 3 cm^{-1} at room temperature (RT) [63]. With the increase of the temperature the peak of the signal moves to lower wave numbers and the line shape widens. In Fig. B 3 a similar behaviour is presented for a mesoporous PS sample.

The PS Raman spectra has been divided in two classes: type-I spectra with bandwidth FWHM of 7 ÷ 9 cm^{-1} and frequency shifted around 2 ÷ 4 cm^{-1}, to lower frequencies, with respect to the single crystalline Si; type-II spectra with wider bands (FWHM of 10 ÷ 40 cm^{-1}) and shifted of 7 ÷ 10 cm^{-1} or more [63].

The Raman band in the spectrum of very oxidized PS samples widens asymmetrically to lower energies showing that the phonon correlation length decreases. An interstitial isolated oxygen in a network of Si produces some changes in the bond charge distribution and in the atomic position of the Si atoms up to the third order of proximity. There will be therefore also a distortion of the bond angles in the crystal that will contribute to increase the number of Raman active modes at lower energy [64].

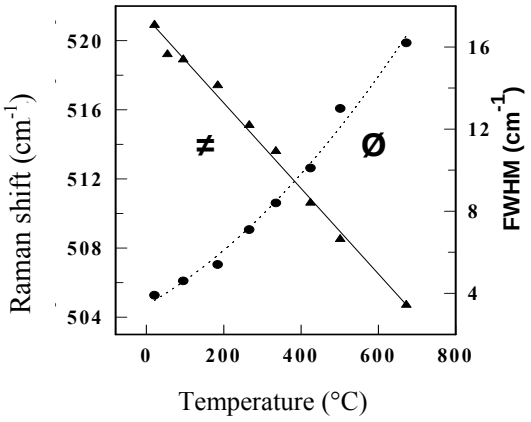

Fig. B 3. The continuous and the dotted lines represent the Raman frequencies and the FWHM, respectivally, as a function of the temperature for a mesoporous PS sample.

The choice of the laser power used for the micro-Raman measures is very important because, as we can see in Fig. B 4, high power density, easily obtainable by micro-Raman, can provoke the heating of the PS sample that is characterized by a thermal conductivity two orders of magnitudes lower than that of the crystalline Si.

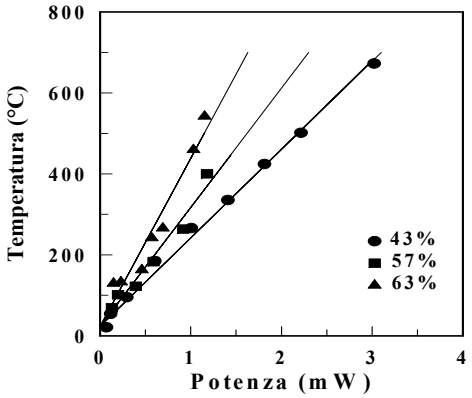

Fig. B 4. Dependence of the temperature of the sample subjected to the micro-Raman measures (of 2 μm laser spot diameter) on the laser beam power for PS samples with different porosity.

In our case the use of a 1 mW laser power with a 2 μm spot diameter means to send on the sample $3.2*10^{-6}$ W/cm^2 causing the obvious local overheating of the sample, and since we already know that a temperature increase moves to lower frequencies and widens the Raman bands, we could erroneously interpret these signals due to the heating as typical signal of the measured PS sample.

C. Fourier Transform Infrared Spectroscopy and Instrumental correction in the case of reflectance spectroscopy.

The general scheme of an FTIR spectrometer is shown in Fig. C 1. FTIR spectroscopy is based on the interference between two IR radiation beams generating an interferogram that changes as a function of the difference in the optical path of the two beams. The two domains of the distance (difference of optical path) and of the frequency (ν) are interconnected through the mathematical method of the Fourier transform.

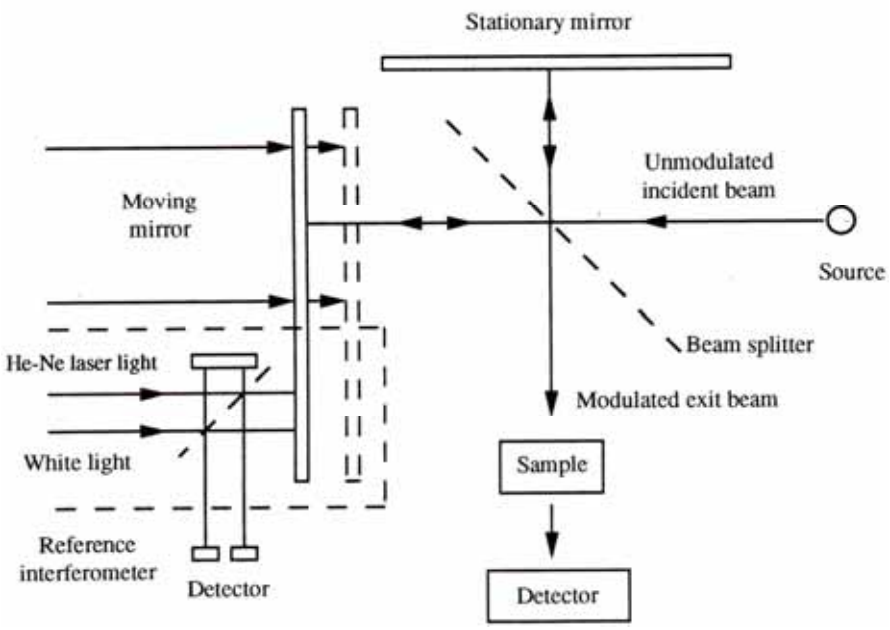

Fig. C1. A Michelson interferometer

The IR radiation emitted from the source is passed to the sample through a Michelson interferometer with a moving mirror, before reaching the detector. In the interferometer, a beam splitter divides the wave beam in two parts (of identical intensity) that are then respectively reflected by the two mirrors. Finally, the reflected beams are recombined by the beam splitter and sent to the sample and then on the detector forming an interferogram. The difference of optical path, δ, between the two beams is due to different positions in the time of the moving mirror.

Generally, different interferograms are added to get a good signal to noise ratio, where a scanning (that is the acquisition of an interferogram) has the duration of fraction seconds.

The modern spectrometers use sophisticated techniques to check the movement of the mirrors that is the crucial part of the Fourier transform spectroscopy (the automatic alignment of the mirror can be obtained using an additional laser beam).

After the amplification of the signal, in which the high frequency contributions have been eliminated by a filter, the data are converted from analogical to digital and then transferred to the computer that applies the Fourier transform. Two fundamental equations correlate the intensity on the detector I (δ), to the spectral power density at a particular wave number ν, B (ν), and they are the followings:

$$I(\delta) = \int_0^{+\infty} B(\nu) \cos 2\pi\nu\delta \, d\nu$$

$$B(\nu) = \int_{-\infty}^{+\infty} I(\delta) \cos 2\pi\nu\delta \, d\delta$$

These two equations are notes as Fourier transform pairs. Each one can be converted into other by the mathematical method of the Fourier transform.

The FTIR spectrometer has different advantages in comparison to the dispersive IR spectrometer:

- The Fellgett advantage is due to an improvement in the signal-to-noise ratio per unit time, which is proportional to the square root of the number of resolution elements being monitored, and results from the large number of resolution elements being monitored simultaneously.
- The Jacquinot advantage is due to the fact that FTIR spectrometry does not require the use of a slit or other restricting devices, particularly to low resolution, the total source output can be passed through the sample continuously. This results in a substantial gain in energy at the detector, which translates to higher signals and improved signal-to-noise ratios.
- The speed advantage is due to the ability of the mirror to move short distances quite rapidly, and this, together with the signal-to-noise ratio improvements due to the Fellgett and Jaquinot advantages, make it possible to obtain spectra on a millisecond timescale. In interferometry the factor that determines the precision of the position of an IR band is the precision with which the scanning mirror position is known. By using a He-Ne laser as reference, the mirror position is known with extremely high precision.

The intrinsic and not oxidized crystalline Si is transparent in the infrared range between 600 and 5000 cm^{-1} and it is in fact often used for realizing prisms and windows useful to transmitting IR radiations. Instead doped Si materials can present significant IR adsorption.

To measure PS samples, in the form of thin films on doped crystalline Si substrates, the most direct way is to record some spectra in reflection since no sample preparation is necessary and a transparent substrate is not needed.

From the IR spectra numerous information can be obtained, not only of vibrational nature. For example, as it is well known [5], the difference of frequency ($\Delta\nu$) between two consecutive interference minima or maxima, present in the IR spectra of thin wafers or film, is inversely proportional to the refraction index (n) and to the thickness (d):

$$d = 1/ (2n\Delta\nu).$$

From such formula, valid for almost normal incidence of the IR radiation on the sample, knowing the refraction index we can obtain the thickness, d, or knowing d, for example by SEM measurements, the refraction index of the sample.

In all of our experiments the intensity of the light reflected from the sample in the IR spectra as obtained from the instrument (R') must be corrected for the contribution, to the reflected light intensity due to the holder (R'_h) that is constituted in our case of a metallic support on which we lean the samples when we perform the reflection measurements. The contribution to the reflected light of the support is illustrated in the Fig. C 2. Hence, identifying with I_s the reflected radiation intensity due to the sample, with I_h the reflected intensity due to the support, with I_m the light reflected intensity of the mirror that is used as reference we have:

$$R' = (I_s + I_h)/ (I_m + I_h)$$

$$R'_h = I_h/ (I_m + I_h)$$

Then, being $R'_m = (I_m + I_h)/ (I_m + I_h) = 1$, the true intensity of the reflected light due exclusively to the sample (R) is:

$$R = I_s/I_m = (R' - R'_h)/ (1-R'_h)$$

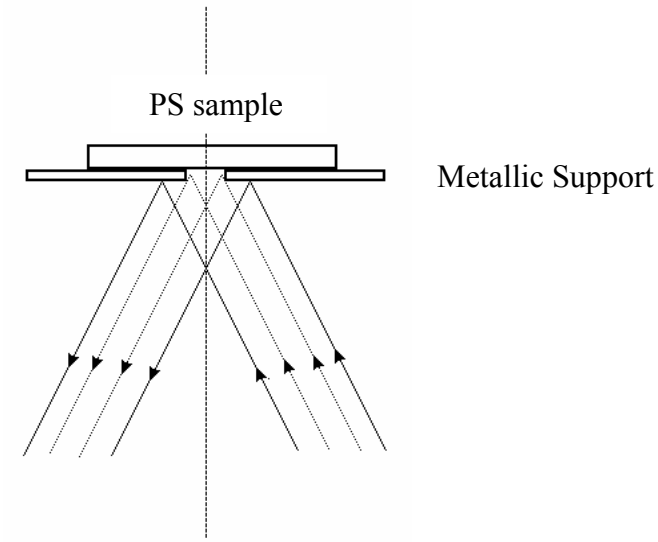

Fig. C 2. Contribute due to the presence of the metallic support to the reflected light intensity.

To help to understand how much the absorption due to the support affects the shape of the absorption spectrum of the sample we can observe Fig. C 3.

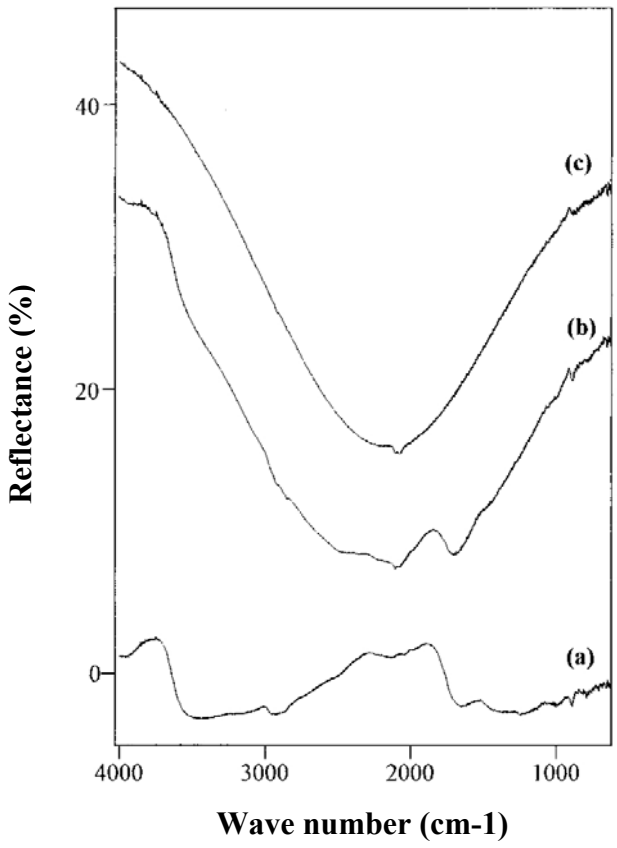

Fig. C 3. IR reflection spectra with angle of incidence of ~10° of the metallic support (a), of the sample, as given from the instrument (b) and after the correction for the contribute due to the support (c). The spectrum (c) has been shifted to higher values of reflectance percentage to allow its contemporary vision to the spectrum (b).

In this figure (a) is the spectrum related to the metallic support, (b) is the spectrum of the sample as measured; and curve (c) represent the true spectrum of the sample obtained after the correction for the contribution due to the support. Looking at this figure it appears clear that without making this correction it is possible to interpret as real bands features that are really due to the reflectivity of the metallic support.

D. SCOUT elaboration and Bruggeman model

The optical properties of an inhomogeneous material can be described by so-called effective dielectric functions if the wavelength of the probing radiation is much larger than the typical sizes of the inhomogeneities of the system, as it is the case of the micro- and meso-porous Si. In this case the response of the mixed material to an incoming electromagnetic wave can be calculated in a quasi-static approximation. Macroscopically the inhomogeneities cannot be seen and the system can be treated then as being quasi-homogeneous. An effective dielectric function $\P_{eff}$ can be introduced which is a nontrivial average of the dielectric functions of the individual components. For the case of a two-phase composite the situation is shown below:

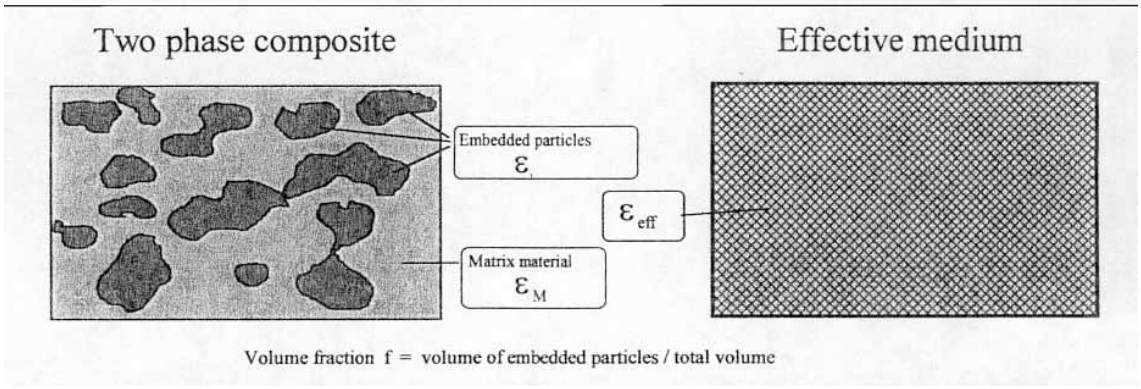

We have used the SCOUT software [62] to obtain the dielectric function of the PS samples. To describe the mixed PS system are necessary two dielectric functions, that of the Si matrix and that of the air contained in the pores, from which obtain the effective dielectric function of the mixed matter. To this aim different formulas are been proposed, we have used that of Bruggeman that is mostly used:

$$f\,(\P-\P_{eff})/\,(\P+2\P_{eff}) + (1-f)\,(\P_M-\P_{eff})/\,(\P_M+2\P_{eff}) = 0$$

where f is the volume fraction occupied by the air, and ¶ its dielectric function (¶ = 1), $\P_M$ the dielectric function of the matrix and $\P_{eff}$ the dielectric function of the mixed material that we want to obtain.

The dielectric function, ¶, that associate the dielectric shift, D, and the electric field vector, E, is strictly correlated to the susceptibility **c**:

$$D = \varepsilon_0 \varepsilon E, \qquad \varepsilon = 1 + \chi$$

The dependence on the frequency, ω, of the susceptibility is strictly characteristic for a material because it includes the effect of the electronic vibrations of the atoms as well as the contributions deriving from the free charge carriers.

Defining ε_M, we have to keep in mind that PS is a complex matrix material where there are the contributions of the crystalline Si, of the forming Si oxide, of the SiH_x species and of the air in the pores. To take into account all these contributions, the dielectric function of the matrix ε_M is the sum of a constant contribution, a harmonic-oscillator like contribution and finally a Drude model term.

The constant contribution is due to the fact that the optical IR properties can be described quite well by the sum of a constant and real dielectric function, often indicated as ε_∞ (indeed, the imaginary part has values close to 0 when the real part is constant), and the contributions describing the IR excitations.

The contribution like harmonic oscillator is due to the fact that the microscopic vibrations that involve the movement of the atomic nucleus generally have their resonance frequencies in the IR region. These characteristic frequencies depend on the masses that oscillate and on the strength of their bond and so they can be used to identify the material. The susceptibility that describes the microscopic vibrations can be described by harmonic oscillators terms:

$$\chi_{\text{Harmonic oscillator}} = \omega^2_S / (\omega^2_{TO} - \omega^2 - i\omega\omega_t)$$

where ω^2_S is the strength of the oscillator, ω_t the damping term, ω_{TO} the resonance frequency and i is the imaginary unit. In the specific case of the PS samples the contribution like harmonic oscillator are due to the vibrations of the species present on the surface of the sample (SiH_x, SiO_2, etc).

The contribution due to the presence of free charge is due to the presence of dopants inserted in the crystalline structure. In fact, in the case of doped semiconductors the charge carriers released from the donors or from the acceptors can be accelerated with very little energies responding to the applied electric field with frequencies in the IR region (the free carriers are responsible in the Si of the structure in the dielectric function below 1000 cm^{-1}). A simple expression (Drude

formula) for the susceptibility of the free carriers (that is also applicable to the metals) where are inserted the carriers concentration and the damping constant is given from:

$$\chi_{Drude} = -\omega^2_P / (\nu^2 - i\nu\omega_t) \quad \text{with } \omega^2_P = ne^2/\varepsilon_0 m$$

Here n is the volume density, e the charge and m the effective mass of the charge carriers, ω_P is the plasma frequency, ω_t the damping constant.

E. SFG Spectroscopy: general information and properties

Being sum frequency generation spectroscopy, SFG, a non linear optical processes of the second order is forbidden in a bulk material that has inversion symmetry. Also an amorphous medium does not generate a sum frequency signal because the bulk is randomly oriented, and second-order mixing is thus forbidden. Only the interface between two materials breaks the symmetry and produces a signal. Besides, polar ordering can occur at the surface of the medium to reduce interfacial energy, resulting in a net orientation of surface molecules, and allowing a sum frequency response. Therefore, SFG is intrinsically surface specific.

In the SFG technique, a pulsed visible laser beam (for example green light λ = 532 nm) is overlapped on a surface with a tunable, pulsed infrared (IR) laser beam (λ = 2 - 10 μm). The two laser pulses combine to produce light at the sum of their frequencies (440 to 500 nm) by a nonlinear process. When the interface is the only not central-symmetrical system by varying the frequency of the sources of SFG signal (IR or visible), some resonances of the interface components can be excited. For example, the vibrational levels of the adsorbates can be investigated by varying the frequencies of the IR light. Indeed this non linear spectroscopy of the interface is a very direct tool to identify the adsorbed species through their vibrational imprint. The light emitted at the sum frequency is detected by a photomultiplier and the spectrum is obtained by tuning the IR beam over the frequency range of interest (see figure 3.10).

Stronger SFG signal occurs when either the IR or visible beam is in resonance with a vibrational mode or electronic state, respectively of the sample. Molecular-level information about the interfacial or surface species can be derived from the vibrational spectrum obtained by tuning the IR beam. This allows both the identity and orientation of surface groups or molecules to be determined.

1. Non linear optics Theory

The interaction of an electromagnetic wave with electric field $\underline{E}$ with matter produces, through the action of its charges (free or bonded) a polarization $\underline{P}$. This process can be reassumed by a relation called **constitutive relation** $\underline{P} = f(\underline{E})$. This polarization produces an electric field that follows the Maxwell's equations. It is a sort of retroaction since this *additional field* modifies the global field. The constitutive relation (Maxwell's equations are already linear) can be

linearized. This linearization consists therefore of developing the relation $P = f(E)$ in series of powers of E following the Taylor's formula, stopping to the first order, getting $P^{(1)} = \chi^{(1)} E$. Nevertheless when the field E amplitude increases this linear approximation it is not correct. The sample does not respond linearly any more but quadratic terms must be considered. We introduce therefore a corrective term to the polarization: $P^{(2)} = b E^2$. We enter into the domain of the non linear optics.

We now suppose that the considered material is radiated by two monochromatic waves sufficiently intense (pulsations ω_1 and ω_2) to generate the non linear effects. We can write the temporal part of these fields under the form:

$$E_1 = (E_{10} e^{-i\omega 1t} + E^*_{10} e^{+i\omega 1t}) = E_{10} e^{-i\omega 1t} + c.c.$$

$$E_2 = E_{20} e^{-i\omega 2t} + c.c.$$

where + c.c. means that the *conjugated complex term* of the term expressly written must be added. The non linear polarization of order 2 takes part to the square of the total field $(E_1 + E_2)^2$. This calculation introduces therefore same terms in $e^{-2i\omega 1t}$, $e^{-2i\omega 2t}$, $e^{-i(\omega 1 + \omega 2)t}$ and $e^{-i(\omega 1 - \omega 2)t}$ and theirs respective complexes conjugated as well as constant terms independent of the time. Besides the constitutive relation imposes that the resultant non linear polarization $P^{(2)}$ is accompanied by its harmonics. Moreover the linearity of the Maxwell's equations does not introduce any harmonics distortion, the resultant electric field oscillates with the same pulsations of the dipolar moment. In the case of the SFG the aim is that to identify some molecular vibrations that fall in the infrared region, typically from 2 to 15 μm. A classical linear vibrational spectroscopy like the absorption spectroscopy (for example FTIR), operates in the infrared region. The SFG radiation is situated in a more favorable spectral domain, namely the visible, where a simple photomultiplier (in "counts of photons") can be used to analyze the signal.

The linear polarization is a vector of which every component depends previously on three components of the electric field. $P^{(1)}$ and E are related therefore by a 2 order tensor (matrix 3x3). At the same way, the 2-order polarization, $P^{(2)}$ depends on all the possible couples (E_j, E_k) formed by the components E_x, E_y or E_z of the field E (since this last appears in the form of a tensorial product). The polarization is written therefore to the order 2:

$$P = P^{(1)} + P^{(2)} = \chi^{(1)} : E + \chi^{(2)} : EE \qquad (1\text{-}1)$$

It is about a tensorial relation where $\chi^{(2)}$ it is a 3 order tensor (27 elements). We can write it in its general form in the following way: for the SFG ($\omega_3 = \omega_1 + \omega_2$)

$$P^{(2)}_i(\omega_1 + \omega_2) = \tfrac{1}{2} \Sigma_{j,k} [\chi^{(2)}_{ijk}(\omega_3, \omega_1, \omega_2) E_j(\omega_1) E_k(\omega_2) + \chi^{(2)}_{ijk}(\omega_3, \omega_2, \omega_1) E_k(\omega_1) E_j(\omega_2)] \quad j \leq k$$
$$= \Sigma_{j,k} \chi^{(2)}_{ijk}(\omega_3, \omega_1, \omega_2) E_j(\omega_1) E_k(\omega_2) \qquad j \leq k \qquad (1\text{-}2)$$

To fix the ideas we can render explicit this relation in the case of two incident waves whose component E_y is null. The component $P^{(2)}_x$ is then the sum of three terms:

$$P^{(2)}_x(\omega_1 + \omega_2) = \chi^{(2)}_{xxx} E_x(\omega_1) E_x(\omega_2) + \chi^{(2)}_{xxz} E_x(\omega_1) E_z(\omega_2) + \chi^{(2)}_{xzz} E_z(\omega_1) E_z(\omega_2). \quad (1\text{-}3)$$

We consider an isotropic and central-symmetrical material or namelly a material that possesses a center of inversion O, for example. This is the case of amorphous medium or of certain liquid crystals. We take a point M individualized by the vector OM = r; we will have its symmetrical, M', in - r. We calculate the term $\chi^{(2)}_{xzz}$ of the tensor: the electric field in M' verifies E (- r) = - E (r). Let us choose a system of axes such that the axis z is collinear to E (r) in the point M: $E = E_z u_z$. The symmetry of the medium also imposes: P (- r) = - P (r).

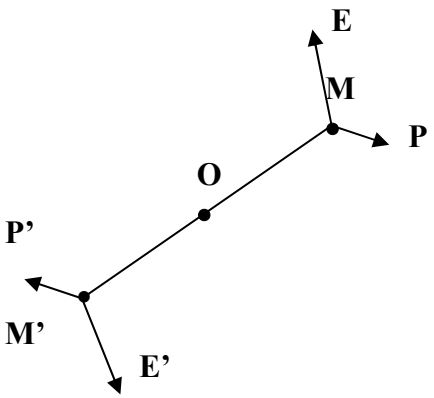

Fig. 1. Direction of the polarization vectors and electric field in a central-symmetrical matter.

$$P^{(2)}_x(-r) = \chi^{(2)}_{xzz} E_z(-r) E_z(-r) = \chi^{(2)}_{xzz} [-E_z(r)] [-E_z(r) = \chi^{(2)}_{xzz} E_z(r) E_z(r) = P^{(2)}_x(r). \quad (1\text{-}4)$$

From it we deduce that $P^{(2)}_x(-r) = P^{(2)}_x(r)$, therefore for all the r, $P^{(2)}_x(r)$ is null, that implicates that the coefficient $\chi^{(2)}_{xzz}$ is zero in all the points r. We can show equally that the other 26 coefficients of the 2 order susceptibility tensor are null. It is one of the fundamental properties

of the SFG: in first approximation **only the not central-symmetrical materials produce a signal SFG**. The SFG, and in general, all the not linear optical processes of order 2, provide a specific signal of the interface. This is not strictly exact in the dipolar electric approximation. A central-symmetrical matter can equally produce a contribution SFG because of a term of quadrupolar field.

2. SFG Intensity Calculation

We now have to calculate the direction and the intensity of the SFG signal beginning from the Maxwell's equations and from the limits conditions created by the interface between two central-symmetrical matters. For the moment we do not go into details about the source of the not linearity, we know only that it is located in the immediate proximities of the interface and that it is contained in the 2 order non linear susceptibility of the interface $\chi^{(2)}$. The 3 order tensor, $\chi^{(2)}$, represents therefore a macroscopic and global vision of the not linearity.

Now we focus the attention on the phase matching, fundamental relation of the non linear optics. We consider an infinite not linear medium in which two planar progressive, monochromatic (of respective pulsations ω_1 and ω_2) waves are propagating. In the following, ω_1 corresponds to a visible wave at 532 nm and ω_2 to an infrared wave of varying wavelength from 3 to 12 μm. The waves 1 and 2 have the wave vectors k_1 and k_2 coplanar (same plan of incidence). The two waves interact in this non linear medium and produce a second order polarization. These dipoles irradiate creating a wave of pulsation ω_3. The emission is a-priori isotropic but because of the dipoles phase correlation it is strongly favorite in a specific direction (destructive interference in the other directions). This condition on the emission angles of the non linear fields is called **condition of phase matching**. We determine it beginning from Maxwell's equations. We suppose that the non linear medium is isotropic, therefore the dielectric permittivity tensor $\varepsilon(\omega_\alpha)$ reduces to a scalar (complex if the matter is absorbent). From Maxwell's equations we deduce the following propagation equation that governs the fields at the interface:

$$[\nabla\wedge(\nabla\wedge) + \partial/\, c^2\partial t^2]\, E(r, t) = -4\pi\partial/c^2\partial t^2\, P(r, t) \qquad (1\text{-}5)$$

The field, E, is it is the overlap of three fields:

$$E(r, t) = E_1(k_1, \omega_1) + E_2(k_2, \omega_2)\, E_3(k_3, \omega_3)$$

where $E_\alpha (k_\alpha,\omega_\alpha)$ (α = 1, 2 o 3) it is a monochromatic plain wave of pulsation ω_α and wave vector k_α given by:

$$E_\alpha (k_\alpha,\omega_\alpha) = \tilde{E}_\alpha e^{i(k\alpha r - \omega\alpha t)}$$

$\tilde{E}_\alpha$ it is the amplitude of the electric field $E_\alpha (k_\alpha,\omega_\alpha)$ at the pulsation ω_α. Linewise, the polarization can be decomposed in linear and not linear polarizations (we look here only at the non linear terms of order 2):

$$\begin{aligned} P(r, t) &= \Sigma_{\alpha = 1, 2, 3} [P^{(1)} (k_\alpha,\omega_\alpha) + P^{(2)} (k_\alpha,\omega_\alpha)] \\ &= \Sigma_{\alpha = 1, 2, 3} \chi^{(1)} (\omega_\alpha) : E_\alpha (k_\alpha,\omega_\alpha) + \Sigma_{\alpha = 1, 2, 3} \tilde{P}^{(2)} (\omega_\alpha) e^{i(k\alpha r - \omega\alpha t)} \end{aligned} \qquad (1\text{-}6)$$

where the suscettivity of order 1 are expressed as a function of the dielectric permittivity of the material (for definition):

$$\varepsilon_\alpha = \varepsilon (\omega_\alpha) = 1 + 4\pi\chi^{(1)} (\omega_\alpha).$$

Keeping in mind these notations, the equation of propagation becomes:

$$[\nabla\wedge(\nabla\wedge) + \omega^2\varepsilon_\alpha/c^2] E_\alpha (k_\alpha,\omega_\alpha) = 4\pi\omega^2/c^2 \tilde{P}^{(2)} (\omega_\alpha) \qquad (1\text{-}7)$$

It is a system of three equations (α = 1, 2 or 3) that allow, once solved, to get the expression (direction and intensity) of the fields E_1, E_2 and E_3.

The polarization $\tilde{P}^{(2)} (\omega_\alpha)$ results from the interaction of the fields present in the medium and such that the sum of their pulsations verifies: $\omega_i + \omega_j = \omega_\alpha$. It results:

for the polarization at ω_1:

$$P^{(2)} (\omega_1) = \chi^{(2)} (\omega_1 = -\omega_2 + \omega_3) : E_2^* (\omega_2) E_3 (\omega_3).$$

for the polarization at ω_2:

$$P^{(2)} (\omega_2) = \chi^{(2)} (\omega_2 = -\omega_1 + \omega_3) : E_1^* (\omega_1) E_3 (\omega_3).$$

for the polarization at ω_3:

$$P^{(2)}(\omega_3) = \chi^{(2)}(\omega_3 = \omega_1 + \omega_2) : E_2(\omega_2)\, E_1(\omega_1).$$

Hence, the energy of the incident waves can be transferred to the non linear waves and then to returned back. The coupling is very strong and it is necessary therefore to impose further simplifying hypotheses. We start writing the field $E_3(k_3, \omega_3)$ in the form of a transvers E_{3tr} and of a longitudinal component E_{3lg}:

$$E_3(k_3, \omega_3) = E_{3tr}(k_3, \omega_3) + E_{3lg}(k_3, \omega_3) \qquad (1\text{-}8)$$

Simplifying Hypothesis

(1) all the waves are plain waves.

(2) *hypothesis of the slowly varying amplitude*: the conversion of energy of the waves pumped at ω_1 e ω_2 toward the non linear waves implicates a negligible relative variation of the amplitude of $E_\alpha(k_\alpha,\omega_\alpha)$ (α =1, 2) that is $E_\alpha(\omega_\alpha)$ it is a constant vector for the wave of pulsation ω_α. We remaind the notations $E_\alpha(k_\alpha,\omega_\alpha) = \tilde{E}_\alpha\, e^{i(k\alpha r - \omega\alpha t)}$. In other words, there is no depletion of the pump: $\tilde{E}_3 << \tilde{E}_1, \tilde{E}_2$.

(3) Effects of birefraction are absent or are negligible it (cubic non linear medium or propagation following an axis of symmetry).

Only the fields generated at the point in which the two pump beams interact (points at z = 0) are considered here. We show then that the relation becomes:

$$\begin{cases} \partial E_{3tr}/\partial z\,(z) = 2i\pi\omega_3^2/k_{3,z}c^2\, \tilde{P}^{(2)}_{3tr}\, e^{i\Delta kz} \\ \varepsilon_3 \partial E_{3lg}/\partial z + 4\pi\partial/\partial z\,(\tilde{P}^{(2)}_{3lg}\, e^{i\Delta kz}) = 0 \end{cases} \qquad (1\text{-}9)$$

where $\Delta k = (k_1 + k_2 - k_3)e_z$ and z represents the distance of interaction of the pump beams. The resultant SFG intensity can be written:

$$I_3(z) = 2\pi\omega_3^2/c\sqrt{(\varepsilon_3)}\cos^2\theta_3\, |\tilde{P}^{(2)}_{3tr}|^2\, [\sin(\Delta kz/2)/\Delta kz/2]^2 \qquad (1\text{-}10)$$

This expression shows that for a given thickness of the non linear material, the field created at ω_3 is maximum for $\Delta k = 0$. This is the case when $k_3 = k_1 + k_2$, this relation is anything else than the **condition of phase matching**.

Remark1: The condition of phase matching can easily be determined considering the case of the corpuscular light model. The phase matching corresponds to the conservation of the impulse, as in the case of a scattering of two particles (in this case of photons). We find again here the fundamental two conservation laws of the mechanics under the form:

the energy's conservation: $\hbar\omega_3 = \hbar\omega_1 + \hbar\omega_2$

the impulse conservation: $\hbar k_3 = \hbar k_1 + \hbar k_2$ where $\hbar$ is the reduced Plank constant

Remark2: In the case of an absorbent material (the wave vectors are therefore complexes), the condition of phase matching is valid only for the real components of the wave vectors. In effects, in the equation (1-9) the imaginary part of Δkz does not contribute to the phase but it appears in the form of damping term.

The condition of phase matching gives the direction for which the intensity of the field to ω_3 is maximum. But it is interesting to notice that out of this direction ($k_3 \neq k_1 + k_2$) the non linear field is not null. The intensity SFG on the phase mismatch Δkz follows a "*sinus cardinal* function". Intensity is maximum for a zero mismatch ($\Delta k = 0$ either $k_3 = k_1 + k_2$) whereas is zero when $\Delta kz = 2\pi$. We also notice that the emission cone of the non linear radiation (given by Δk) is the more open the more short is the non linear interaction length, z. We can think therefore that measuring this angular opening we can get an order of magnitude for the thickness of the matter that contributes to the SFG. To estimate the order of magnitude of this effect let us suppose a non linear interaction thickness of 1 nm. If we differentiate the relation $\Delta kz = 2\pi$, we get the angular opening of the SFG beam: $\Delta\theta_3 = \pi/k_3 z \sin\theta_3$. If we choose the following values for the different parameters: $\theta_1 = 50°$, $\theta_2 = 60°$, $\lambda_1 = 532$ nm, $\lambda_2 = 5$ µm, we obtain: $\theta_3 = 51°$ $\Delta\theta_3 = (6*10^{-5})°$. The effect is very difficult to be measured, especially when the pumps beams are not parallel at all. For (e.g. $\theta_1 = 50° \pm 1°$, $\theta_2 = 60° \pm 4°$) the angular dispersion of the SFGbeam is: $\theta_3 = 51° \pm 10°$. To exploit this property of the SFG, is necessary to use therefore well collimated pump beams to minimize at the best geometric causes of angular dispersion of the SFG beam.

3. Direction of the reflected SFG wave

When a wave meets a discontinuity, gives rice to a reflected and a transmitted wave. In the case of the generation of a nonlinear field E_3 by an interface, it is necessary to distinguish 2 interfaces separating 3 media: the media (a) and (b) and the “film" of the interface (e.g. adsorbates) that has a very thin thickness compared to the wavelength. The media (a) and (b) are considered both center-symmetric, therefore only the interface is source of non linearity (cf. § 1). One supposes that the media (a) and (b) are isotropic, therefore their dielectric permittivities $\varepsilon_a(\omega)$ and $\varepsilon_b(\omega)$ are scalar. The medium (a) is supposed transparent $\varepsilon_a(\omega)$, therefore, is real. On the other hand $\varepsilon_b(\omega)$ can be complex (absorbing medium,e.g. a metal).

The waves 1 and 2 are transmitted in the nonlinear film with the wave vectors k'_1, and k'_2 (law of the refraction of Snell-Descartes). The condition of phase matching requires then $k'_3 = k'_1 + k'_2$. On the x axis projection, this relation is written (see Fig. 2):

$$k'_3 \sin\theta'_3 = k'_1 \sin\theta'_1 + k'_2 \sin\theta'_2 \qquad (1\text{-}11)$$

The angles are counted positively toward the left for the incident waves and positively toward the right for the emergent waves (SFG or DFG) in accordance with the conventions traditionally used for this problem (see for example [3-5]).

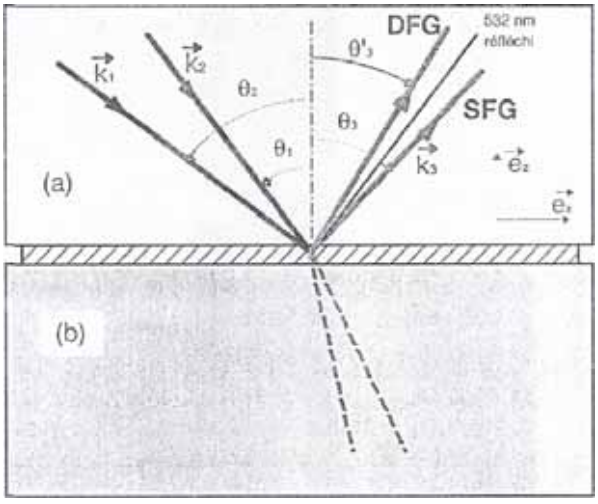

Figure 2. Scheme of the incident beams of the SFG and DFG “reflected” waves in the case of an interface between two center-symmetric media. The wave of wave vector k_1 is at a fixed wavelength (532 nm) while the varied wave vector k_2 is tunable in the infrared (5-12 μm).

A part of the SFG wave (k'_3) is reflected on the interface between the nonlinear film and medium (b) according to the usual reflection law (equality of the incidence and reflection angles). Then it is refracted and transmitted in medium (a). The emergent SFG wave verifies therefore: $k'_3 \sin\theta'_3 = k_3 \sin\theta_3$. If we express all angles and the wave vectors for every wave as a function of their value in the medium (a), one finally find:

$$k_3 \sin\theta_3 = k_1 \sin\theta_1 + k_2 \sin\theta_2 \qquad (1\text{-}12)$$

Where k_α (α = 1, 2 or 3) is related to the complex refraction index $\underline{n}$ by

$$k_\alpha = \underline{n}(\omega_\alpha)\omega_\alpha/c,$$

with $\underline{n}(\omega_\alpha) = n(\omega_\alpha) + k(\omega_\alpha)$ (real and imaginary parts of $\underline{n}$), c the speed of light in vacuum.
We can write the phase matching relation as:

$$n^a(\omega_3)\,\omega_3 \sin\theta^a_3 = n^a(\omega_1)\,\omega_1 \sin\theta^a_1 + n^a(\omega_2)\,\omega_2 \sin\theta^a_2 \qquad (1\text{-}13)$$

The relation (1-13) permits to calculate the angle with which the SFG beam emerges. We can note that this angle only depends on the index of the medium (a). If the all indexes $n^a(\omega_\alpha)$ have almost the same value. The relation simplifies further:

$$\theta^a_{SFG} = \theta^a_3 = \text{Arcsin}\,(\omega_1 \sin\theta^a_1 + \omega_2 \sin\theta^a_2)/(\omega_1 + \omega_2) \qquad (1\text{-}14)$$

Remark 1. The SFG spectroscopy consists in varying the wave number $\sigma_2 = \omega_2/(2\pi c)$ of the infrared beam. For a spectrum between 2000 and 2200 cm^{-1} if we choose $\theta_1 = 50°$ and $\theta_2 = 60°$, the SFG emerges then with an angle that varies between 50,86° and 50,94°, From an experimental viewpoint, this angular deviation is weak enough that does not require to move the detector.

Remark 2. Formula (1-14) is worth only for a co-propagating configuration (the 2 pump- beams arrive from the same side respect to the normal to the surface). In the case of the counter-propagating configuration, the sign" +" of the numerator must be replaced by a sign "-" (cf. [1], equation (3.5)).

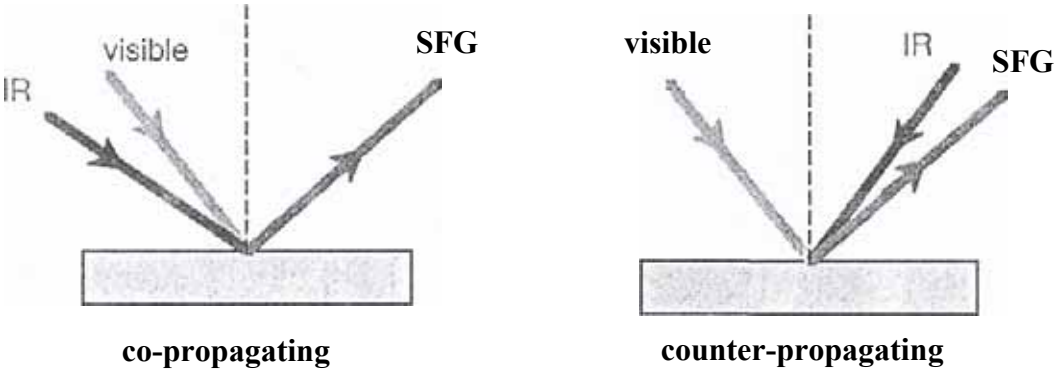

Fig. 3. Schemes of the beams in the cases of a co-propagative configuration and counter-propagative.

4. Intensity of the field electric SFG

Two strategies are possible to approach this calculation. Some authors perform the calculation inside the already evoked nonlinear film where the overtones are originated. The solution of the equation of field propagation (1-7) making reference to the sources of $P^{(2)}(\omega_3)$, is expressed as a sum of two waves: a homogeneous wave (solution of the differential equation without the second member) and an inhomogeneous solution [1, 4, 6]. This field propagates and produces the non linear emergent field to ω_3 in the medium (a), linked to the previous one by the" boundary conditions".

Another method is to consider the nonlinear film as infinitely thin. We define, in this case, a surface non-linear polarization $P^{(2)S}$ oscillating at $\omega_3 = \omega_1 + \omega_2$. Since the pump beams transfer only very little energy to the overtones, we can consider that their crossing of the interface is governed by the usual linear optics. We can calculate therefore (Fresnel formulas) the reflected fields in the medium (a). Knowing the incident fields in the nonlinear film, P^{NLS} can be determined then. In generalizing Fresnel formulas to the case of the nonlinear optics, we can express all emergent electric fields at ω_3 [3, 5, 7, 8].

Annex E References

[1] N. Bloembergen and P. S. Pershan, *Phys. Rev.* 128, 606 – 622, **1962**.

[2] P. Guyot-Sionnest, J. H. Hunt and Y. R. Shen, *Phys. Rev. Lett.* 59, 1597 – 1600, **1987**.

[3] C. Hirose, N. Akamatsu, D. Kazunari, *Appl. Spectr.* 86, 1051-1072, **1992**.

[4] B. Dick, A. Gierulski, G. Marowski, *Appl. Phys. B* 38, 107-116, **1985**.

[5] A. V. Petukhov, *Phys. Rev. B* 52, 16901-16911, **1995**.

[6] Y. R. Shen, *The Principles of Nonlinear Optics* (Wiley) 67-85, **1984**.

[7] Y. R. Shen, *The Principles of Nonlinear Optics* (Wiley) 479-504, **1984**.

[8] E. W. M. Van der Ham Thesis, *Sum Frequency Generation at interfaces a study employing the Felix free-electron laser* (Leiden), **1998**.

List of Publication

International Journals

1. *An FTIR study of porous silicon layers exposed to humid air with and without pyridine vapors at room temperature*, G. Mattei, V. Valentini, V. A. Yakovlev, **Surf. Sci.** 502-503 (2002), 58-62.
2. *An FTIR study of hexamethylenetetramine in Porous Silicon*, V.A. Yakovlev, V. Valentini and G. Mattei, **Phys**. **Stat. Sol.** 197 (1), 158-162 (2003).
3. *In Situ Functionalization of Porous Silicon during the electrochemical Formation Process in Ethanoic Hydrofluoric Acid Solution*, G. Mattei, V. Valentini**, JACS Commun.** 125 (2003), 9608-9609.
4. *Sum-frequency generation from surface species in porous silicon,* G. Mattei, V. Valentini, V. A. Yakovlev, A. A. Mani, Y. Sartenaer, P. A. Thiry, A. Peremans, Y. Caudano, L. Dreesen, B. Busson, F. Vidal, C. Humbert and A. Tadjeddine, **Phys. Stat. Sol.** Accepted for publication.

Presentation at International Conferences:

5. *Infrared study of hexamethylenetetramine in porous silicon*, V.A. Yakovlev, V. Valentini and G. Mattei, abstract for the 3rd. international conference "Porous Semiconductors-Science and Technology", Tenerife-Spain, 10-15 Marzo 2002.
6. *In situ functionalization-formation of porous silicon layers and structures: the method and its features*, V. Valentini, G. Mattei, abstract for the 4th. international conference "Porous Semiconductors-Science and Technology", Cullera-Valencia, 14-19 Marzo 2004.
7. *Sum-frequency generation from surface species and adsorbates in porous silicon,* G. Mattei, V. Valentini, V. A. Yakovlev, A. A. Mani, Y. Sartenaer, P. A. Thiry, A. Peremans, B. Busson and A. Tadjeddine, abstract for the 4th. international conference "Porous Semiconductors-Science and Technology", Cullera-Valencia, 14-19 Marzo 2004.